Display Scaling of Degraded Visual Environment Helicopter Symbology in Station-Keeping Tasks

by

Fabian Erazo, B.Eng.

A thesis submitted to the
Faculty of Graduate and Postdoctoral Affairs
in partial fulfillment of the requirements for the degree of

Master of Applied Science in Aerospace Engineering

Ottawa-Carleton Institute for Mechanical and Aerospace Engineering
Department of Mechanical and Aerospace Engineering
Carleton University
Ottawa, Ontario
September, 2017

The undersigned hereby recommends to the
Faculty of Graduate and Postdoctoral Affairs
acceptance of the thesis

Display Scaling of Degraded Visual Environment Helicopter Symbology in Station-Keeping Tasks

submitted by **Fabian Erazo**, **B.Eng.**

in partial fulfillment of the requirements for the degree of

Master of Applied Science in Aerospace Engineering

_____
Professor C. Herdman, Internal Examinor

_____
Professor M. Ahmadi, Member of Department

_____
Professor E. Lanteigne, Member of Joint Institute

_____
Professor J. Etele, Thesis Supervisor

_____
Mr S. Jennings, Thesis Co-supervisor

_____
Professor R. Miller, Chair,
Department of Mechanical and Aerospace Engineering

Abstract

Unexpected encounters with degraded visual environments (DVE) pose a serious risk to rotary-wing aircraft. Due to the loss of outside visual references, pilots engaged in DVE become entirely reliant on cockpit displays and instrument information to land safely. Flight symbology systems have been accordingly developed which offer a set of symbolic cues meant to replace the pilot's lost visual cues. Prior to engaging in operational use, symbology systems must undergo a certification process in part comprised of tuning the display scaling (i.e. the manner in which physical states are scaled to units representable on the display). At present, tuning is conducted through trial-and-error according to the feedback of the test team, without applying quantitative rigor to the process. The premise of this investigation is therefore to prove the existence of a predictable relationship between display scaling and pilot response, and in doing so provide a quantifiable and defendable basis for the tuning process. An experiment is designed in which participants conduct a single-axis precision hover using a pared-down, non-conformal symbology system. During the experiment, three display scalings are varied: the acceleration cue scaling K_a, the velocity cue scaling K_v, and the position cue scaling K_x. A fourth independent variable, *Lead*, is also considered, which represents the amount of velocity prediction afforded by the acceleration cue. The response is measured according to the root-mean-square (RMS) of the position error, the control activity, and the Bedford workload ratings. From the generated trends, suggested scaling and *Lead* levels are selected as those simultaneously resulting in low RMS, low control activity, and low workload: $K_x = 175 \frac{ft}{screen}$, $K_v \approx 22 \frac{kts}{screen}$, $K_a = 15 \frac{\frac{ft}{s^2}}{screen}$, and *Lead* = 2-2.5 *s*. Participant control aggression is then captured through the maximum attitude excursion and the time taken to complete the precision hover in an attempt at explaining anomalous responses.

Acknowledgments

Preface

This thesis is an original work by Fabian Erazo. The research project, of which this thesis comprises in part, received research ethics approval from the National Research Council's Ethics Board, Project Name "Helicopter Symbology Assessment Metric", Project No. 2016-79, 31 January 2017. Secondary approval was obtained from the Carleton University Research Ethics Board (CUREB-B), Project Name "Helicopter Symbology Assessment Metric", Project No. 106515, 03 March 2017.

Table of Contents

List of Tables

List of Figures

Nomenclature

A	state matrix
$\vec{a}_B$	body-axis acceleration vector [ft/s/s]
$\vec{a}_W$	world-reference acceleration vector [ft/s/s]
a_{X_B}	longitudinal acceleration [ft/s/s]
a_{Y_B}	lateral acceleration [ft/s/s]
a_{Z_B}	upward acceleration [ft/s/s]
B	control matrix
D	drag force [lbs]
ES	effect size
EE_{Main}	estimated effect for main-variable effect
$EE_{Interaction}$	estimated effect for N-way interaction
$\vec{E}_B$	body-axis position error vector [ft]
$\vec{E}_W$	world-reference position error vector [ft]
E_{North}	position error northward [ft]
E_{East}	position error eastward [ft]
E_{Vert}	position error vertical [ft]
E_{X_B}	longitudinal position error [ft]
E_{Y_B}	lateral position error [ft]

E_{Z_B}	downward position error [ft]
F	ANOVA statistics variable
$\vec{F}_B$	body-axis external force vector [lbs]
$\vec{F}_W$	world-reference external force vector [lbs]
F_{X_B}	external longitudinal force (alternate notation) [lbs]
F_{Y_B}	external lateral force (alternate notation) [lbs]
F_{Z_B}	external downward force (alternate notation) [lbs]
$\vec{G}_B$	body-axis external moment vector [ft-lbs]
G_{X_B}	external longitudinal moment (alternate notation) [ft-lbs]
G_{Y_B}	external lateral moment (alternate notation) [ft-lbs]
G_{Z_B}	external downward moment (alternate notation) [ft-lbs]
$\vec{g}_W$	world-reference gravity vector [ft/s/s]
$\vec{g}_B$	body-axis gravity vector [ft/s/s]
g	gravity constant [32.174 ft/s/s]
$\vec{h}_B$	body-axis angular momentum
$\vec{I}_B$	body-axis inertia vector $[ft^4]$
I_{xx}	second moment area along the longitudinal axis $[ft^4]$
I_{yy}	second moment area along the lateral axis $[ft^4]$
I_{zz}	second moment area along the vertical axis $[ft^4]$
K_a	acceleration cue scaling factor [ft/s/s/screen]
K_x	longitudinal position cue scaling factor [ft/screen]
K_y	lateral position cue scaling factor [ft/screen]
K_v	velocity vector scaling factor [kts/screen]

K_ϕ	roll indicator scaling factor [deg/screen]
K_θ	pitch indicator scaling factor [deg/screen]
$\vec{L}_{BW}$	world-to-body Euler transformation matrix
$\vec{L}_{BW}$	body-to-world Euler transformation matrix
L	vehicle lift [lbs]
M	external pitching moment [ft-lbs]
M_I	external pitching moment normalized w.r.t. I_{yy}
M_U	speed stability derivative
M_{U_I}	speed stability derivative normalized w.r.t. I_{yy} [rad/(ft-sec)]
M_Q	pitch damping derivative
M_{Q_I}	pitch damping derivative normalized w.r.t. I_{yy} [1/sec]
$M_{\delta_{long}}$	cyclic control moment derivative
M_{δ_I}	cyclic control moment derivative normalized w.r.t. I_{yy} [rad/sec^2-in]
m	vehicle mass [slugs]
N	external yawing moment [ft-lbs]
n	number of position error measurements taking in a 20-second hover phase
N_c	number of unique trials in an experiment matrix [$\Longrightarrow$ 64]
N_R	number of control reversals in a 3-second window
N_S	number of samples
p	body-axis roll rate [deg/s]
q	body-axis pitch rate [deg/s]

r	body-axis yaw rate [deg/s]
S_L	edgelength of position cue [screen units]
$\vec{S}_P$	position cue location vector [screen units]
S_{P_X}	position cue longitudinal location [screen units]
S_{P_Y}	position cue lateral location [screen units]
$\vec{S}_V$	velocity vector location [screen units]
S_{V_X}	velocity vector longitudinal location [screen units]
S_{V_Y}	velocity vector lateral location [screen units]
$\vec{S}_a$	acceleration cue location vector [screen units]
S_{a_X}	acceleration cue longitudinal location [screen units]
S_{a_Y}	acceleration cue lateral location [screen units]
u	longitudinal velocity [ft/s]
$u_{control}$	control input vector
$\vec{V}_B$	body-axis velocity vector [ft/s]
V_{X_B}	longitudinal velocity (alternate notation) [ft/s]
V_{Y_B}	lateral velocity (alternate notation) [ft/s]
V_{Z_B}	downward velocity (alternate notation) [ft/s]
$\vec{V}_W$	world-referenced velocity vector [ft/s]
v	lateral velocity [ft/s]
w	vertical velocity [ft/s]
$\bar{x}$	group mean
X	external longitudinal force [lbs]
X_m	external longitudinal force normalized w.r.t. mass [lbs/slug]

X_U	drag damping coefficient [slug/s]
X_{U_m}	drag damping coefficient nomralized w.r.t. mass [1/sec]
Y	external lateral force [lbs]
Y_i	trial response
$Y_{Aligned}$	ART aligned data
Y_{ART}	ART aligned-and-ranked data
Z	external downward force [lbs]
α_{SIG}	significance criterion
δ_{long}	cyclic control longitudinal input [inches]
θ	vehicle pitch angle [deg]
$\dot{\theta}$	world-referenced vehicle pitch rate [deg/sec]
$\mathcal{L}$	external rolling moment [ft-lbs]
ϕ	vehicle roll angle [deg]
$\dot{\phi}$	world-referenced vehicle roll rate [deg/sec]
ψ	vehicle heading [deg]
η_q	pitch damping derivative augmentation factor
$\sigma_{population}$	standard deviation of the population
σ_δ	standard deviation of the control deflections in a 3-second moving window [inches]
$\vec{\omega}_B$	body-axis angular rate vector [deg/s]
ω_{X_B}	body-axis roll rate (alternate notation) [deg/s]
ω_{Y_B}	body-axis pitch rate (alternate notation) [deg/s]
ω_{Z_B}	body-axis yaw rate (alternate notation) [deg/s]

$\vec{\omega}_W$ world-referenced angular rate vector [deg/s]

$\vec{\chi}$ state space vector

$\vec{\chi}_D$ gust-disturbed state space vector

ζ cyclic control derivative reduction factor

Shorthand

Longitudinal	$\implies$	body-axis along X_B
Lateral	$\implies$	body-axis along Y_B
downward	$\implies$	body-axis along Z_B
Northward	$\implies$	world-reference north
Eastward	$\implies$	world-reference east
Vertical	$\implies$	world-reference up
Screen Units	$\implies$	the fraction of normalized screen limits, -1 to 1
W.R.T	$\implies$	with respect to

Units

The methodology and results are largely presented in English units in keeping with North American aerospace industry practice. Apply the following conversion factors as necessary:

English Unit	S.I. Conversion
inch	2.54 cm
feet	0.3048 m
lbf	4.45 N

Abbreviations

AOA	Angle of Attack
ADS	Aeronautical Design Standards
ANOVA	Analysis of Variance
ART	Align Rank Transform
BOSS	BrownOut Symbology Simulation
C.G.	Center of Gravity
DIMS	Dynamic Interface Modeling and Simulation
DoD	Department of Defense
DVE	Degraded Visual Environment
FBD	Free-Body Diagram
FOV	Field-of-View
HDD	Head-Down Display
HMD	Head-Mounted Display
HUD	Head-Up Display
HITS	Highway-in-the-Sky
IC	Initial Conditions
LOS	Line of Sight
L-ViS	Low Visibility Symbology

MRT	Main Rotor Thrust
PIO	Pilot-Induced Oscillation
PVA	Position-Velocity-Acceleration
RMS	Root-Mean-Square
SDT	Small Disturbance Theorem
STOL	Short Take-Off and Landing
TTA	Time-to-Approach
USB	Universal Serial Bus
VTOL	Vertical Take-Off and Landing

Chapter 1

Background

Unexpected encounters with degraded visual environments (DVE) pose a serious safety risk to rotorcraft and their crew. To combat some of the inherent risks with DVE flight, symbology systems are developed in which the pilot's lost visual cues are replaced with symbolic representations of helicopter position and state. Every symbology system, regardless of the manner in which symbols are presented, must be certified prior to operational use—a process which currently involves tuning symbology parameters through trial-and-error. Under this strategy, tuning is conducted according to the feedback of the test team without quantitative means to support their suggestions. Furthermore, tuning is expensive and time-consuming as it is necessarily an in-flight process. The present research aims to prove that the relationship between pilot response and display scaling (that is, display gain, where display laws and symbol filtering remain constant) can be quantitatively predicted. The existence of a predictable relationship is impactful in two ways: first, system designers can identify display scaling levels which promote the desired pilot response, thereby providing a quantifiable and denfendable basis for the tuning process; second, the ability to methodically tune symbology characteristics through simulator trials rather than in flight greatly reduces the associated costs. To better situate the research, the following sections describe degraded visual environments and the loss of spatial awareness they induce. The symbology systems developed to minimize DVE effects are discussed, contrasting the suitability of conformal and non-conformal symbology for different phases of flight. The design of symbology is then examined by considering how certain elements affect the human user: head-mounted displays (HMD) vs. head-up displays (HUD) vs. head-down displays (HDD), visual clutter, field of view, symbol size and rate information, and symbol contrast and colour.

1.1   Degraded Visual Environments

As a rotorcraft nears the ground, its propeller downwash disturbs any loose terrain or debris. If present in great enough quantities, the recirculating matter produces a degraded visual environment, partially or totally obscuring the outside visual field (Figure 1). The resulting spatial disorientation makes maintaining a controlled flight difficult, and has recurrently caused the loss of aircraft and personnel. Landing under such conditions has been described as severely as "...essentially flying a controlled crash into the ground with no outside reference" [1]. In fact, the European Safety Agency identifies unexpected DVE encounters as the number one risk to rotary wing assets [2], a claim supported by the U.S. Department of Defence (DoD) findings which concluded that between 2001 and 2009 65% of their combat non-hostile losses during low-speed flight could be attributed to DVE conditions [3].

Minimizing the adverse effects of DVE flight, particularly during low-speed and hover manoeuvres, is plainly a priority issue, and DoD has accordingly compiled a number of candidate solutions for reducing DVE rotorcraft losses. Many suggestions are geared towards improving the methods already in practice, such as increased pilot training in simulator settings and updating crash-worthiness criteria for the rotorcrafts themselves. However, DoD has placed a large emphasis on introducing active means of addressing DVE flight, most notably the continued development of flight symbology to improve pilot awareness [3].

Figure 1: Helicopter engaging DVE conditions. Adapted from [4].

1.2   Flight Symbology

Conventionally, helicopter state information is presented through a series of gauges and meters on the cockpit panel. With such systems, pilots must inspect individual elements to extract salient information. On more modern aircraft, panel-mounted displays are used as a means of centralizing state information, reducing the time spent visually scanning the cockpit. Particularly when operating in DVEs, however, critical information must be immediately available—searching for and consciously interpreting cockpit elements is not a viable strategy. Flight symbology systems are thus an attractive means of providing all necessary information "at a glance" by combining pictographic and alpha-numeric features within the pilot's direct line-of-sight. Flight symbology can be broadly categorized as either conformal or non-conformal, and in the following sections an overview of both is provided.

1.2.1   Conformal Flight Symbology

Conformal flight symbology is predicated on the principles of augmented reality: virtual landing zones and ground references (e.g. physical obstacles) are superimposed on a synthetic forward-view of the terrain, which is generated either through topographical databases or using real-time sensors. Such systems provide the pilot with an intuitive representation of the task and surroundings. Conformal symbology can be subdivided into two formats: egocentric, in which the symbology is displayed from the perspective of the pilot, and; exocentric, in which the symbology is displayed as though from a tethered distance behind the rotorcraft (Figure 2). Wickens and Prevett [5] found that egocentric conformal symbology exhibits a pronounced advantage with respect to vertical and lateral tracking when compared to exocentric symbology. They posit the "ecological consistency", or naturalness, of the first-person configuration as the reason for this discrepancy. McGreevey and Ellis [6] concur: they found that exocentric judgements of position are intrinsically biased, and can lead to errors in closed-loop position tracking tasks. However, while the naturalness of egocentric symbology is superior for local guidance, exocentric symbology provides better global awareness because the pilot is able to directly view the position of the rotorcraft with respect to its surroundings [5]. This indicates that neither display perspective is capable of providing high levels of fidelity in both tracking (guidance) tasks *and* situational awareness. The ability to toggle between modes is therefore an attractive
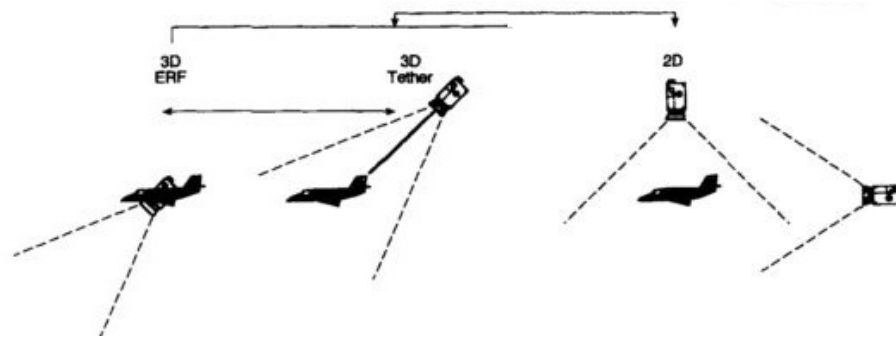
Figure 2: Helicopter symbology perspectives. Left: Conformal egocentric; Middle: Conformal exocentric; Right: Non-conformal. Adapted from [5].

feature on future conformal symbology systems, enabling the user to, for example, conduct the approach phase of a landing manoeuvre from an egocentric perspective and switch to an exocentric view when nearing the ground.

Though conformal symbology is largely 3D, such systems are often augmented with 2D instrument information, such as alpha-numeric representations of heading and altitude. Such symbols must be judiciously applied: as noted by McCann and Foyle [7], improper superposition of the descriptive information may lead to attention tunneling where the pilot becomes fixated on either the near domain (instrument information being displayed at the forefront) or the far domain (terrain information in the background). This is because overlapping but incoherent sets of information may result in the serial processing of the two domains of information, rather than parallel processing [8, 9]. Properly formatted conformal symbology, in which the near-domain imagery moves concomitantly with that of the far-domain, is necessary to facilitate the mental integration of both sets of information.

An example of one commonly-adopted conformal symbology configuration is Highway-in-the-Sky (HITS). In a general sense, a HITS display is a "three-dimensional representation of the aircraft's intended flight path, as seen through the cockpit forward window" [10] (refer to Figure 3). As is the case with conformal symbology at large, instrument information is often superimposed on the HITS display. Such displays have the potential to reduce pilot cognitive workload by integrating attitude and navigation information into a single source, and by allowing the pilot to apply the same laws of spatial relationship and interaction as is inherently applied in other arenas of life [11, 12]. They also provide an amount of predictive information because the pilots can extrapolate the future state of the aircraft given the current control

inputs. HITS displays enable the pilot to fly complex approaches with low amounts of tracking error and good path awareness [10, 13], though it has been noted that a pilot reaction time to unexpected events (incursions, obstacles, etc.) was much increased, contrary to prevailing assumptions [14].
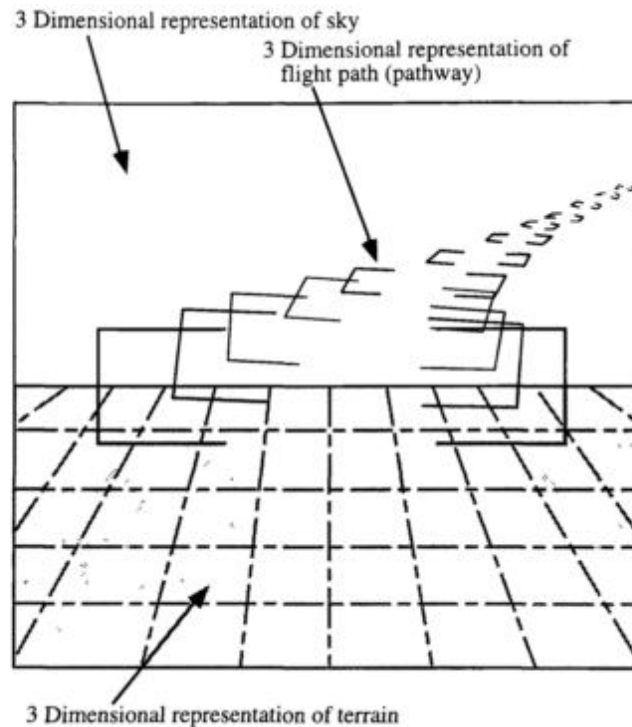
Figure 3: Highway-in-the-sky conformal symbology. Source: [10].

1.2.2 Non-Conformal Flight Symbology

Non-conformal symbology depicts the rotorcraft state through a series of two-dimensional symbols belonging to either a plan (top) view or a profile (side) view (refer to Figure 2, right). A number of core elements found in modern non-conformal symbology can be found in Figure 4, and are inherited from such systems as the NASA V/STOL HUD of the early 1990's [15]. In the plan view, the center of the screen denotes the helicopter position (aircraft ref.), and symbols denoting horizontal information move relative to that location. For example, a velocity vector extends from the center of the screen whose length and orientation denote the magnitude and direction of the helicopter's body-axis planar velocity. A target location is also depicted in some fashion, in this case a rectangle denoting a landing pad. A horizontal

acceleration cue is often added, referenced to the end of the velocity vector and thus acting as a predictor for the velocity. Using plan-view symbology, a pilot manipulates the helicopter controls to bring the landing zone cue to the center of the screen— once accomplished, the helicopter's horizontal position is coincident with the desired ground location. In non-conformal systems, it is found that the large amount of delay between a cyclic input and its associated steady-state horizontal velocity could lead to pilot-induced oscillations (PIO), but that the predictive capability afforded by the acceleration cue mitigated such problems [16]. Properly configuring the acceleration cue is therefore of great importance, and is a large focus of the research in this thesis.

Proper navigation of a flight vehicle requires more information than is provided by plan-view symbols. The addition of profile-view symbols on the same displays has received positive feedback from pilots due to the saliency of the information provided, despite the added workload necessary to consolidate both views [13, 17]. Referring once more to Figure 4, profile symbols often include a vertical velocity cue, vertical acceleration cue, and rising ground (landing deck, in this case). Information belonging to neither perspective is assigned to an "unreferenced" view. Unreferenced symbols (e.g. torque bars and alpha-numerics) have been added to non-conformal symbology systems such as the Brown Out Symbology Simulation (BOSS) developed by NASA-Ames (Figure 5), and the AH-64 symbology set of the U.S. Army [18, 19].

As described earlier, conformal symbology is formatted as either egocentric or exocentric, with the latter affording better situational awareness. However, research conducted by Wickens [5] found that non-conformal symbology affords better situational awareness than *either* egocentric or exocentric conformal symbology because the pilot is not restricted to the viewport of the camera or image generator. Note that this is at a cost of task awareness (e.g. how well the pilot can follow a flight path) because all ecological cues inherently present in a first-person perspective are lost—instead, non-conformal symbology requires the pilot to interpret abstract and dissociated symbols. Despite the task awareness limitations, non-conformal symbology is preferred for touchdown and low-altitude manoeuvres [13, 20] because errors in position and attitude are more readily identifiable, even if such excursions must be mentally transformed from symbol motion to meaningful information. This predilection towards non-conformal symbology for low-altitude tasks presents a strong case for the further development of such systems in particular.
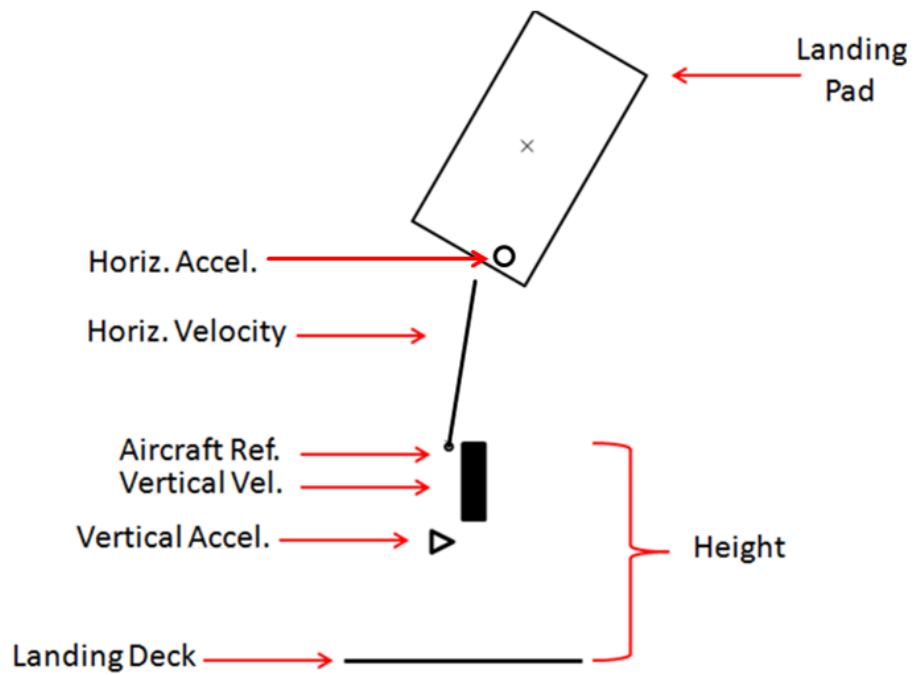
Figure 4: Representative non-conformal symbology system
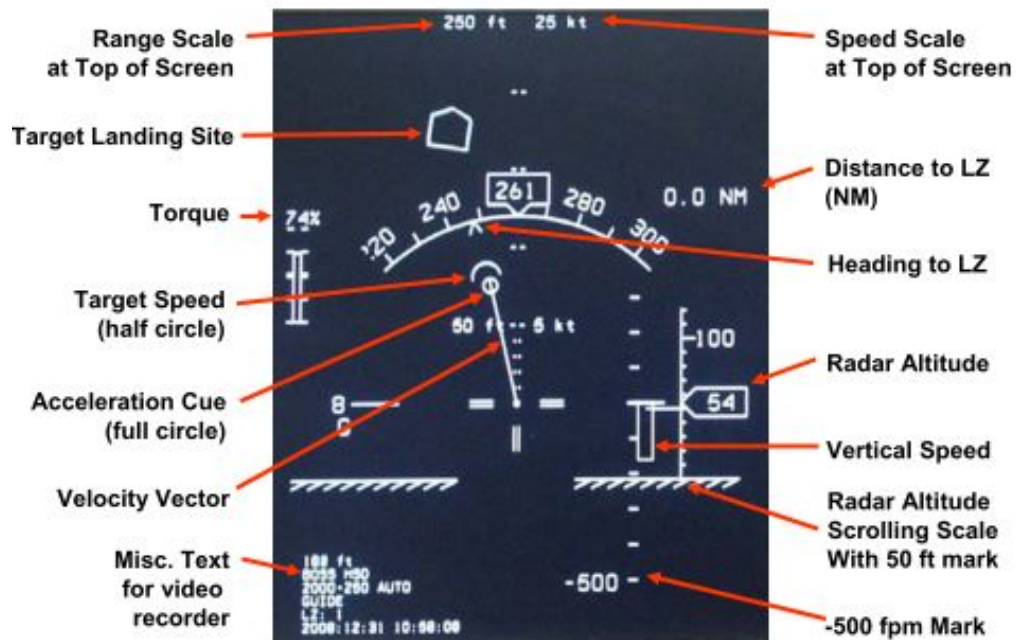
Figure 5: NASA-Ames BOSS Symbology. Source: [16].

1.3   Head-Up vs. Head-Down vs. Head-Mounted Displays

In a rotorcraft, three systems are available for displaying flight symbology: a head-down display (HDD), a head-up display (HUD), and a head-mounted display (HMD). An HDD quite simply amounts to a computer screen affixed in the cockpit, initially installed as a means of centralizing cockpit information to reduce pilot scanning time. As DVE-dedicated non-conformal symbology systems were developed, these too were displayed on HDDs. HDDs cannot be used for conformal symbology since it offers no outside view, so data orientation is crucial [21].

Head-up displays were the first see-through display option developed, with their use in the military dating back to the 1960's [21, 22]. HUDs are comprised of a transparent display mounted between the pilot and the windscreen (i.e. in the pilot boresight), and enable pilots to maintain a heads-up posture during flight by displaying symbology overlaid onto the outside world; in this respect, HUD systems enable conformal symbology (refer to Figure 6 [23]). The HUD introduces a new set of challenges for pilots: for example, they require the pilot to focus at infinity [24], however the eye rarely does so and instead tends to drift towards a point of focus. This tendency is exacerbated by fatigue, reduction in luminance, and low visibility conditions where the eye is unlikely to be stimulated by objects at infinity [25]. It also seems that pilots are unable to readily make the mental rotation of horizontal information presented on a vertical HUD, which is more easily done on a vertical HDD displaying non-conformal symbology. Such transformation difficulties have been attributed to the fact that real-world information is being presented simultaneously with symbolic information [21], and often lead pilots to misjudge distances [26]. With HUDs, the phenomenon of attention tunnelling for the first time became apparent, in which pilots fixate on the symbology presented in the near-domain and thereby interrupt their scanning patterns of the far-domain (i.e. outside world). Larsh and Wickens [27] found that attention tunnelling caused pilots to miss low-probability events, such as the appearance of alerts or intruders, when flying conformal symbology on an HUD. It is for this reason that HUDs are generally designed to provide the pilot with the option to select/deselect symbology elements on the display [24].

Figure 6: Commercial airliner head-up display

As HUD technology improved and hardware components shrank, it became possible to mount the display system directly on the pilot's helmet—head-mounted displays (also called helmet-mounted displays) were the result. HMDs allow the pilot to look elsewhere than the boresight while still retaining the same information otherwise presented on HDDs or HUDs. In addition to issues inherent to see-through display systems such as HUDs, a number of complications arise due to the image projection configurations and the non-static nature of the HMD itself. For example, information can be projected through monocular, bi-ocular, or binocular configurations, where the former two may cause optical distortions since the images presented to each eye are different (symbology vs. real-world for monocular; two differing sets of symbology for bi-ocular). However, for binocular HMDs in particular, vertical retinal image disparities are a concern as they are liable to cause diplopia (double vision) [24].

To properly use HMDs, pilot head tracking is required to establish their line-of-sight (LOS) and generate the imagery presented in their viewfield. Head tracking can be accomplished mechanically (direct-connect linkages), optically (emitters or fiducials), magnetically (magnetic field radiated through the cockpit and measured through helmet sensor), accoustically, or gyroscopically [21]. Each of these methods

introduces its own set of complexities, and the additional layer of computationally-intensive processing raises concerns of accuracy and latency. Newman [28] empirically determined that head tracking responses of at least 4 times quicker than the measured data rate is required to established the precise portrayal of symbology on an HMD, and Dudfield [24] found that image lags greater than 100 ms result in pilot nausea. Slewable information (e.g. information that travels across the HMD independent of the head motion of the pilot) in particular has the potential for illusory effects when the tracking response and image latency thresholds are crossed. Head motion also greatly complicates the representation of attitude information, since such information must be presented in an unambiguous manner in every orientation. For example, the designer must consider if the horizon line should remain fixed the real-world horizon and thus present both helicopter pitch and roll information, or if the symbol should remain fixed to the orientation of the HMD and thus solely denote pitch.

From an operational perspective, HMD weight is a critical factor when flying for extended periods—a factor not present with HDDs or HUDs. Aside from the physical fatigue induced by the additional weight, the increased inertia of the HMD could slow the pilot's lateral head movements and hence limit the fundamental benefit of an HMD [24]. Furthermore, variations in head geometry means that HMDs must be re-fitted to each new pilot prior to flight, again adding to the operational complexities.

1.4   Human Factors Considerations

Symbology systems are designed for human use and must therefore be considerate of the nuances and limitations of cognitive capabilities. Particularly when operating in DVE conditions, when spatial disorientation becomes a concern and vestibular stimuli (i.e. sense of balance and orientation) are suspect, the visual cues provided by symbology become the most important mode of rotorcraft control. Symbology definition will be divided into a few areas of consideration, each of which are discussed in the following sections: (1) symbol clutter, (2) field-of-view (FOV), (3) the shape, size, and meaning of individual symbols, and (4) the motion of symbols (rate). Aside from the symbology configuration, display system issues affecting visual interpretation of the symbology, such as luminance and colour (5), must also be considered.

1.4.1 Visual Display Clutter

Visual clutter is an inhibitory phenomenon in which added information increases visual search time. While the term "clutter" may be subjective, Alexander et al. [29] assert that a pilot will consider a display to be cluttered when the visual density exceeds the information density required for the task. Alexander, Wickens and Hardy [30] further suggest that a pilot's perception of clutter is affected by his/her knowledge and *use* of information within the task domain—under both of these definitions, therefore, clutter is a matter of redundant information. Symbol colours, it has been found [29], can also cause a display to seem cluttered if the colour scheme results in symbols clashing in a confusing manner. The effect of clutter is particularly detrimental in HUDs and HMDs because, aside from disrupting information processing, clutter limits the view of the far-domain imagery [24]. Ververs and Wickens [31] found that in such cases a cluttered display slows pilot response time by up to 0.5 seconds when compared to an uncluttered display. Clutter effects are greatly reduced in HDDs because only near-domain imagery is presented.

Newman and Greeley [21] define clutter reduction as one of the primary goals of display design, and strongly suggest that symbology systems provide pilots with de-clutter options to clear warning indicators and reduce symbols to a minimalistic set. In practice, reducing the number of symbols may not always be possible, but delays in response time can still be somewhat mitigated by presenting non-attention cueing to peripheral rather than focal areas: for example, Doyle [32] found that attitude information presented in the periphery was unaffected by clutter and attention tunnelling. Others means of improving response time include replacing symbols by more easily-interpretable equivalents: Hosman et al. [33] determined that digital representations of airspeed resulted in faster interpretation than analog counterparts, and that yet better responses were obtained when isolated airspeed indicators (analog or digital) were replaced with an indicator-predictor pair.

Studies conducted by Fadden & Wickens [34] and by Yeh et al. [35] found that the mental cost associated with clutter is generally outweighed by the cost of scanning—that is, it is preferable to search for information in a region of high symbol concentration than it is to scan for information across the display. These findings support the arguments of Doyle and Hosman (above) which assert that reducing clutter is not as simple as reducing symbol density, but is more a matter of improving symbol saliency and clarity.

1.4.2 Field-of-View

The intent of HUDs and HMDs is to provide a sense of naturalness while flying, and to do so their field-of-view (FOV) must be compatible with the functions of the human eye. A complete sense of immersion would require the system to match the human eye's forward-facing FOV of approximately 200 degree horizontal (with 120 degrees of binocular overlap, if system-applicable) and 130 degrees vertical [36]. Furthermore, symbology systems must consider that human vision is also anatomically subdivided into two pathways: one activated by stimulation in the center of the retina and one activated by stimulation of the periphery [37]. A restricted field of view may therefore fail to activate either of these two paths in a natural way. However, an appropriate field-of-view is greatly dependent on the task, and much of the time a significantly reduced FOV may be tolerable. For example, Patterson [37] found that a FOV as small as 40 degree is adequate for target recognition since it requires little peripheral information. For tasks requiring peripheral information, e.g. visual orientation, a FOV greater than 60 degrees is required. By contrast, a 127-degree FOV is required for adequate control in a low-altitude flight simulation, with subjective workload measures increasing dramatically in a more restricted FOV [38]. Richman et al. [39] also found that forward flight while using the HITS systems require large FOVs, else the observer becomes desensitized to increases in forward velocity and loses their sense of spatial orientation. The transition from HUDs to HMDs therefore greatly increases the range of applicability: HUD FOVs are limited to about 25 degrees (with wide-FOV HUDs extending up to 45 degrees) [24], making their use unsuitable for many tasks. However, since HMDs are mounted closer to the user's eye they can offer much broader FOVs, and are therefore a promising choice when displaying conformal symbology. Caution must be applied when using HMDs in a binocular configuration, however, as they must provide at least 50 degrees of visual overlap to avoid disorientation [37].

With respect to HDDs, research by Szobozslay et al. [40] revealed that the FOV greatly affects the amount of pilot compensation required to achieve desired performance: at 20 degrees FOV, compensation is considerable; at 40-80 degrees FOV, compensation is moderate; at 100 degrees FOV, compensation is still moderate but the achievable performance is better. In keeping with the findings of Richman and Szoboszlay, Newman and Greeley [21] insist that HDD target acquisition is more readily achieved with wide HDD FOVs.

1.4.3   Symbol Size and Detectability

Symbol size and behaviour must be carefully considered to ease detection and reduce the likelihood of providing overwhelming distraction. For symbol size, U.S. military standard MIL-STD-1295A suggest that a symbol should not subtend less than 20 minutes of arcangle (where 1 minute of arcangle is 1/60th of a degree) [42]. Particularly when contrast is low, larger symbols are required for detection. Appropriate symbol sizes will therefore depend on the type of display system being used: for a HMD, the physical size of the symbol will be smaller because the display is very close to the eye. For HUDs and HDDs, however, symbol sizes will vary according to the size of the display and its distance from the user. In terms of detectability, each symbol should be unique (by virtue of at least two "coding characteristics" [21], such as shape and scaling, or colour and display law) and flashing symbols should be minimized—flashing, it is suggested, may be used to draw attention to a symbol but not by itself to denote error. Bernsten [43] also found that using symbols to *directly* identify error or excursions, rather than having to extract error information indirectly through symbol *motion*, leads to superior performance. For example, it is preferable to include error indicators which appear when position excursions are nearing the prescribed limits, rather than having to interpret that information from the motion of the position cue.

1.4.4   Rate Information

Reaction time is defined as the "interval between the presentation of a stimulus to a subject and the subject's response" [44]—in other words, the latency of the response as a result of neuromuscular lag. To determine pilot reaction time criteria, Morris and Hamilton [45] conducted an experiment in which 62 subjects were tasked with pressing the joystick upon the appearance of a spot target, and found a reaction time range of 0.143-0.461 seconds [45]. The subjects in question were all F-14 fighter pilots, and their reaction times are therefore presumably exemplary. The 0.1-0.5 second reaction time range is likewise adopted as a consolidated neuromuscular lag term in digital pilot models, such as that of Pollard [46].

   The 0.5 second reaction time presented above is a *simple* reaction time, in that it is elicited when performing a simple task (e.g. press a button when the bulb lights up). As task complexity increases (e.g. press a button when only one of two bulbs light up,

but not when both light up) reaction time likewise increases because the pilot must make a decision prior to executing a response. Reaction time further increases when the subject is presented with multiple means of executing the response, not only because the alternatives exists, but because the alternatives introduce uncertainty [47]. For example, the helicopter pilot must contend with multiple sets of controls to perform a multi-axis task and must therefore undergo a decision-making loop to predict and correct excursions in many directions. Cummings [48] postulates that reaction time is linearly related to the amount of information transmitted (i.e. number of discrete tasks and response options), and Schweizer [49] found that reaction time equally increases with pilot stress.

To mitigate the effects of reaction time, pilots will use rate information (the rate at which the symbol tracks across the display) to project errors forward in time: for fast-moving signals, the projection may only be enough to compensate for the neuromuscular delay; in slower-moving signals, it may lend an amount of prediction to their control inputs. For example, due to the higher-order dynamics of helicopter controls, pilots must perceive the attitude as well as the attitude rate [50], i.e. the rate at which the attitude indicator travels. The heavy use of symbol rates strongly suggests that display scaling (refer to Section 1.5, where display scaling is defined as the manner in which physical helicopter states are mapped to the symbology display) is of utmost importance since the scaling ultimately *defines* the rate at which symbols track across the display.

1.4.5   Luminance and Colour

At the system level, display issues can include insufficient luminance (brightness), particularly in bright ambient lighting [51]. According to MIL-STD-1295A [42], information must be presented such that it is easily interpretable in sunshine reflecting off fresh snow. A display luminance of 10,000 foot-Lamberts was suggested, though Newman argues that this is excessive particularly for displays intended for use in adverse weather, wherein DVE falls [21]. Rash et al. [52] recommend a value of roughly 3000 foot-Lamberts as appropriate for displays, with weapon aiming sights perhaps warranting higher requirements. While these provides adequate guidelines, proper luminance levels are a function of task and display system. Ververs and Wickens [22] found that tasks which involve visually searching for a target on an HDD are better accomplished when irrelevant information is low-lighted, but that the same is not the

case for HUDs. It was determined that the low-lighting enables relevant information to be more readily extracted, leading to more head-up time when operating on an HDD—however, with a HUD the pilot need not switch his attention from the display to real-world scanning. More elaborate luminance issues arise when operating an HMD, since designers must be considerate of the relative luminance between eyepieces: for binocular configurations, luminance differences of more than 30% between the two views has been found to cause disorientation [37].

Along the same vein as luminance issues is the concern for insufficient symbology-real world contrast: monochrome green is often used for symbology displays [53] because many colours are not suitable against the constantly-changing real-world background. Colour should therefore "only be used when an appreciable improvement over monochrome can be proven" [21]. Though no clear indication of universal benefits has yet been established, colour may find its way into use because it has the advantage of providing realism [24], and because it offers the prospect of encoding high- and low-importance events.

1.5   Display Laws vs. Display Scaling

To appreciate the nuances of symbology design, it is prudent to make a distinction between display *scaling* and display *laws*. Display laws (sometimes called display dynamics) refer to the equations containing the scaling, filtering, and overall dynamics which determine the behaviour of symbology cues on a display [54]. For example, the designer will modify the display laws depending on their desired acceleration cue behaviour, where common options include: 1) the status display, where the acceleration cue represents the rotorcraft's acceleration; 2) the predictor display, where the acceleration cue predicts the position of the tip of the velocity vector (i.e. the equations driving the position of the acceleration cue are dependent not only on the acceleration of the rotorcraft, but also upon the body-axis velocity of the rotorcraft); and, 3) the command display, where the acceleration cue is a flight director symbol, and is referenced to the center of the display rather than to the tip of the velocity vector. Note that elements of the helicopter model are not included in display laws, since by definition the display laws refer to the terms affecting the representation of the helicopter states on the display, but assume that the states themselves are known (e.g. *pitch, velocity, etc.*).

The discussion presented thus far impresses upon the reader that, most fundamentally, display laws describe the equations and filtering driving symbol motion—that is, they describe the *behaviour* of the symbols. Display *scaling* (sometime called display gain) are the conversion factors, used to convert physical units (e.g. ft/s^2, kts, etc.) to display units. Display scaling is subsumed within display laws (i.e. the helicopter dynamics must be scaled to the appropriate units prior to being presented as cue motion on a display). Since the display scaling determines how many feet, knots, etc. are displayed on a screen, it determines not only the *position* of a symbol on the screen but also the *rate* at which the symbol tracks across the screen. For example, a position cue will track across the screen differently for two different scaling levels, even if the helicopter velocity were to remain constant in both cases. This concept is touched upon in Section 1.4.4. In the present research, it is the *scaling* values which shall be modified, leaving the underlying *laws* unchanged.

Establishing an appropriate display scaling scheme is accomplished on a "That Looks About Right" directive [21], sometimes predicated on existing systems. For example, the U.S. Army's night-time attack helicopter symbology [56] was designed with a baseline position cue scaling, K_x, of 35 feet/screen, which was subsequently deemed overly sensitive for use in the intended hover applications. This deficiency prompted a re-evaluation of the display scaling, from which a non-linear position cue display scaling was devised where the cue sensitivity decreased as the helicopter strayed from the target location. At the development stage, determining appropriate display scaling is sometimes a matter of matching the transfer function properties of a modified helicopter-symbology system to its predecessor. Such was the case in the follow-up night-time attack helicopter symbology research, which was conducted to investigate variations in control system characteristics and display formats [57]. During the experiments, system designers adopted linear display scalings of $K_v =$ 8.88 knots/screen, $K_x = 66$ feet/screen, and $K_\theta = K_\phi = 39$ deg/screen to preserve open-loop transfer function properties. Some display scaling guidelines can also be extracted from physical manoeuvre limitations and system resolution: the critical lateral drift during helicopter landing is 0.4 kts above which the helicopter is liable to roll-over [58], meaning such excursions must be readily identifiable on an HDD. Largely, however, display scaling is inconsistent even between systems designed for the same phases of flight: compare the above scaling to that implemented by BOSS during hover manoeuvres, where $K_x = 150$ feet/screen, $K_v = 15$ knots/screen, and K_θ

= 22.5 deg/screen. Also consider the logarithmic altitude cue scaling (with a maximum displayed altitude of 500 feet) implemented by SAE International in their hover symbology [59], as compared to the 150 ft/screen (or 75 ft/screen, mode-dependent) altitude scaling in BOSS. Clearly, the volume of display scaling possibilities is staggering, and furthermore, establishing the display scaling during developmental trials does not suffice to meet operational certification, which dictates that the symbology must be tuned by a trained flight test crew. This process is accomplished in-flight, and follows a trial-and-error approach without quantitative means of supporting the test crew's decision—selecting appropriate scaling levels therefore heavily depends on the test team's preferences and competencies.

Chapter 2

Research Direction

Minimizing the adverse effects of DVE flight is of evident importance, and one way to do so is by ameliorating the symbology systems tailored for operation in such conditions. Rather obviously, unexpected DVE encounters most frequently occur during touchdown and low-altitude manoeuvres—logically, therefore, improving low-altitude symbology systems would ultimately improve DVE flight safety. As discussed in Chapter 1, non-conformal symbology systems are often preferred for low-altitude use because position and attitude excursions are more easily identified through discrete symbols than when interpreting them in a conformal environment. Improving *non-conformal* symbology systems tailored for *low-altitude* use therefore presents itself as a promising means of reducing the hazards of DVE rotorcraft operation.

The introduction sections have outlined attempts made at improving symbology systems through symbol layout, display laws, symbology perspectives, field-of-view, and so on. Engineering efforts have equally been directed towards improving approach guidance algorithms for non-conformal symbology in specific [13]. However, the literature presented in Section 1.5 emphasizes the drastically non-uniform display scaling even for similarly-formatted symbology systems, and exposes the lack of quantitative methodology being applied when determining such scaling levels. The importance of having more rigorous methods is demonstrated through a simple example: how many degrees of helicopter pitch should map to the display, i.e. if a symbol denoting helicopter pitch were to be located at either limit of the display, how many degrees of pitch should it represent? Since display scaling directly affects the manner in which symbols track across the display, an overly sensitive display may result in pilot-induced oscillations. Conversely, an insufficiently sensitive display will misrepresent large excursions as small visual discrepancies.

2.1 Research Statement

At present, tuning the display scaling of a non-conformal symbology system is accomplished during certification according to a trial-and-error approach. This process is conducted based on the feedback of the test team, without quantitative means to support their suggestions—Newman [21] refers to this subjective approach as a "That Looks About Right" directive. In reality, however, very few guidelines *are* available for such tuning, and those which exist largely consist of platitudes such as "...should be clean-shaped, clear and explict" or "...must perform its intended task" [21]. Nor do military standards provide any better guidance: MIL-STD-1295A [42] identifies symbology system hardware specifications, environmental tolerances, and latency requirements, but offers nothing by way of symbology behaviour suggestions. In addition to the plaguing lack of defendable guidelines, tuning is necessarily conducted in flight, and certification processes dictate that a symbology system must be re-evaluated for each new helicopter upon which it is installed, as well as following any major changes to the symbology software. The cost associated with so many in-flight hours is extraordinary.

Through simulator trials, this research aims to prove the existence a predictable relationship between non-conformal symbology display scaling and pilot response. If the research statement is substantiated, the implications are twofold: first, system designers can use the results to identify appropriate display scaling, thereby providing a quantifiable and defendable basis for the tuning process. Second, while minor tuning can be conducted in-flight as necessary, the display scaling will be selected according to simulator results, greatly reducing the associated cost. When considering this investigation, it is important to recognize that the research is fundamental in nature: the display scaling suggested in forthcoming sections is specific to the helicopter model implemented. Nonetheless, the implication of such results is universal in that the *existence* of a predictable scaling-response relationship holds true regardless of the model of choice—replacing the helicopter model and re-performing the experiment will produce equally valid results.

2.2   Experiment Layout

To meet the objectives of this research, the following approach will be undertaken:

- Define and rationalize the experiment task

- Establish a non-conformal symbology system with low-altitude and hover cueing capabilities from commons

- Tailor the symbology to the experiment task

- Define a helicopter model and gust model. Coupled with the symbology system, these complete the pilot-in-the-loop feedback system.

- Establish a display scaling test matrix

- Conduct human-participant experiments on the simulator, performing the prescribed task under all display scaling combinations presented in the test matrix

Chapter 3

Methodology

3.1   Experiment Task

The participant is tasked with performing a *precision hover* along the longitudinal axis. In a precision hover, the helicopter begins at a distance from the target location, and the pilot must translate to the target and subsequently maintain a hover. This manoeuvre is selected from the Aeronautical Design Standards ADS-33E [60], and is meant to assess the ability to shift from translating flight to a stabilized hover. For the purposes of this document, the precision hover is formally separated into two phases: the approach phase and the hover phase. The transition from approach phase to hover phase occurs when the helicopter is within 10 feet of the target location. In the experiment, the simulated helicopter position is initially offset from the target location by 50 feet. The duration of a single trial is subject to the aggressiveness of the participant: a 20-second timer begins counting down once the helicopter enters the hover phase—through preliminary studies, it was determined that the average trial takes roughly 30 seconds in total. This task is limited to single-axis to isolate the effect of display scaling from other sources (e.g. refer to Section 1.4 for a discussion of the effects of multi-task decision-making, visual clutter associated with more comprehensive symbology, etc.). Off-axis inputs and coupling effects are therefore ignored in this experiment.

3.2   Position-Velocity-Acceleration Architecture

In representing planar information, one of the most commonly-adopted non-conformal symbology configurations is the position-velocity-acceleration (PVA) format. Under

PVA architecture, the acceleration cue is the primary controlled element—in other words, cyclic control inputs are used to drive the location of the acceleration cue on the display. A velocity vector is used to denote the helicopter's instantaneous planar velocity, and a position cue to denote the error between the helicopter's position and the target location. To maintain a hover while operating a PVA system, the pilot places the acceleration cue on the position cue and maintains that arrangement as the latter converges to the reticle (center of the screen). Refer to Figure 8, where the central PVA elements are illustrated. The location of the PVA cues on the screen are obtained through a series of transformations whereby world-reference position, velocity, and acceleration are rotated into body-axis through the relevant Euler angles, and subsequently converted to units representable on the display. The world-referenced position error vector $\vec{E}_W$ is defined as having components of northing, easting, and vertical position errors

$$\vec{E}_W = \begin{bmatrix} E_{North} & E_{East} & E_{Vert} \end{bmatrix}^T \tag{1}$$

and the body-axis position error vector $\vec{E}_B$ can be defined as having components acting along the longitudinal axis (X_B), lateral axis (Y_B), and downward axis (Z_B), where downward is defined as a axis orthogonal to both X_B and Y_B, with positive acting out the bottom of the aircraft.

$$\vec{E}_B = \begin{bmatrix} E_{X_B} & E_{Y_B} & E_{Z_B} \end{bmatrix}^T \tag{2}$$

The body-axis position errors are obtained through the world-to-body Euler transformation matrix defined as $\vec{L}_{BW}$, where c is shorthand for cos, s is shorthand for sin, θ is the aircraft pitch, ϕ the aircraft roll, and ψ and aircraft yaw:

$$\vec{L}_{BW} = \begin{bmatrix} c\theta c\psi & c\theta s\psi & -s\theta \\ s\phi s\theta c\psi - c\phi s\psi & s\phi s\theta s\psi - c\phi c\psi & s\phi c\theta \\ c\phi c\theta c\psi + s\phi s\psi & c\phi s\theta s\psi - s\phi c\psi & c\phi c\theta \end{bmatrix} \tag{3}$$

thus

$$\vec{E}_B = \vec{L}_{BW} \vec{E}_W \tag{4}$$

Consider the scenario in Figure 7, which depicts the planar (2D) position error of the helicopter (i.e. the *horizontal* distance between the helicopter and the desired location). For this system, the transformation matrix L_{BW} is reduced to elements of heading, ψ, since out-of-plane aircraft rotations are ignored (therefore $\phi = \theta = 0$). The vertical position error E_{Vert} is likewise ignored, meaning Equation 4 is reduced to the following

$$
\begin{bmatrix} E_{X_B} \\ E_{Y_B} \\ E_{Z_B} \end{bmatrix} = \begin{bmatrix} c\psi & s\psi & 0 \\ -s\psi & c\psi & 0 \\ 0 & 0 & 1 \end{bmatrix} \begin{bmatrix} E_{North} \\ E_{East} \\ 0 \end{bmatrix}
\tag{5}
$$
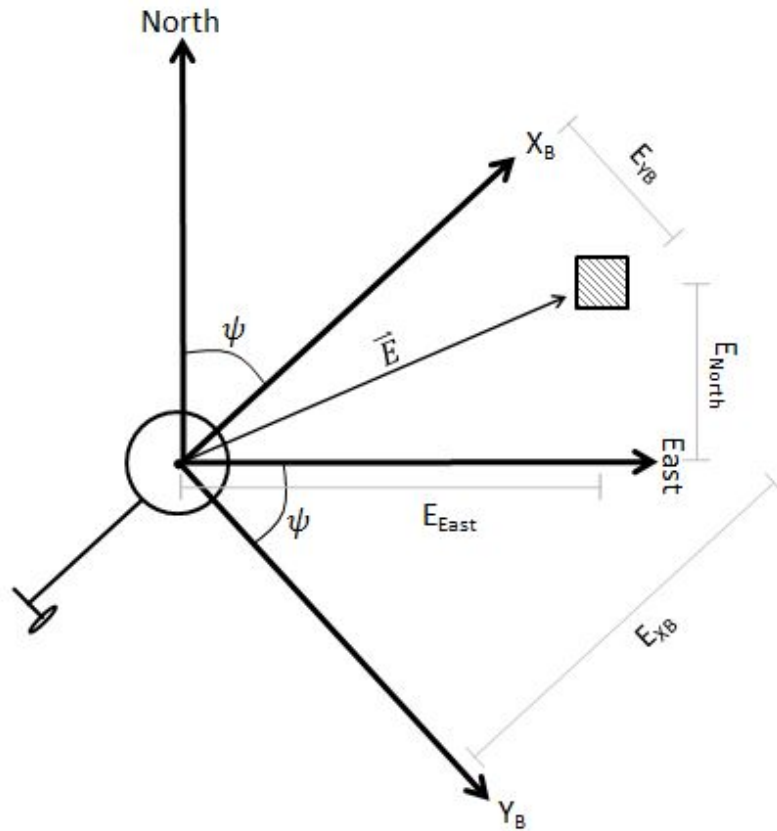
Figure 7: World-to-body transformation of planar position error. The hatched square denotes the target location.

where after multiplying through, the longitudinal and lateral components of the body-axis position error take the form

$$E_{X_B} = cos(\psi)E_{North} + sin(\psi)E_{East} \tag{6}$$

$$E_{Y_B} = -sin(\psi)E_{North} + cos(\psi)E_{East} \tag{7}$$

$$E_{Z_B} = 0 \tag{8}$$

Transforming the velocity from world-reference to body-axis follows a similar procedure. Let the world-reference and body-axis velocity vectors, $\vec{V}_W$ and $\vec{V}_B$, be defined

$$\vec{V}_W = \begin{bmatrix} V_{North} & V_{East} & V_{Vert} \end{bmatrix}^T \tag{9}$$

$$\vec{V}_B = \begin{bmatrix} u & v & w \end{bmatrix}^T \tag{10}$$

respectively. As with the position error, the velocity is transformed from world-reference to body-axis according to

$$\vec{V}_B = \vec{L}_{BW}\vec{V}_W \tag{11}$$

or alternatively

$$\vec{V}_B = \vec{L}_{BW}\dot{\vec{X}}_W$$
$$\vec{V}_B = \dot{\vec{X}}_B \tag{12}$$

and expressing $\vec{V}_B$ in component form yields

$$\vec{V}_B = \begin{bmatrix} u \\ v \\ w \end{bmatrix} = \begin{bmatrix} \dot{E}_{X_B} \\ \dot{E}_{Y_B} \\ \dot{E}_{Z_B} \end{bmatrix} \tag{13}$$

In keeping with the planar analysis introduced in Figure 7, the Z-component of the body-axis position error, E_Z, is set to zero. The vertical component of the velocity, w, is also set to zero. The body-axis accelerations can be obtained according to the time-derivative of the body-axis velocities, following identical logic to that shown in

Equation 11. In reality, however, the accelerations are measured through accelerometers installed on the aircraft and aligned with the body-axes; thus, the accelerations are by default referenced to the body-axes and require no transformations. For consistency, the body-axis acceleration vector is defined as:

$$\vec{a}_B = \begin{bmatrix} a_{X_B} & a_{Y_B} & a_{Z_B} \end{bmatrix}^T \tag{14}$$

recalling once more that a_Z is zero in the planar analysis.

With the position, velocity, and acceleration now expressed in the body-axis frame, the next step is to express these quantities in a manner representable on the display— that is, the body-axis position, velocity, and acceleration must be converted from physical units (ft, knots, ft/s/s) to "display units" of some description. The location of the position cue on the display, $\vec{S}_P$ will be defined as the following

$$\vec{S}_P = \begin{bmatrix} S_{P_X} & S_{P_Y} \end{bmatrix}^T \tag{15}$$

with the location of the velocity vector $\vec{S}_V$ and the acceleration cue $\vec{S}_a$ adhering to similar notation

$$\vec{S}_V = \begin{bmatrix} S_{V_X} & S_{V_Y} \end{bmatrix}^T \tag{16}$$

$$\vec{S}_a = \begin{bmatrix} S_{a_X} & S_{a_Y} \end{bmatrix}^T \tag{17}$$

In a general form, the location of the symbol on the display can be expressed as a scalar function dependent on the appropriate display scaling and body-axis helicopter quantities.

$$S_{P_X} = f_p(K_x, E_{X_B}, E_{Y_B}, u, v, a_{X_B}, a_{Y_B}, \psi)$$

$$S_{P_Y} = f_p(K_y, E_{X_B}, E_{Y_B}, u, v, a_{X_B}, a_{Y_B}, \psi)$$

$$S_{V_X} = f_v(K_v, E_{X_B}, E_{Y_B}, u, v, a_{X_B}, a_{Y_B}, \psi)$$

$$S_{V_Y} = f_v(K_v, E_{X_B}, E_{Y_B}, u, v, a_{X_B}, a_{Y_B}, \psi)$$

$$S_{a_X} = f_a(K_a, E_{X_B}, E_{Y_B}, u, v, a_{X_B}, a_{Y_B}, \psi)$$

$$S_{a_Y} = f_a(K_a, E_{X_B}, E_{Y_B}, u, v, a_{X_B}, a_{Y_B}, \psi)$$

Recalling the discussion from Section 1.5, the functions f_* represent the display *laws*, which describe the position, motion, and filtering of the symbols on the display. It is for this reason that each function can be expressed as a combination of the any of the available helicopter quantities: consider the predictor-PVA format, where the acceleration cue location is dependent also on the body-axis velocity. Often, however, the display laws do not make use of the majority of secondary terms. The display laws specific to the symbology used in the present research are discussed in Section 3.3.2. The display *scaling* is denoted as K_x, K_v, and K_a, and are the conversion factors from physical units to display units—display scaling is subsumed within the display laws.

As a final matter, the interpretation of the display units themselves must be considered. Designers often cite the display units as the angle subtended in the user's visual field (i.e. if the display is a certain distance from the user, and is of a certain height and width, physical units are converted to an angular region within the user's field of view). This system of display units is adequate for HMDs because the screen is a known and constant distance from the user's eye; however, with the HDD set-up decided upon for this research (discussed later) the distance from the user to the display is variable. To describe the location of display symbols in an unambiguous manner regardless of the user-display separation, the coordinate system is selected such that the limits of the display (bottom and top, left and right) are normalized to (-1, 1). This is illustrated in the PVA symbology in Figure 8, where the longitudinal (X_B) and lateral (Y_B) axes are aligned with the up-down and left-right axes of the display: within the first quadrant of the display, both axes have a range of (0-1) screen units. These ranges would be extended to include -1 to 1 if all 4 quadrants were depicted. Within the scope of Figure 8, therefore, the X-component and Y-component of the position cue, velocity vector, and acceleration cue all lie somewhere within 0-1.
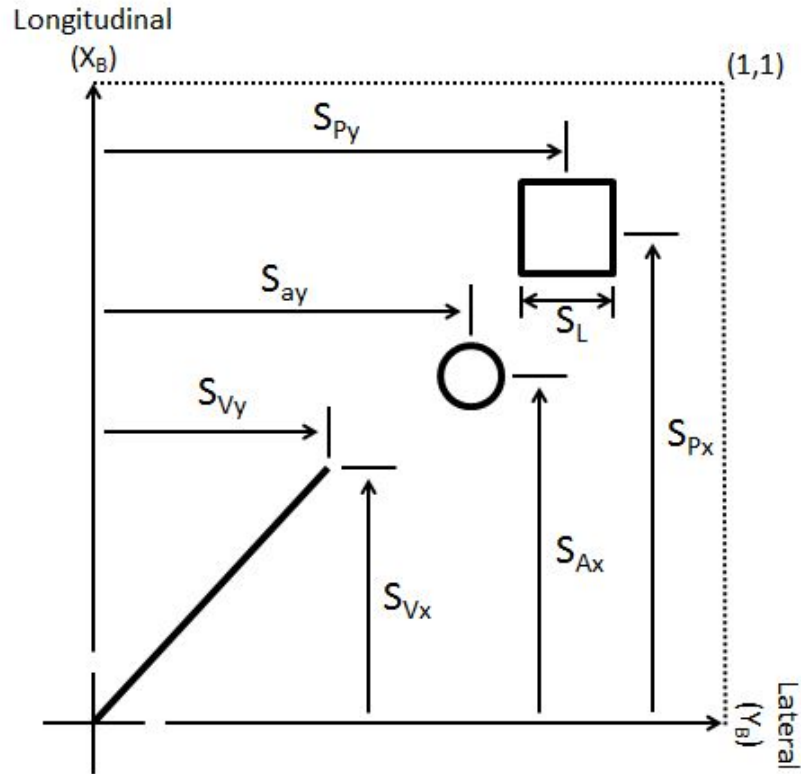
Figure 8: Generalized position-velocity-acceleration symbology format

3.3 L-ViS Symbology System

A non-conformal symbology system dubbed L-ViS (**L**ow **Vi**sibility **S**ymbolgy) was developed in collaboration with the National Research Council of Canada's Flight Research Laboratory for the purposes of this research. L-ViS has its roots in NASA-Ames' BOSS symbology [16] and affords many of the same features. The approximate placement and colour scheme are likewise largely inherited from BOSS. The L-ViS system was developed with full-axis cueing capabilities, and is configured to provide flight information in a format appropriate for low-altitude, low-speed manoeuvres (e.g. approach, hover, landing). For example, vertical situational awareness information is included which would not necessarily be required under cruise conditions. Unreferenced symbols such as torque and engine parameters are not incorporated in this version. The location of alpha-numeric indicators, such as the compass and altimeter, are static within the display. The pitch indicator is a quasi-conformal symbol in that it moves not only vertically with the pitch, but also rolls to properly characterize the
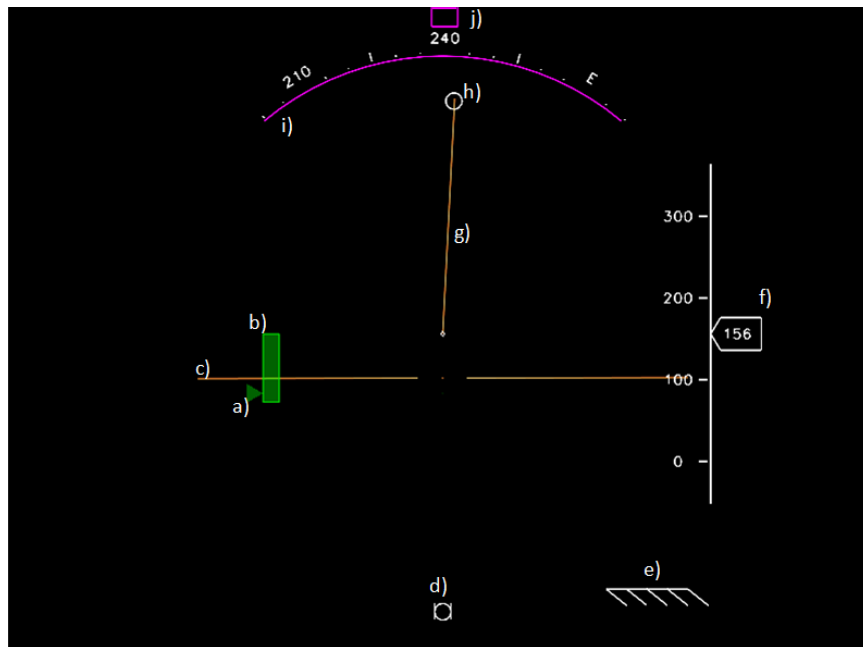
Figure 9: L-ViS symbology system

Table 1: L-ViS cue nomenclature

Assigned Nomenclature (Figure 9)	Symbology Cue
a)	Vertical Acceleration Cue
b)	Vertical Velocity Cue
c)	Pitch (Horizon) Indicator
d)	Sideslip Ball
e)	Rising Ground
f)	Altimeter
g)	Horizontal Velocity Vector
h)	Horizontal Acceleration Cue
i)	Compass
j)	Position Cue

orientation of the horizon—this behaviour is *descriptive*, and in no way conforms to the real-world horizon. A full list of symbology nomenclature is provided in Table 1, and details regarding the symbology functionality pertinent to the experiment is provided in Section 3.3.2.

3.3.1 Pared-Down L-ViS Symbology System

A pared-down version of the L-ViS system is implemented for the single-axis experiment, as shown in Figure 10. It contains only those cues necessary to complete the longitudinal precision hover task: the pitch indicator, the horizontal position cue, the horizontal velocity vector, and the horizontal acceleration cue.
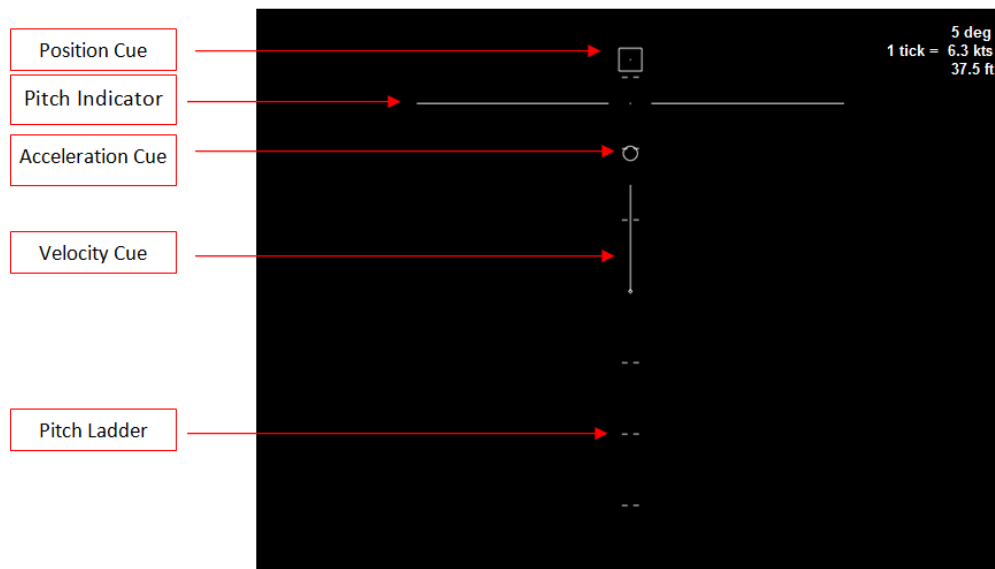
Figure 10: Pared-Down ELVIS Symbology

Qualitatively, the functionality of the provided cues follow position-velocity-acceleration (PVA) format described in Section 3.2. The position cue denotes the relative distance between the helicopter position (referenced to the center of the screen) and the target location—if the cue is above the center of the screen, the helicopter is behind the target location. The velocity cue is an indication of body-axis velocity, with a cue extending upwards from the center of the screen denoting forward velocity. The acceleration cue is referenced to the end of the velocity vector: thus, the direction of acceleration is indicated by the position of the acceleration cue

relative to the tip of the velocity vector, and the magnitude of acceleration is indi-
cated by the separation distance between the two. In this format, the acceleration
cue is intended as the primary indicator through which the pilot manages the velocity
and position.

The pitch indicator is included because the underlying helicopter model is rate
controlled (Section 3.4), and preliminary studies found that the helicopter could not
be properly flown without attitude indication. The pitch indicator scaling is kept
constant at +/-20 degrees per screen (i.e. +/-20 degrees at either display limit).
This is in keeping with the sensitivity of a helicopter's cockpit attitude indicator.
Note also that a pitch ladder is included, which is a feature not available in the
full-axis L-ViS arrangement. This pitch ladder provides a means of interpreting not
only the intermediate pitch values, but also the display scaling which is presented
alpha-numerically in the top-right corner of the screen (i.e. 1 ladder tick denotes a
certain number of feet of distance, knots of speed, and degrees of pitch). In keeping
with the findings of Section 1.4.5, the symbology system is achromatized to remove
distractions caused by visual clutter. Visual angles subtended by the cues are variable
since the participant is allowed to adjust the orientation and position of the computer
screen (ref. Section 3.8)

3.3.2   Symbology Display Laws

The display *laws* driving the position, velocity, and acceleration cue behaviour are
described in Equations 18, 19, and 20, respectively. Only the longitudinal laws are
defined as no other axes are considered in the experiment. In keeping with the
notation presented in Section 3.2:

$$S_{P_X} = f_p(K_x, \vec{E}_W, \psi)$$

$$S_{V_X} = f_v(K_v, u)$$

$$S_{a_X} = f_a(K_a, a_{X_B}, S_{V_X})$$

with the functions f_* are defined as

$$f_p(K_x, \vec{E}_W, \psi) = \frac{1}{K_x}(E_{North}cos(\psi) + E_{East}sin(\psi)) \tag{18}$$

$$f_v(K_v, u) = \frac{1}{K_v} u \tag{19}$$

$$f_a(K_a, a_{X_B}, S_{V_X}) = \left(\frac{1}{K_a} a_{X_B}\right) + S_{V_X} \tag{20}$$

where

K_x is the position cue scaling ($ft/screen$)

K_v is the velocity cue scaling ($kts/screen$)

K_a is the acceleration cue scaling ($ft/s^2/screen$)

E_{North} is the vehicle world-axis position error, northward (in ft)

E_{East} is the vehicle world-axis position error, eastward (in ft)

ψ is the vehicle heading (arbitrarily assumed 0 $degrees$)

u is the body-axis longitudinal velocity (in kts)

a_{X_B} is the body-axis longitudinal acceleration (in ft/s^2)

The distinction between display law and display scaling is once more apparent in the above equations, where K_x, K_v, and K_a act as conversion factors from physical units to units representable on the display. Since the pared-down L-ViS symbology is intended for the hover and low-speed domains, the display scaling linearly maps physical to display units (whereas a symbology set intended for use through the entirety of an approach may employ logarithmic or piece-wise display scaling [13]). As previously described, the acceleration cue is referenced to the end of the velocity vector—this behaviour is reflected in Equation 20 in which the position of the tip of the velocity vector S_{V_X} is summed with the scaled acceleration. Thus, if no acceleration is present, the acceleration cue and velocity cue tip occupy the same display region.

The acceleration cue, pitch indicator, and ladder are coded to remain a constant size within the display. For example, the acceleration cue is a circle with a radius of 0.025 screen units (recall that the display limits are normalized to +/- 1 screen units). Clearly, the behaviour of the velocity vector requires the cue to lengthen and shorten according the velocity being displayed. Less obvious is that, since the position cue is meant to represent a physical landing zone, the size of the cue as presented on the display is designed to vary. Referring once more to Figure 8, the

position cue's edgelength S_L represents a physical distance of 20 feet, and its visual depiction depends on the scaling level K_x as per Equation 21. To clarify, consider looking down at the ground from a bird's-eye view, and imagine that a 20ft x 20ft landing pad is demarcated on the ground. If one maintains a constant altitude the size of the landing pad doesn't change; however, increasing or decreasing altitude, while not affecting the FOV, will cause the landing pad appear to vary in size. This is artificially replicated in the symbology by changing the position cue scaling K_x: decreasing K_x in this analogy is equivalent to increases altitude, i.e. the perceivable field increases so the size of the target appears to decrease.

$$S_L = 20 * \frac{1}{K_x} \tag{21}$$

3.4   Helicopter Model

In the following sections, the general force and moment equations are derived for a helicopter in flight, and are subsequently reduced to the longitudinal set. The longitudinal equations are then linearized about an equilibrium condition (trim) according to the Small Disturbance Theorem (SDT). The aerodynamic and control forces and moments acting on a helicopter in motion are then described, thereby defining the stability and control derivatives. Finally, the linearized force and moment equations are presented in state space format.

3.4.1   Definition of Assumptions

Prior to engaging in the lengthy derivation, it is important to outline several overarching assumptions applied to the process: 1) the helicopter is a rigid body; 2) the velocity of the helicopter is small compared to the rotation of the Earth, so the latter can be considered an inertial frame of reference (i.e. the relative angular acceleration is zero); 3) the X_B-Z_B plane is a plane of symmetry. Additional assumptions pertaining to specific elements of the derivation are introduced as necessary.

3.4.2   Definition of Terms

A free-body diagram (FBD) of a helicopter in 3-dimensional flight is presented in Figure 11. In this diagram, the externally-acting body-axis forces and moments are

defined in general terms as F_B and G_B, respectively:

$$\vec{F}_B = \begin{bmatrix} F_{X_B} & F_{Y_B} & F_{Z_B} \end{bmatrix}^T = \begin{bmatrix} X & Y & Z \end{bmatrix}^T \tag{22}$$

and

$$\vec{G}_B = \begin{bmatrix} G_{X_B} & G_{Y_B} & G_{Z_B} \end{bmatrix}^T = \begin{bmatrix} \mathcal{L} & M & N \end{bmatrix}^T \tag{23}$$

where aerospace convention adopts the nomenclature found in Equation 23 to describe the externally-acting moment, such that $\mathcal{L}$ is the rolling moment, M is the pitching moment, and N is the yawing moment.

The specific forces considered in the forthcoming description of the stability derivatives are presented in Figure 11: the lift, L, is the component of the main rotor thrust (MRT) acting upwards (i.e. in opposition of the helicopter weight, W); the thrust, T, is the component of the MRT acting in the forward direction; and, the drag, D, opposing the vehicle thrust. The body-axis linear velocities are defined in Equation 13, and are presented again for consistency:

$$\vec{V}_B = \begin{bmatrix} V_{X_B} & V_{Y_B} & V_{Z_B} \end{bmatrix}^T = \begin{bmatrix} u & v & w \end{bmatrix}^T$$

As per Figure 11, the angular velocities are defined as

$$\vec{\omega}_B = \begin{bmatrix} \omega_{X_B} & \omega_{Y_B} & \omega_{Z_B} \end{bmatrix}^T = \begin{bmatrix} p & q & r \end{bmatrix}^T \tag{24}$$

where p is the roll rate, q is the pitch rate, and r is the yaw rate. Finally, for purposes of the force and moment derivations, the body-to-world Euler angle transformation matrix $\vec{L}_{WB}$ is required

$$\vec{L}_{WB} = \begin{bmatrix} c\theta c\psi & s\phi s\theta c\psi - c\phi s\psi & c\phi c\theta c\psi + s\phi s\psi \\ c\theta s\psi & s\phi s\theta s\psi - c\phi c\psi & c\phi s\theta s\psi - s\phi c\psi \\ -s\theta & s\phi c\theta & c\phi c\theta \end{bmatrix} \tag{25}$$

which is simply the transpose of the world-to-body Euler angle transformation matrix, $\vec{L}_{BW}$, found in Equation 3.
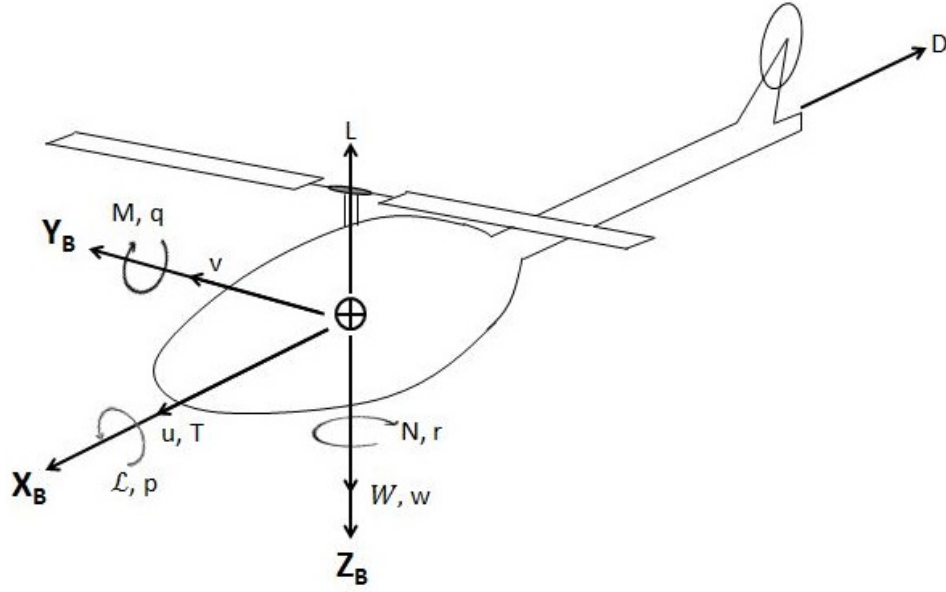
Figure 11: Body-axis coordinate system with origin at the C.G.

3.4.3   Force Equations

Taking the Earth as the *inertial frame*, the external forces acting on an aircraft's center of mass can be described by the principle of the conservation of linear momentum, where m is the vehicle mass and a_W is the acceleration

$$\vec{F_W} = ma_W \tag{26}$$

Replacing the acceleration with its time-derivative and replacing the world-axis elements with body-axis elements and $\vec{L}_{WB}$ yields

$$\vec{F_W} = m\frac{d\vec{V}_W}{dt} \tag{27}$$

$$\vec{L}_{WB}\vec{F}_B = m\frac{d}{dt}\{\vec{L}_{WB}\vec{V}_B\} \tag{28}$$

$$\vec{L}_{WB}\vec{F}_B = m\{\dot{\vec{L}}_{WB}\vec{V}_B + \vec{L}_{WB}\dot{\vec{V}}_B\} \tag{29}$$

The first term in Equation 29 can be replaced according to

$$\dot{\vec{L}}_{WB}\vec{V}_B = \vec{L}_{WB}\{\omega_B \times \vec{V}_B\} \tag{30}$$

thus

$$\vec{L}_{WB}\vec{F}_B = m\{\vec{L}_{WB}(\omega_B \times \vec{V}_B) + \vec{L}_{WB}\dot{\vec{V}}_B\} \tag{31}$$

Multiplying both sides by the world-to-body Euler angle transformation matrix and recognizing that $\vec{L}_{BW}\vec{L}_{WB} = \vec{I}_N$, where $\vec{I}_N$ is the identity matrix, yields

$$\vec{L}_{BW}\{\vec{L}_{WB}\vec{F}_B\} = \vec{L}_{BW}\{m\{\vec{L}_{WB}(\omega_B \times \vec{V}_B) + \vec{L}_{WB}\dot{\vec{V}}_B\}\} \tag{32}$$

$$\vec{F}_B = m\{\dot{\vec{V}}_B + (\vec{\omega}_B \times \vec{V}_B)\} \tag{33}$$

The term $\vec{F}_B$ in Equation 33 represents the external forces acting on the aircraft, comprised of the aerodynamics forces, control forces, and gravity. Commonly, the gravity term is explicitly written. To do so, let $\vec{g}_W$ be the world-axis force of gravity

$$\vec{g}_W = \begin{bmatrix} 0 & 0 & g \end{bmatrix}^T \tag{34}$$

such that the body-axis gravitational force is

$$\vec{g}_B = \vec{L}_{BW}\vec{g}_W \tag{35}$$

thus mg_B can be written as $m\vec{L}_{BW}g_W$ and Equation 33 can be expressed as

$$\vec{F}_B + m\vec{L}_{BW}\vec{g}_W = m\{\dot{\vec{V}}_B + (\vec{\omega}_B \times \vec{V}_B)\} \tag{36}$$

Expanding Equation 36, one obtains

$$\begin{bmatrix} X \\ Y \\ Z \end{bmatrix} - msin(\theta)g = m\begin{bmatrix} \dot{u} \\ \dot{v} \\ \dot{w} \end{bmatrix} + m\overbrace{\begin{bmatrix} 0 & -r & q \\ r & 0 & -p \\ -q & p & 0 \end{bmatrix}}^{crossproduct}\begin{bmatrix} u \\ v \\ w \end{bmatrix} \tag{37}$$

and considering the longitudinal component (i.e. the one pertinent to the experiment task), the force equation reduces to

$$X - mgsin(\theta) = m\{\dot{u} - rv + qw\}$$

The longitudinal force, X, is in fact the summation of all externally applied forces

acting in that direction. For clarity, therefore, X is explicitly written as a summation:

$$\Sigma X - mgsin(\theta) = m\{\dot{u} - rv + qw\} \tag{38}$$

3.4.4 Moment Equations

In a manner similar to the external forces, the external moments acting on an aircraft's center of mass can be describe by the principle of conservation of angular momentum when operating in an inertial frame

$$\vec{G}_W = \frac{d\vec{h}_W}{dt} \tag{39}$$

and converting the world-axis elements to body-axis while taking the time-derivative

$$\vec{L}_{WB}\vec{G}_B = \frac{d}{dt}\{\vec{L}_{WB}\vec{h}_B\} \tag{40}$$

$$\vec{L}_{WB}\vec{G}_B = m\{\dot{\vec{L}}_{WB}\vec{h}_B + \vec{L}_{WB}\dot{\vec{h}}_B\} \tag{41}$$

$$\vec{L}_{WB}\vec{G}_B = m\{\vec{L}_{WB}(\omega_B \times \vec{h}_B) + \vec{L}_{WB}\dot{\vec{h}}_B\} \tag{42}$$

where $\vec{h}_B$ is the angular momentum defined as product of the body-axis inertia vector, $\vec{I}_B$, and the body-axis angular velocities

$$\vec{h}_B = \vec{I}_B\vec{\omega}_B \tag{43}$$

$$\vec{I}_B = \begin{bmatrix} I_{xx} & -I_{xy} & -I_{xz} \\ -I_{yx} & I_{yy} & -I_{yz} \\ -I_{zx} & -I_{zy} & I_{zz} \end{bmatrix} \tag{44}$$

Multiplying both sides of Equation 42 by the world-to-body Euler transformation matrix simplifies the moment equation to

$$\vec{L}_{BW}\{\vec{L}_{WB}\vec{G}_B\} = \vec{L}_{BW}\{m\{\vec{L}_{WB}(\omega_B \times \vec{h}_B) + \vec{L}_{WB}\dot{\vec{h}}_B\}\} \tag{45}$$

and distributing terms, one arrives at

$$\vec{G}_B = \vec{\omega}_B \times (\vec{I}_B\vec{\omega}_B) + \vec{I}_B\dot{\vec{\omega}}_B \tag{46}$$

while noting that

$$\vec{h}_B = \vec{I}_B \vec{\omega}_B$$

$$\dot{\vec{h}}_B = \dot{\vec{I}}_B \vec{\omega}_B + \vec{I}_B \dot{\vec{\omega}}_B$$

$$\vec{I}_B = const$$

$$\dot{\vec{I}}_B = 0$$

Expanding Equation 46 results in the following

$$
\begin{bmatrix} \mathcal{L} \\ M \\ N \end{bmatrix} = \vec{I}_B \begin{bmatrix} \dot{p} \\ \dot{q} \\ \dot{r} \end{bmatrix} + \overbrace{\begin{bmatrix} 0 & -r & -q \\ r & 0 & -p \\ -q & p & 0 \end{bmatrix} \begin{bmatrix} (pI_{xx} - qI_{xy} - rI_{xz}) \\ (-pI_{yx} + qI_{yy} - rI_{yz}) \\ (-pI_{zx}) - qI_{zy} + rI_{zz}) \end{bmatrix}}^{crossproduct}
\tag{47}
$$

where assuming an $X_B - Z_B$ plane of symmetry reduces some of the coupling moments of inertia to zero:

$$I_{xy} = I_{yx} = I_{xz} = I_{zx} = 0$$

Therefore, the moment acting in the longitudinal direction (i.e. the pitching moment acting about the Y_B axis), is established as

$$M = \dot{q}I_{yy} + rp(I_{xx} - I_{zz}) + I_{xz}(p^2 - r^2)$$

As with the force derivation, the pitching moment M is in fact the summation of all externally applied forces acting in that sense. For clarity, therefore, M is explicitly written as such:

$$\Sigma M = \dot{q}I_{yy} + rp(I_{xx} - I_{zz}) + I_{xz}(p^2 - r^2) \tag{48}$$

3.4.5   Linearized Equations of Motion

Solving Equations 38 and 48 for the general dynamic motion of the aircraft is difficult because the aerodynamic forces and moments acting on the aircraft are not linear functions for all time. To simplify the solution, the Small Disturbance Theorem is

commonly adopted wherein the aircraft begins at a reference state at time $t = t_o$, and the analysis is conducted for small disturbances *about* this state. This process results in a linearized set of force and moments equations. In applying the SDT, a frame of reference coinciding with principle body-axes is assumed (i.e. the frame is aligned with the $X_B - Y_B - Z_B$ triad). The "B" subscript is therefore implicit.

$$p = p_o + \Delta p$$

$$q = q_o + \Delta q$$

$$r = r_o + \Delta r$$

$$X = X_o + \Delta X$$

$$M = M_o + \Delta M$$

$$\theta = \theta_o + \Delta\theta$$

The longitudinal force equation (Equation 38) can be written as the following, dropping the summation sign for convenience:

$$(X_o + \Delta X) - mgsin(\theta_o + \Delta\theta) = m\{\frac{d}{dt}(u_o + \Delta u) - (r_o + \Delta r)(v_o + \Delta v) \\ + (q_o + \Delta q)(w_o + \Delta w)\} \tag{49}$$

and if the reference state is taken as hover, the reference angular and linear velocities are all zero

$$\vec{\omega}_o = \begin{bmatrix} p_o \\ q_o \\ r_o \end{bmatrix} = \begin{bmatrix} 0 \\ 0 \\ 0 \end{bmatrix} \quad \& \quad \vec{V}_o = \begin{bmatrix} u_o \\ v_o \\ w_o \end{bmatrix} = \begin{bmatrix} 0 \\ 0 \\ 0 \end{bmatrix}$$

thus,

$$(X_o + \Delta X) - mgsin(\theta_o + \Delta\theta) = m\{\frac{d}{dt}(\Delta u) - (\Delta r)(\Delta v) + (\Delta q)(\Delta w)\} \tag{50}$$

Note that while the angular rates are zero in hover, the attitudes themselves (θ_o, for the purposes of the longitudinal analysis) are not necessarily so. It is assumed,

however, that the hover pitch angle is small (i.e. small angle theorem $\implies sin(\theta_o) = \theta_o, \ cos(\theta_o) = 1$). Since each disturbance Δ is small to begin with, products of the disturbances are considered negligible. Equation 50 therefore reduces to

$$(X_o + \Delta X) - mgsin(\theta_o + \Delta\theta) = m\{\frac{d}{dt}(\Delta u)\} \tag{51}$$

Considering now only those variables associated with the reference condition of hover and invoking the small angle theorem

$$X_o - mgsin(\theta_o) = 0$$

$$X_o - mg\theta_o = 0 \tag{52}$$

Similarly, in applying trigonometric identities:

$$sin(\theta_o + \Delta\theta) = sin(\theta_o)cos(\Delta\theta) + cos(\theta_o)sin(\Delta\theta)$$

$$sin(\theta_o + \Delta\theta) = \theta_o(1) + (1)\Delta\theta \tag{53}$$

Substituting Equations 52 and 53 into Equation 51 yields the following

$$mg\theta_o + \Delta X - mg(\theta_o + \Delta\theta) = m\dot{\Delta u}$$

$$\Delta X - mg\Delta\theta = m\dot{\Delta u}$$

The externally-applied forces are normalized against the vehicle mass, the reason for which will become apparent when defining the stability and control derivatives.

$$\frac{\Delta X}{m} = \Delta\dot{u} + g\theta$$

and finally reinstating the summation sign, which was originally dropped to ease interpretation of the derivation, yields the linearized longitudinal force equation

$$\frac{\Sigma(\Delta X)}{m} = \Delta\dot{u} + g\theta \tag{54}$$

An identical procedure can be applied for the moment equation. Starting with Equation 48 and replacing the external moments, angular rates, and attitudes with perturbations about the equilibrium state:

$$(M_o + \Delta M) = \frac{d}{dt}(q_o + \Delta q)I_{yy} + (r_o + \Delta r)(p_o + \Delta p)(I_{xx} - I_{zz})$$
$$+ I_{xz}([p_o + \Delta p]^2 + [r_o + \Delta r]^2) \tag{55}$$

where assuming rotational rates equalling zero at the equilibrium state yields

$$(M_o + \Delta M) = \frac{d}{dt}(\Delta q)I_{yy} + (\Delta r)(\Delta p)(I_{xx} - I_{zz}) + I_{xz}([\Delta p]^2 + [\Delta r]^2) \tag{56}$$

and recalling that the products of small disturbances are negligible, one obtains

$$(M_o + \Delta M) = \frac{d}{dt}(\Delta q)I_{yy}$$

$$M_o + \Delta M = \dot{\Delta q}I_{yy} \tag{57}$$

By considering only those quantities in Equation 57 associated with the equilibrium state, it is apparent that the equilibrium pitching moment M_o is zero (that is, no other equilibrium quantities are present), so the linearized moment equation is

$$\Delta M = \dot{\Delta q}I_{yy}$$

and in a manner similar to the linearized force equation, the linearized pitching moment equation is resolved by restoring the summation and normalizing the externally-applied moments against the vehicle's lateral moment of inertia:

$$\frac{\Sigma(\Delta M)}{I_{yy}} = \Delta \dot{q} \tag{58}$$

3.4.6   Stability Derivatives

With the force and moment equations now in a linear form, the actual forces and moments acting on the center of gravity (other than gravity itself, which was already included in obtaining the force and moment equations) must be resolved. In the longitudinal sense, the drag force D dominates the external forces, and arises from three sources: the main rotor, the fuselage, and the tailplane (horizontal stabilizer). Examining first the main rotor effects, consider that as a rotorblade reaches the advancing side of the rotor disc, the blade will experience an increase in relative oncoming airspeed due to the vehicle's forward velocity. The advancing blade will

flap up, and assuming a phase offset of 90 degrees, it will reach its maximum up-flap displacement over the nose of the aircraft. The opposite will occur as the blade retreats: the decrease in relative oncoming airspeed causes the blade to flap down, reaching its maximum down-flap displacement over the tail of the aircraft. This phenomenon is termed "flap-back", and results in the rotor disc tilting backwards in forward flight. Aside from the main rotor flap-back, the fuselage and tailplane contribute to the drag force simply by virtue of being a body in motion in a fluid. Drag and flap-back are functions of the vehicle's forward velocity, u, and this relationship is canonically simplified to a single term, X_u, called the Drag Damping Coefficient.

In the simplified single-axis model, drag and flap-back are the major longitudinal forces arising due to changes in velocity. The summation of forces is therefore:

$$\Sigma(\Delta X) = X_u \Delta u \tag{59}$$

where in practice the drag damping coefficient is negative since both flap-back and fuselage/tailplane drag produce a rearward force on a forward-moving helicopter.

Examining now the external moments applied to the aircraft, one can begin by again considering the effects of forward velocity, u. The contributions largely arise from the offset between the main rotor thrust vector and the C.G., as well as from the forces generated on the tailplane acting about the C.G. However, at higher speeds aeroelastic effects are a concern as they will alter the magnitude and direction of the forces produces by the rotor and tailplane. These effects are subsumed into a single term, M_u, called the Static Speed Stability Derivative.

The pitch rate q also contributes to the external moments, where a changing pitch angle produces a stabilizing moment response due to aerodynamic damping, largely dominated by the rotor hub [63]. This phenomenon is described by the Pitch Damping Derivative, M_q, and is the most potent term in longitudinal handling qualities.

With the above two moment-stability derivatives defined, the summation of moment reduces to:

$$\Sigma(\Delta M) = M_u \Delta u + M_q \Delta q \tag{60}$$

3.4.7   Control Derivatives

The above stability derivatives describe the external forces and moments arising from aerodynamic phenomena. However, the vehicle can also experience forces and moments deliberately induced by the pilot through control activity. In the single-axis model, the only control action contributing to vehicle motion is the longitudinal cyclic, δ_{long}. Applying a cyclic input tilts the main rotor hub, thereby offsetting the MRT vector from the C.G. and causing a pitching moment. This effect is described by the Cyclic Control Derivative, $M_{\delta_{long}}$. Equation 60 is therefore expanded to include this term, such that

$$\Sigma(\Delta M) = M_u \Delta u + M_q \Delta q + M_{\delta_{long}} \delta_{long} \tag{61}$$

3.4.8   State Space Representation

The forces and moment equation can be rewritten as follows, substituting the stability and control derivatives for the amorphous summations:

$$\frac{X_u}{m}\Delta u - g\theta = \Delta \dot{u} \tag{62}$$

$$\frac{M_u}{I_{yy}}\Delta u + \frac{M_q}{I_{yy}}\Delta q + \frac{M_{\delta_{long}}}{I_{yy}}\delta_{long} = \Delta \dot{q} \tag{63}$$

and by evaluating the derivatives at the equilibrium condition $(t = t_o)$, then they become linear functions of the aerodynamic variables at $t = t_o$ (e.g. M_u changes linearly with changes in u about equilibrium), reflecting the premise of the Small Disturbance Theorem. Equations 62 and 63 can now be expressed in a compact state space format

$$\dot{\vec{\chi}} = A\vec{\chi} + B\vec{u}_{control}$$

by selecting the state variables to be the body-axis speed u, the pitch rate q, and the pitch angle θ. The formatted state matrix A, control matrix B, state vector $\vec{\chi}$, and control input $\vec{u}_{control}$ therefore take the following form

$$
\begin{bmatrix} \Delta \dot{u} \\ \Delta \dot{q} \\ \Delta q \end{bmatrix} = \begin{bmatrix} \frac{X_U}{m} & 0 & -g \\ \frac{M_U}{I_{yy}} & \frac{M_Q}{I_{yy}} & 0 \\ 0 & 1 & 0 \end{bmatrix} \begin{bmatrix} \Delta u \\ \Delta q \\ \Delta \theta \end{bmatrix} + \begin{bmatrix} 0 \\ \frac{M_{\delta_{long}}}{I_{yy}} \\ 0 \end{bmatrix} \begin{bmatrix} \delta_{long} \end{bmatrix} \tag{64}
$$

Moving forward, the variables in the state space model will be presented according to modified nomenclature for ease of interpretation. First, recognizing that the stability and control derivatives are divided by mass (or moment of inertia) in Equations 62 and 63, the following shorthand is introduced:

$$
X_{u_m} = \frac{X_U}{m}
$$

$$
M_{u_I} = \frac{X_U}{I_{yy}}
$$

$$
M_{Q_I} = \frac{M_Q}{I_{yy}}
$$

$$
M_{\delta_I} = \frac{M_{\delta_{long}}}{I_{yy}}
$$

Next, through the normalization processes in Equations 62 and 63 the linear acceleration $\dot{u}$ is now equal to the total longitudinal force X divided by mass, and the angular acceleration $\dot{q}$ is now equal to the total moment M divided by the moment of inertia. Using similar shorthand notation as above:

$$
\Delta \dot{u} = \frac{\Sigma(\Delta X)}{m} = \Delta X_m
$$

$$
\Delta \dot{q} = \frac{\Sigma(\Delta M)}{I_{yy}} = \Delta M_I
$$

and the state space model in small disturbance form can now be written as

$$
\begin{bmatrix} \Delta X_m \\ \Delta M_I \\ \Delta q \end{bmatrix} = \begin{bmatrix} X_{u_m} & 0 & -g \\ M_{U_I} & M_{Q_I} & 0 \\ 0 & 1 & 0 \end{bmatrix} \begin{bmatrix} \Delta u \\ \Delta q \\ \Delta \theta \end{bmatrix} + \begin{bmatrix} 0 \\ M_{\delta_I} \\ 0 \end{bmatrix} \begin{bmatrix} \delta_{long} \end{bmatrix}
$$

Since the experimental task is ultimately to regulate the *position error* of the helicopter, E_X, it is added to the state space model as an additional state variable. When running the simulation, the initial condition is set such that E_X begins at 50 feet. Augmentation factors of η_q and ζ were included for the M_{Q_I} and M_{δ_I}, respectively, the reasons for which are expanded upon in Section 3.4.9. Finally, the Δ's are dropped from the model, though it is understood that the equations have been linearized about hover conditions and are therefore only valid within that region.

$$
\begin{bmatrix} X_m \\ u \\ M_I \\ q \end{bmatrix} = \begin{bmatrix} X_{U_m} & 0 & 0 & -g \\ 1 & 0 & 0 & 0 \\ M_{u_I} & 0 & M_{Q_I} * \eta_q & 0 \\ 0 & 0 & 1 & 0 \end{bmatrix} \begin{bmatrix} u \\ E_{X_B} \\ q \\ \theta \end{bmatrix} + \begin{bmatrix} 0 \\ 0 \\ \frac{M_{\delta I}}{\zeta} \\ 0 \end{bmatrix} \delta_{long} \qquad (65)
$$

3.4.9   Augmentation

As previously discussed, the $M_{\delta_{long}}$ term in Equation 65 converts the longitudinal cyclic input to a pitching moment about the helicopter's C.G. In the present experiment, $M_{\delta_{long}}$ is reduced by a factor of $\zeta = 5$ to correct for the discrepancy between full cyclic travel in a full-scale UH-1H (15 inches) and that available on the desktop simulator (3 inches). ζ is therefore simply a gearing ratio. Having collapsed the helicopter model to a single-axis representation, pitch damping augmentation is also required to produce helicopter behaviour which pilots found consistent with real-world flight. Preliminary studies yielded the value $\eta_q = 3$ as sufficient.

3.4.10   Assigned Derivative Values

While analytical methods can be employed to solve the stability and control derivatives (albeit requiring iterative methods to determine the main rotor effects), a common approach is to fly the helicopter through a series of manoeuvres and empirically determine the stability and control derivatives which would produce the recorded response. The values assigned to the derivatives in Equation 65 were determined through this empirical method, and comprise the Bell UH-1H state space model as found in [64]: X_{U_m} is -0.0034, M_{U_I} is 0.0019, M_{Q_I} is -0.19, and $M_{\delta I}$ is -0.1691.

These values are obtained for sea level conditions, while in hover (near 1 knot), at a helicopter weight of 8000 lbs. Recall that the derivatives are obtained assuming a small disturbance theorem, so deviating from the prescribed conditions will results in erroneous simulated responses. The gravity constant g is taken as 32.174 ft/s/s.

3.5   Wind Model

A wind model is required to disturb the position of the helicopter during the experiment—without such perturbations, the participant could maintain a hover with very little control input, necessary only to mitigate the mild oscillations arising due to the natural instability of a helicopter. The wind model assumes the form of a sum of nine incommensurable sine waves adopted from [65], whose amplitude and frequencies are listed in Table 2. Note in Table 2 that the wind amplitudes are being scaled by a factor of 1/450, which is required because the "wind" is actually applied directly to the helicopter longitudinal velocity u, rather than as an externally-acting disturbance. For example, a wind of 1 knot buffeting an aircraft would cause a change in the vehicle's velocity of much less than that. The phase offsets of the sine waves are generated at the beginning of each experiment matrix (defined in Section 3.7) by seeding a random number generator using the system clock. A 30-second sample of the injected wind disturbance is presented in Figure 12. The sum-of-sines method is preferred over a Dryden or Von Karmen gust model because the disturbance sought is low-amplitude, low-frequency, and for use in low-altitude manoeuvres; Dryden and Von Karmen methods are generally used to inject highly destabilizing disturbances more suited to high-altitude flight. Preliminary assessment made by a professional test pilot indicated that the system properly emulates in-flight responses, and that the "wind" disturbance feels realistic.

Table 2: Wind model as a sum of nine sine waves

No.	Amplitude (ft/s)**	Frequency (rad/s)
1	1	0.47
2	1	0.7
3	1	1.16
4	0.5	1.86
5	0.2	3.49
6	0.05	6.48
7	0.025	11.17
8	0.015	15.96
9	0.010	18.62

** Amplitude multiplied by 1/450 when applied as disturbance
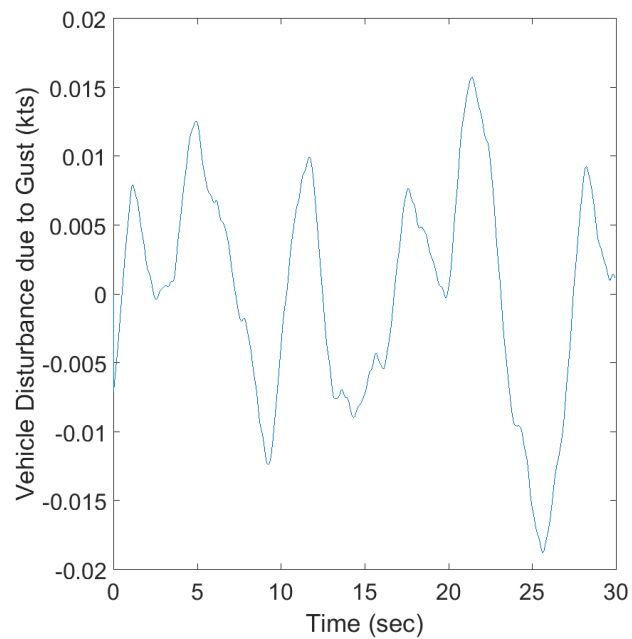
Figure 12: 30-second sample of injected disturbance, applied directly to the vehicle longitudinal velocity. Positive indicates forward, negative indicates rearward.

3.6 Pilot-in-the-Loop Feedback System

The open-loop system consists of an input generated from the a pilot-wielded joystick, the helicopter model, and a wind disturbance model. Closing the loop in the experiment is the symbology presented to the pilot on the HDD. The closed-loop feedback diagram representing the pilot-in-the-loop system is presented in Figure 13. As per this notation, the pilot interprets the discrepancy between the target location (the reticle, i.e. the center of the screen) and the location of the position cue on the symbology, S_{P_X}. This discrepancy is denoted $[e]$. The pilot applies an appropriate corrective action $[\delta_{long}]$ through the joystick, producing a helicopter response $[\dot{\chi}]$ according to the state space model in Equation 65. The response elements consist of the longitudinal force, X_m, the velocity u, the pitching moment M_I, and the pitch rate q. The response is summed with the destabilizing sum-of-sines gust producing $[\dot{\chi}_D]$, which is fed back into the helicopter dynamic model as initial conditions (I.C.) for the following iteration. The time-integral of $\dot{\chi}_D$ is generated to produce a position term (i.e. $E_{X_B} = \int u$, where the integrals of other terms in the state vector are not required). The state vector and its time derivative are both applied to the display laws found in Equations 18, 19, and 20 and subsequently displayed through the L-ViS symbology as the position cue (S_{P_X}), velocity vector (S_{V_X}), and acceleration cue (S_{a_X}).
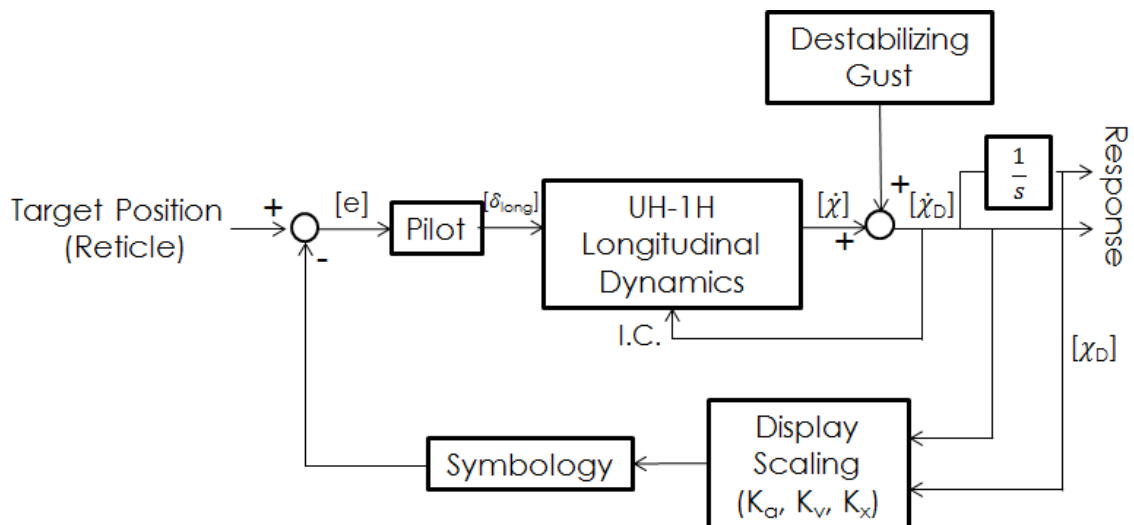
Figure 13: Pilot-in-the-loop feedback diagram

3.7 Experiment Design

The experiment is implemented as a 4x4x4 within-subject factorial design, where the factors assessed are the position scaling (K_x), the velocity scaling (K_v), and the acceleration scaling (K_a). Each factor is tested at 4 levels, producing a test matrix containing 64 trials in total (i.e. containing every possible permutation). The levels of each factor are empirically determined through preliminary studies, and are meant to encompass the range of values outside of which the symbology is deemed unusable. The selected levels are found in Table 3. Note that these levels are presented in terms of *units per screen*, indicating the number of *units* represented at either limit (top or bottom) of the display. For example, a K_x value of ± 100 $\frac{ft}{screen}$ means that a position cue located at the top of the screen indicates a target location 100 feet forward, and a position cue at the bottom of the screen indicates a target location 100 feet rearward. For illustration purposes, Table 15 contains the first few combinations of the test matrix. The full 64-trial matrix is available in Appendix C. For brevity, the "$\pm$" sign is dropped from the scaling levels in the remainder of the document.

Mather and Sharman [66] propose that prolonged exposure to visual stimuli can cause a bias in a subject's response to subsequent stimuli—essentially, that the subjects will continually adapt to the task, and that such adaptation will be reflected in their performance. To mitigate such effects, the trials comprising each experiment matrix are presented in a randomized order. With 64 combinations per matrix, the randomization process is deemed adequate to ensure that performance improvements due to residual learning (adaptation) would be easily distinguishable from improvements due to favourable display scaling combinations. For example, if the results show unilateral improvement as the experiment proceeds (when considering individual participants in isolation), it can be stated that adaptation effects are the cause since it is highly unlikely that such systematic behaviour would result from such a randomized field.

Table 3: Scaling levels

Display Scaling	Level 1	Level 2	Level 3	Level 4
$K_x \ [\frac{ft}{screen}]$	±100	±125	±175	±200
$K_v \ [\frac{kt}{screen}]$	±20	±22.5	±27.5	±30
$K_a \ [\frac{\frac{ft}{s^2}}{screen}]$	±10	±15	±25	±30

Table 4: Illustrative test matrix combinations (5 of 64)

Trial No.	K_x Level	K_v Level	K_a Level
1	1	1	1
2	1	1	2
3	1	1	3
4	1	1	4
5	1	2	1
⋮	⋮	⋮	⋮

Each individual trial within the experiment matrix consists of the participant completing a longitudinal precision hover, described in Section 3.1. During the trial, the facilitator records if the participant loses control of the helicopter (e.g. if pilot-induced oscillation occurred, if the participant lost focus and subsequently abandoned the task, etc.). For each trial, a new display scaling combination is randomly selected from among those remaining in the matrix of 64. The participant has no knowledge of the upcoming combination. After each individual trial, a pause initiated at which point the participant is prompted to rate their perceived workload by entering a value on the keyboard (0-9). The workload rating scheme follows that of the Bedford rating scale [67], which is discussed in Section 3.11.5 and is available for reference in Appendix D.

3.8   Experiment Set-Up

The experimental set-up consists of a desktop computer and monitor, a standard USB keyboard, and a CombatStick gaming joystick (shown in Figure 14). The joystick is characterized in Appendix D. The experiment room is comfortably lit, and contains windows whose blinds can be opened at the participant's discretion. The participant is allowed to adjust the brightness, contrast, position and orientation of the monitor to suit their preferences. The participant can position the joystick in accordance with their dominant hand, and equivalently reposition the keyboard to maintain access between trials. The experiment facilitator remains in the room at all times to answer any questions (within the scope of allowable information), to troubleshoot software issues, and to record any anomalous events.

The experiment is conducted at the National Research Council's Flight Research Laboratory, Bldg U-61, 1920 Research Road, Ottawa, Canada. The experiment takes approximately 4 hours to complete. The experiment schedule is found in Appendix D. A screening questionnaire and consent form are presented to the participant, both also available for reference in Appendix D. No penalty is levied should the participant decide not to sign the consent form and instead opt out of the experiment. If the participant elects to continue with the experiment, they are then briefed on their task, and introduced to the experiment set-up and symbology display.

Figure 14: Experiment Set-up

3.9   Number of Participants

The number of required participants is predicted through an F-test power analysis following the methods presented by Cohen [68]. For this analysis, we define the *null hypothesis* as "the hypothesis that the phenomenon to be demonstrated is in fact absent" [68]. When conducting statistical analyses, one hopes to reject the null hypothesis, thereby disproving the non-existence of a phenomenon. However, rejecting the null hypothesis only indicates that a phenomenon exists, but is no guarantee of a statistically significant result—that is, the phenomenon may not *warrant* the conclusion that it exists, as it may have been a product of random chance. Statisticians accordingly define the term *power* to indicate the likelihood that a study will detect an effect when there is *actually* an effect to be detected. The *power* of a statistical test is dependent on three parameters: the significance criterion α_{SIG}, the reliability of the sample results, and the effect size ES [68].

The significance criterion α_{SIG} represents the risk of mistakenly rejecting the null hypothesis. When assigning this value during a statistical test, it therefore represents the user's willingness to incorrectly identify a statistical difference when none are present. While one may assume that assigning a very small value to α_{SIG} is best, consider that the more stringent the standard of proof (i.e. low α_{SIG}), the lower the likelihood that a effect will be detected (i.e. lower power). Typical α_{SIG} values fall within the range of 0.01 to 0.1 [68]. The reliability of sample results refers to the *precision* of the results, which can be expressed as, for example, the standard deviation σ. Measures of reliability are greatly dependent on the number of samples, N_S, in that the larger the sample size, the smaller the error and thus the greater the reliability. It is for this reason that, in practice, the number of samples N_S is often used as an indirect measure of reliability. Finally, the effect size ES is used to interpret the difference between the means of two groups. Consider for example two narrow distributions with very little overlap, whose means differ by some amount "x". If two wider distributions with a great deal of overlap were to exhibit the same difference in means, "x", the latter difference would seem much less significant. The effect size is therefore a standardized difference of means, described by the following:

$$ES = \frac{\bar{x}_1 - \bar{x}_2}{\sigma_{population}} \tag{66}$$

where $\bar{x}$ is the group mean and $\sigma_{population}$ is the standard deviation of the population's worth of data. An effect size of, for example, $ES=0.1$ thus implies that the two groups' means do not differ by more than 0.1 standard deviations—this would suggest a wide distribution of the sample data. As a rule of thumb, a small effect size is $ES = 0.1$, a moderate effect size is 0.2, and a large effect size is 0.4 [68] .

Thus far, the description of statistical elements has been geared towards determining *power* from α_{SIG}, N_S, and ES; however, investigators can equally determine the number of samples N_S required to ensure a desired *power*, given α_{SIG} and ES. This approach provides a rational basis for determining the sample size required for future experiments, and is thus applied to the present research. In efforts to avoid confusion, it is prudent to first explicitly introduce the terminology used in determining N_S. Consulting Table 5, the first row denotes the *independent variables*—in this research, the scaling factors K_x, K_v, and K_a. Each of the three independent variables are tested at 4 *levels*, and a unique $K_x - K_v - K_a$ level combination defines a *trial* (see the leftmost column of Table 5). As per Section 3.7, in a single test *matrix* there are 64 trials, which therefore produces 64 *responses* (measured data or metric). Response entries can be grouped according to independent variable levels (e.g. all responses observed when $K_x =$ Level 1) or combinations of independent variables levels (e.g. all responses observed when $K_x =$ Level 1 and $K_a =$ Level 1 simultaneously). Such groupings are called *cells*.

Table 5: Illustrative definition of the terminology employed when computing the required number of participants

	Indep. Var (K_x)	Indep. Var (K_v)	Indep. Var (K_a)	Response (Y_i)
Trial 1	Level 1	Level 1	Level 1	Y_1
Trial 2	Level 1	Level 1	Level 2	Y_2
Trial 3	Level 1	Level 1	Level 3	Y_3
Trial 4	Level 1	Level 1	Level 4	Y_4
Trial 5	Level 1	Level 2	Level 1	Y_5
⋮	⋮	⋮	⋮	⋮

As the penultimate terminology definition, let the term *samples* refer to the number of repetitions of a *unique* trial. For example, completing a single test matrix

produces 1 sample, 2 matrices produce 2 samples, etc. Finally, the concepts of main-variable effect, two-way interaction, and three-way are introduced. In brief, a main-variable effect is obtained when looking at the effect of changing the level of a single variable: for example, how does the response differ from K_x level 1 to K_x level 2? A two-way interaction considers whether the effect of changing the level of a single variable is *dependent* on the level of the second variable. This concept is examined in further detail in Section 4.1.5. A three-way interaction is a simple expansion of a two-way interaction wherein the effect of a change in level of the first variable is dependent on the level of two other variables.

To determine the number of samples, the investigator must compute the numerator degree of freedom u_N, which is the product of the number of levels of each independent variable of interest, less one. For example, consider the experiment elucidated in this document which consists of 3 independent variables each with 4 levels. When testing for main-variable effects, u_N will be 3 (4 levels to a single variable, less 1). When testing the same set of data for two-way interactions, u_N will be 9 (two variables each with 4 levels $\implies (4-1)(4-1) = 9$). Knowing u_N, the investigator assigns values to *power*, α_{SIG}, and ES, and determines the intermediate sample size n' via the look-up tables provided in Appendix E. These tables are taken from Cohen pp.381-389 [68]. The n' is subsequently applied to Equation 67 to determine the number of required samples, recalling that there are $N_c = 64$ unique trials in a matrix. The result is the number of samples, N_S.

$$N_S = \left\{ \frac{(n'-1)(u_N+1)}{N_c} + 1 \right\} N_c \tag{67}$$

In computing the number of samples, the statistical parameters are assigned as: $\alpha_{SIG} = 0.1$, $ES = 0.2$, and desired *power* $= 0.8$ (where 0.8 is a conventionally-used value [68]). The total number of samples necessary to ensure that main-variable effects of statistical significance (if present) are detected is 104. When determining the number of required samples to properly detect two-way interactions, the effect size ES of the velocity cue scaling K_v relaxed to 0.1 —in preliminary studies, velocity is identified as the least likely to display interaction effects, so the relaxation is deemed acceptable. The total number of samples required to ensure that two-way interactions of statistical significance (if present) are detected is 112. It was deemed unlikely that three-way interactions would be present in a simplified longitudinal task. The target

number of samples N_S is therefore established as 112, with 100 being considered adequate. In other words, 100 repetitions of *each unique trial* are required, i.e. 100 completions of the entire 64-trial matrix. Within the allotted schedule (Appendix D), each participant is able to complete the 64-trial matrix 4 times; thus, 25 participants are required to meet the number of samples N_S.

Of the 25 participants sought, only 23 eventually completed the experiment. Analyses were conducted regardless, and as is made evident by the results, all trends displaying statistical significance did so in a compelling manner, and all trends not displaying significance are equally unequivocal. The participants were assembled from among the National Research Council's Flight Research Laboratory personnel and from Carleton University's Master of Applied Science candidates. Piloting experience among the participants included professional helicopter pilots (2/23), those with private pilot licenses (3/23), and those with no flight experience at all (18/23). Both male (22/23) and female (1/23) participants completed the experiment.

3.10 Participant Instruction and Training

To complete the precision hover task, the participant is instructed to translate the position cue to the center of the screen and regulate its position. In keeping with the predictor PVA format described in Section 1.5, participants are informed that the most effective way to do so is by keeping the acceleration cue centred on the position cue as it tracked towards the center of the screen. No instructions are given as to how aggressively the participant should approach the target position, with the intent that the participant adjust their strategy according the display scaling rather than trying to maintain the same strategy throughout.

Training is provided to the participant to familiarize themselves with the symbology, task, and controls. During the training phase, the participant repeatedly attempts a single trial wherein the display scaling is kept constant at $K_a = 20 \; \frac{ft/s^2}{screen}$, $K_v = 25 \; \frac{kt}{screen}$, and $K_x = 150 \; \frac{ft}{screen}$. These values are taken as the middle of each respective set of scaling levels from Table 3. The root-mean-square (RMS) of the position error is computed in real-time during the hover phase and is displayed at the end of each trial to the experiment facilitator for review. The training phase terminates when the RMS position error remains below 5 feet for 5 consecutive attempts, though discretionary power is afforded to the facilitator in that they can extend or end the

training for reasons outside the termination criterion. For example, the facilitator may modify the participant training time if: a sequence of more than 5 attempts converges to within 5 feet RMS, but is interrupted by a single attempt producing an RMS above 5 feet (e.g. Figure 39 in Appendix B); the participant performance plateaus at an RMS marginally greater than 5 (i.e. 6-7); or, the participant requests more training time as they do not feel sufficiently competent despite having met the RMS criterion. This element of subjective assessment introduced by the facilitator is not foreign to human-participant experiments, having been equally implemented by NASA in vertical motion simulator trials [69]. The training data for each of the 23 participants is available in Appendix B for review.

3.11   Data Analyses

In this section, a fourth independent variable, *Lead*, is introduced as an independent variable alongside display scaling factors K_x, K_v, and K_a. In proving the existence of a predictable relationship between display scaling and pilot response, the response itself is divided into two categories: performance and workload. The performance is captured according to the normalized root-mean-square (RMS) during the hover phase. The workload is further subdivided into two measured: the DIMS (Dynamic Interface Modeling Simulation), which is a numerical estimate of workload according to pilot control activity, and the Bedford workload ratings, which is a subjective measure of participant control effort. Each of these three response measures as well as their respective normalization techniques are described in greater detail in the following sections. The ANOVA process adopted to establish statistical significance of any obtained trends is then described. Finally, the characterization of participant control strategy through the time-to-approach (TTA) the hover phase and the maximum attitude excursions is discussed.

3.11.1   Lead

As described in Section 3.7, the effects of 3 independent variables are tested in this experiment: K_a, K_v, and K_x. For purposes of the analysis a fourth independent variable, *Lead*, is also considered. *Lead* is generated as the quotient of K_v and K_a (Equation 68), and describes by how many seconds the acceleration cue predicts the position of the tip of the velocity vector. For example, consider again Figure 10 and

imagine that only the velocity vector is allowed to move: it will take *Lead* number of seconds for it to reach to the position of the acceleration cue. *Lead* has implications from a human-user perspective, in that too little lead will result in insufficient time for the pilot to recognize and react to a change in acceleration prior to the velocity vector catching up, likely leading to performance degradation. This is a direct result of the finite reaction time of a human user, as discussed in Section 1.4.4.

$$Lead = \frac{K_v}{K_a} \tag{68}$$

Note that *Lead* is not analyzed in the same manner as a two-way K_a-K_v interaction. *Lead* consists of all possible K_v-K_a quotient permutations (16, since K_v and K_a have 4 levels each) and is analysed as a main variable effect; in other words, how does the number of seconds of velocity prediction afforded by the acceleration cue affect pilot response? The two-way K_a-K_v interaction instead considers if changing the value of K_a affects how pilots respond to changes in K_v, and if so, how changing K_a affects the K_v *trend*. The *Lead* analysis will produce a single trend of 16 points; the two-way interaction analysis will produce 4 trends of 4 points each. This distinction is made explicit in Section 4 when considering the two-way interactions in Figure 31.

3.11.2 RMS Position Error

The participant performance is measured according to the root-mean-square (RMS) of the position error, computed during the hover phase of a trial; the approach phase is not included. The RMS is computed according to Equation 69, where the position error measurements E_X are the *raw* data, and in a single trial approximately 1200 E_X data points are generated (i.e. a 20-second hover with a simulation operating at 60 Hz $\implies$ $n \approx 1200$). A single RMS value is generated per trial—going back to the terminology presented in Table 5, the RMS data are the responses Y_i. For each participant, the RMS values of all four matrices are normalized against the median RMS of the *first* matrix (i.e. the median RMS across the 64 responses belonging to the first matrix) so that results can be compared across participants with varying levels of piloting experience. It was found that participant position error largely degraded throughout the experiment due to fatigue, and the median of the first matrix therefore offered a "best performance" normalization benchmark—thus, in subsequent sections, strong performance is characterized as a normalized position error RMS at or below

unity. Note that in all forthcoming sections, the normalized RMS position error is colloquially referred to as either the "position error" or the "RMS" for brevity.

$$RMS = \sqrt{\frac{(E_X)_1^2 + (E_X)_2^2 + (E_X)_3^2 + ... + (E_X)_n^2}{n}} \qquad (69)$$

$(E_X)_i$ is the ith measurement of the vehicle longitudinal position error (ft)

n is the number of measurements in a given 20-second hover phase (≈ 1200)

3.11.3   DIMS

When considering workload, the Dynamic Interface Modeling and Simulation (DIMS) metric [70] is used to generate a *numerical* estimate of pilot workload based on control activity. The DIMS value, though carrying units of *inches*, does not represent a physical phenomenon: it can therefore only be used as an indicator of control effort relative to other points on the plot (e.g. trial 1 required double the control effort as trial 2). Equation 70, a control reversal is defined as a "local maximum or minimum in the control inceptor deflection time history" [70]—in other words, a change in joystick travel *direction*, not a crossing of the joystick's neutral position. Reversals at frequencies above 3.3 Hz are filtered, following the widely accepted practice that the majority of pilot control movements reside in the frequency band between 0.2-2 Hz.

$$DIMS = N_R \sigma_\delta \qquad (70)$$

N_R is the number of control reversals in a 3-second moving window

σ_δ is the standard deviation of control deflections in a 3-second moving window (*inches*)

3.11.4   ANOVA

Both the RMS position error and DIMS data underwent an ANOVA (Anlysis of Variance) procedure, which is a commonly-adopted process to test for statistical significance (i.e. were the observed trends genuine or due to random chance?). ANOVA was selected over the t-test because the former is capable of handling independent variables of more than 2 levels, whereas the latter cannot. The ANOVA process requires that the data adhere to the following 6 assumptions [68]:

1. the dependent variable (position error or DIMS, in this case) is continuous (i.e. measured on a continuous scale, rather than "yes or no")

2. the independent variable consists of 2 or more levels

3. the data must have independence of observations; that is, no relation between one response entry (cell) and the next

4. the data must have no significant outliers

5. the data must be approximately normally distributed for each level of the independent variable

6. there must be an equal number of samples for each level (i.e. each trial number be repeated the same number of times)

The steps to conduct an ANOVA are as follow:

1. for a single independent variable, group the responses Y_i according to the levels (i.e. generate the cells corresponding to K_x=level 1, K_x=level 2...). In a single matrix, each level of each variable occurs 16 times (64 trials divided equally over 4 levels). In total, over all 92 matrices completed (23 participants times 4 matrices per), each cell contains 1472 response entries.

2. compute the sum of the cell's responses $\Sigma(Y_i)_{G1}, \Sigma(Y_i)_{G2}, ...$

3. compute the sum-of-squares of the cell's responses $(\Sigma Y_i^2)_{G1}, (\Sigma Y_i^2)_{G2}, ...$

4. compute the square-of-sums of the cell's responses $(\Sigma Y_i)_{G1}^2, (\Sigma Y_i)_{G2}^2, ...$

5. compute n_l, which is the number of samples N_S (i.e. the number of repetitions of a *unique* trial (64) as defined in Section 3.10) divided by the number of levels per independent variable, $r=4$ (Eq. 71)

6. compute the total sum-of-squares, SS_{total} (Eq. 72)

7. compute the sum-of-squares *between* the cell's responses, SS_{bt} (Eq. 73)

8. compute the sum-of-squares *within* the cell's responses, SS_{wi} (Eq. 74)

9. compute the degrees of freedom between/within levels, df_{bt} and df_{wi} (Eq. 75/76)

10. compute the mean squares between/within levels, MS_{bt} and MS_{wi} (Eq. 77/78)

11. compute the statistic variable F (Eq. 79). Statistical significance is established by consulting an F-significance probability table (Appendix E), and interpolating between the p-value (significance level). The rule of thumb is that a

p − value less than 0.05 indicates statistically significant data (and the trends exhibited are therefore not a product of random chance).

12. repeat steps 1-11 for each unique independent variable

$$n_l = \frac{N_S}{r} \tag{71}$$

$$SS_{total} = (\Sigma(Y_i^2)_{G1} + \Sigma(Y_i^2)_{G2} + ...) - \frac{[(\Sigma Y_i)_{G1} + (\Sigma Y_i)_{G2} + ...]^2}{N_S} \tag{72}$$

$$SS_{bt} = [\frac{(\Sigma Y_i)_{G1}^2}{n_l} + \frac{(\Sigma Y_i)_{G2}^2}{n_l} + ...] - \frac{[(\Sigma Y_i)_{G1} + (\Sigma Y_i)_{G2} + ...]^2}{N_S} \tag{73}$$

$$SS_{wi} = SS_{total} - SS_{bt} \tag{74}$$

$$df_{bt} = r - 1 \tag{75}$$

$$df_{wi} = N - r \tag{76}$$

$$MS_{bt} = \frac{SS_{bt}}{df_{bt}} \tag{77}$$

$$MS_{wi} = \frac{SS_{wi}}{df_{wi}} \tag{78}$$

$$F = \frac{MS_{bt}}{MS_{wi}} \tag{79}$$

"Between levels" describes the systematic variance, which explains the difference in responses between one level of independent variable and the next. "Within levels" describes the error variance, and represents the variance between responses within the same level of independent variable. As an example of the above procedure, an ANOVA analysis is conducted on a single matrix of normalized RMS data (Table 7) to test for a statistically significant K_x main variable effect (an equivalent process would be applied to K_v and K_a). The results are presented in Table 6, noting again that the ruling on statistical significance is accomplished by consulting the F-significance probability table provided in Appendix E. In practice, all 5888 normalized RMS responses ([23 participants]x[4 matrix repetitions]x[64 responses per matrix]) are included, but a single matrix of 64 data points suffices for illustration purposes.

Table 6: Sample RMS ANOVA summary table

Response Cell	ΣY_i	$\Sigma(Y_i^2)$	$(\Sigma Y_i)^2$	SS_{bt}	SS_{wi}	df_{bt}	df_{wi}	F
G1 (K_x Level 1)	32.19	111.39	1036.8					
G2 (K_x Level 2)	19.80	40.35	393.2	10.05	68.36	3	60	2.939
G3 (K_x Level 3)	16.23	20.32	263.5					
G4 (K_x Level 4)	17.53	21.31	307.5					

Table 7: Sample RMS data

Trial No. (i)	K_x Level	K_v Level	K_a Level	Response, Y_i	
				Normalized RMS	Bedford
1	1	1	1	7.408	3
2	1	1	2	12.536	4
3	1	1	3	18.433	8
4	1	1	4	9.206	7
5	1	2	1	6.144	8
6	1	2	2	5.679	3
7	1	2	3	7.998	4
8	1	2	4	6.594	4
9	1	3	1	5.805	4
10	1	3	2	6.488	5
11	1	3	3	11.38	5
12	1	3	4	33.65	8
13	1	4	1	3.657	4
14	1	4	2	2.305	3
15	1	4	3	2.415	2

16	1	4	4	2.899	3
17	2	1	1	7.659	3
18	2	1	2	6.475	3
19	2	1	3	2.828	3
20	2	1	4	3.029	2
21	2	2	1	7.405	3
22	2	2	2	5.199	3
23	2	2	3	3.336	3
24	2	2	4	4.975	4
25	2	3	1	5.07	3
27	2	3	3	3.457	7
28	2	3	4	21.387	8
29	2	4	1	3.065	3
30	2	4	2	2.286	7
31	2	4	3	3.935	5
32	2	4	4	4.739	5
33	3	1	1	7.716	4
34	3	1	2	3.265	4
35	3	1	3	2.19	2
36	3	1	4	2.891	3
37	3	2	1	11.369	5
38	3	2	2	4.05	4
39	3	2	3	3.356	2
40	3	2	4	4.158	3

41	3	3	1	5.568	4
42	3	3	2	4.942	3
43	3	3	3	2.657	3
44	3	3	4	4.305	7
45	3	4	1	3.261	6
46	3	4	2	3.854	4
47	3	4	3	4.066	4
48	3	4	4	4.243	3
49	4	1	1	6.518	3
50	4	1	2	3.352	6
51	4	1	3	3.28	5
52	4	1	4	4.035	6
53	4	2	1	7.279	3
54	4	2	2	3.444	4
55	4	2	3	4.552	5
56	4	2	4	8.541	9
57	4	3	1	3.626	4
58	4	3	2	3.507	5
59	4	3	3	3.679	2
60	4	3	4	4.812	4
61	4	4	1	3.618	5
62	4	4	2	5.362	7
63	4	4	3	7.022	6
64	4	4	4	5.031	6

3.11.5 Bedford Ratings

The DIMS estimate of pilot workload is supplemented through the Bedford workload ratings, which are subjective measures of pilot effort based on spare cognitive processing ability (refer to Appendix D for the rating scale). The Bedford ratings are a relative measure; that is, one cannot presume that a rating of "2" indicates a pilot was working twice as hard as for a rating of "1", simply that they perceived having worked harder. Therefore, the Bedford scale can only indicate if one trial (i.e a unique $K_x - K_v - K_a$ level combination as per Table 5) requires more effort than another in a binary sense—this is expanded upon in Chapter 4. Through the subjective workload, an important facet to symbology scaling is captured: even if a scaling scheme should prove the most effective from a performance standpoint, it would be imprudent to deem it suitable for actual flight if the amount of effort required to pilot the aircraft should be unrealisable.

The collected Bedford workload ratings underwent a non-parameterized analysis equivalent to the factorial ANOVA, called Align-Rank-Tranform (ART), as described by Wobbrock et. al [71]. This non-paramterization is necessary because each participant does not necessarily assign the same numerical value for the same level of mental workload (e.g. participant A's Bedford rating of 4 could be participant B's rating of 6). ART in particular can be used to examine interaction effects, which is not the case with other non-parameterization processes (e.g. Kruskal-Wallis and Friedman tests [71]). In the ART process, each main variable or interaction effect is aligned in such a manner so as to strip all effects other than the one of interest.

Consider the ART example below, in which the Bedford data presented in Table 7 is non-parameterized and tested for a main variable (K_x, in this case) effect and a two-way K_x-K_v interaction effect. Recalling once more that a "cell" is a group of responses associated with the same independent variable level (e.g. all responses observed when K_x = Level 1) or the same combination of independent variables' levels (e.g. all responses observed when K_x = Level 1 and K_a = Level 1 simultaneously), the first step in the ART process is to compute the cell means (listed in Tables 8 for the $K_x - K_v$ interactions effect and in Table 9 for the K_x main-variable effect).

Table 8: Cell means of Bedford data for two-way interactions. Original data taken from Table 7.

Cell	Cell Condition	Cell Mean
1	K_x Level 1, K_v Level 1	5.5
2	K_x Level 1, K_v Level 2	4.75
3	K_x Level 1, K_v Level 3	5.5
4	K_x Level 1, K_v Level 4	3
5	K_x Level 2, K_v Level 1	2.75
6	K_x Level 2, K_v Level 2	3.25
7	K_x Level 2, K_v Level 3	5.25
8	K_x Level 2, K_v Level 4	5
9	K_x Level 3, K_v Level 1	3.25
10	K_x Level 3, K_v Level 2	3.5
11	K_x Level 3, K_v Level 3	4.25
12	K_x Level 3, K_v Level 4	4.25
13	K_x Level 4, K_v Level 1	5
14	K_x Level 4, K_v Level 2	5.25
15	K_x Level 4, K_v Level 3	3.75
16	K_x Level 4, K_v Level 4	6

Table 9: Cell means of Bedford data for K_x main variable effect. Original data taken from Table 7.

Cell	Cell Condition	Cell Mean
1	K_x Level 1	4.68
2	K_x Level 2	4.13
3	K_x Level 3	3.81
4	K_x Level 4	5

The **residuals** are then computed according to the following equation, where again Y_i refers to the individual response entries from Table 7

$$\textbf{residual} = Y_i - CellMean \tag{80}$$

Consider K_x, with levels $h = 1...4$ and K_v, also with levels $j = 1...4$. Let $\bar{Y}_{K_x}^h$ be the mean of all responses for which K_x was at level h, let $\bar{Y}_{K_v}^j$ be the mean of all

responses for which K_v was at level j, and let $\bar{Y}$ be the grand mean of all responses. The estimated effects, EE, are then computed for the main and interaction effect:

$$EE_{Main} = \bar{Y}_{K_x}^h - \bar{Y} \tag{81}$$

$$EE_{Interaction} = \bar{Y}_{K_x}^h \bar{Y}_{K_v}^j - \bar{Y}_{K_x}^h - \bar{Y}_{K_v}^j + \bar{Y} \tag{82}$$

The EE_{Main} is computed for each variable level h (when conducting ART for a main-variable effect), and $EE_{Interaction}$ for each level combination h, j (when conducting ART for a two-way interaction effect). The aligned data point $Y_{Aligned}$ is then computed, and replaces the original responses Y_i. This is repeated for each main-variable and interaction effect of interest, producing a new column of aligned data each time.

$$Y_{Aligned} = \mathbf{residual} + EE \tag{83}$$

The aligned responses are ranked by numerical weight, and averaged in the case of ties. This produces the aligned-and-ranked responses, Y_{ART}. Finally, ANOVA is performed on the aligned-and-ranked data, Y_{ART}.

3.11.6   Control Strategy

In addition to performance and workload, the participant control strategy is examined through two pilot aggressiveness metrics. The time-to-approach the target (i.e. the time taken to reach hover phase) is examined as a means of potentially explaining unpredicted trends (e.g. high degrees of control activity may arise from a preferred control strategy, and not truly reflect elevated levels of workload). The maximum attitudes (i.e. the maximum/minimum pitch values) are examined for similar reasons.

3.11.7   Anomalous Trials

During the analyses, when confronted with an anomalous trial (e.g. participant indicated that they had abandoned the task for one reason or another), the position error and workload measures are replaced with the mean values generated from the remaining valid trials of that matrix. Further, data residing at more than 3σ outside the matrix mean are considered outliers, and are equally replaced in the same manner. Replacing the data rather than discarding them was necessary to maintain an equal number of samples per independent variable level for ANOVA purposes.

Chapter 4

Results

In the following sections, "performance" is meant to indicate "normalized position error RMS", i.e. the root-mean-square of the discrepancy between the helicopter position and target location, normalized against the median RMS value of the first matrix for each participant. An improvement in performance is characterized as a decrease in position error. While "performance" is a general term, within the context of this experiment and its documentation it is decidedly unambiguous. DIMS is often referred to simply as control activity, and Bedford ratings as subjective workload or perceived effort. These terms are to be taken as interchangeable.

Ideally, the position error, DIMS, and Bedford data will follow concurring trends because there exists an intuitive assumption that control activity and subjective workload increase in response to decaying performance. If such assumptions hold true, certain display scaling levels will result in large position error, high DIMS, and high Bedford ratings simultaneously, and other scaling levels in low position error, low DIMS, and low Bedford ratings. From these trends, suggested scaling levels can therefore be obtained. The data presented in this Section's figures represent the mean values across all participants and across all levels of those display scalings not being immediately considered (e.g. in Figure 15a, every K_x and K_v level is considered at each unique level of K_a, and the resulting data points describe the mean values of that process across all participants). The error bars represent a consolidated standard error (i.e. where standard error is the square root of the standard deviation σ) which includes both the variation between participants and variation in the other display scalings. Larger K_a, K_v, and K_x values indicate less sensitive scaling, and smaller values indicate more sensitive scaling.

4.1 Performance and Control Activity (DIMS)

Figures 15 and 16 depict the participant response according to performance and control activity. In Figure 15, the main variable effects of K_a, K_v, and K_x are shown, each having been tested at 4 distinct states. In Figure 16, *Lead* is the main variable whose effects are being assessed. *Lead* has 16 distinct states, i.e. every permutation of the quotient $\frac{K_v}{K_a}$. When interpreting these results, strong performance is indicated by normalized RMS position error values near or below unity (refer to Section 3.11.2 for an explanation of the normalization process). Low control activity is characterized by smaller DIMS values, though recall that DIMS is a figurative metric and does not represent a physical phenomenon—as stated in Section 3.11.3, the DIMS values can only be used as an indicator of control effort relative to other points on the plot (e.g. point 1 required double the control effort as point 2). The ANOVA-generated p-values indicating statistical significance of the results can be found in Table 11 in Section 4.1.6.

4.1.1 Acceleration Cue Scaling

According to the means depicted in Figure 15a), the minimum position error and workload both correspond to an acceleration scaling level of $K_a = 15 \; \frac{\frac{ft}{s^2}}{screen}$. However, the error bars make such a definite statement difficult to maintain—more correctly, therefore, the data conclusively demonstrates that the minimum position error and workload both occur somewhere between $K_a = 10$ and $25 \; \frac{\frac{ft}{s^2}}{screen}$. This uncertainty notwithstanding, $K_a = 15 \; \frac{\frac{ft}{s^2}}{screen}$ is still the recommended starting value within the tested range, and thus affords a quantitative criterion against which system designers can tune the symbology.

With respect to the performance, a sharp increase in position error is seen as the acceleration scaling is changed from $15 \; \frac{\frac{ft}{s^2}}{screen}$ to $10 \; \frac{\frac{ft}{s^2}}{screen}$ (increasing sensitivity). Likewise as the acceleration cue scaling increases towards $30 \; \frac{\frac{ft}{s^2}}{screen}$ (decreasing sensitivity), performance degrades, albeit more slowly. The steeper degradation observed at small values of K_a is likely due to the fact that cue becomes overly-responsive, making the cue's position difficult to regulate. In contrast, large values of K_a result in behaviour which is more predictable. However, while very insensitive cues are predictable, small visual cue excursions correspond to large physical accelerations. This means that even if the cue deviates by only small amounts on the display before being
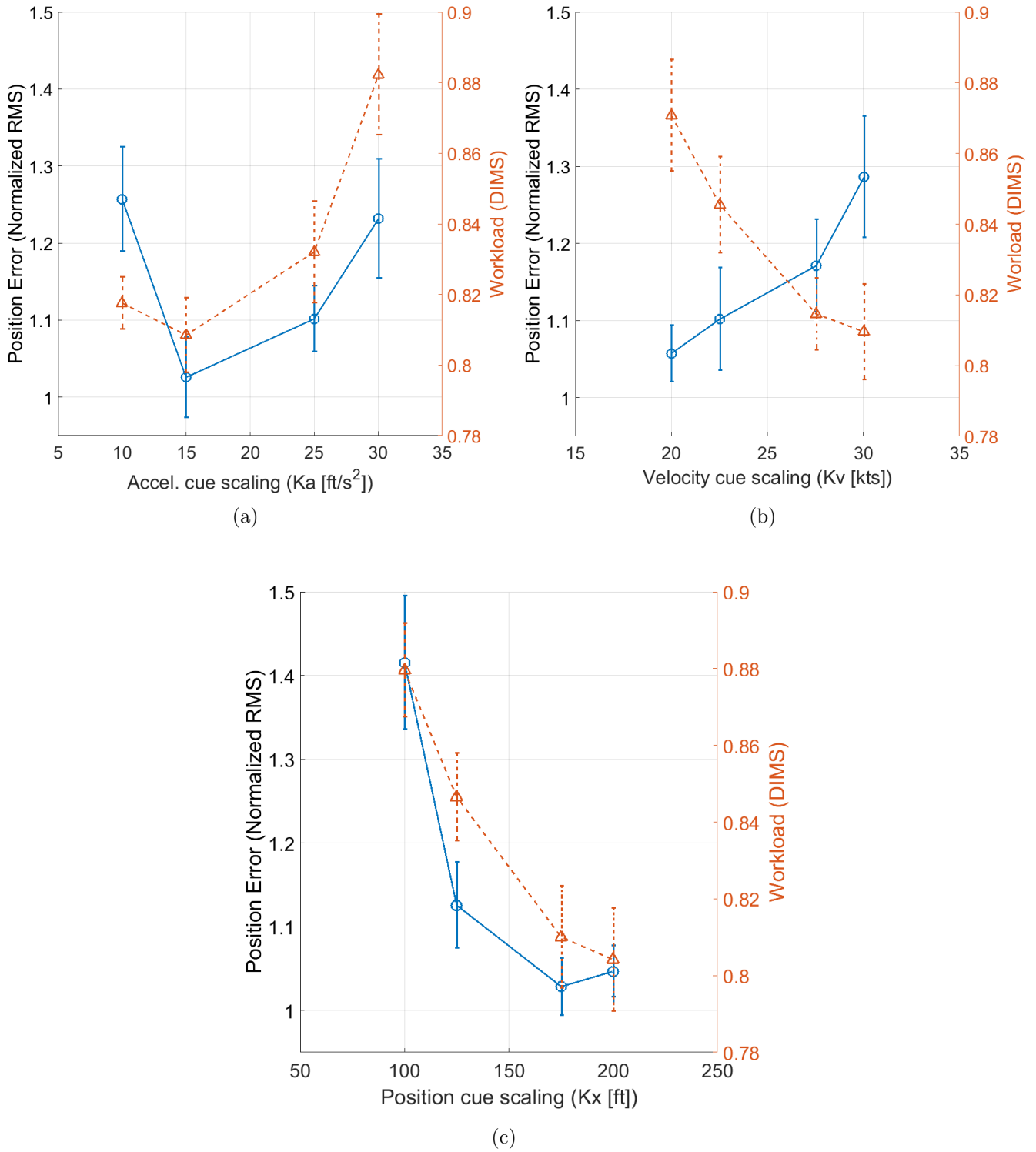
Figure 15: Position error (—o—) and control workload (- -△- -) as a function of position cue scaling, velocity cue scaling, and acceleration cue scaling
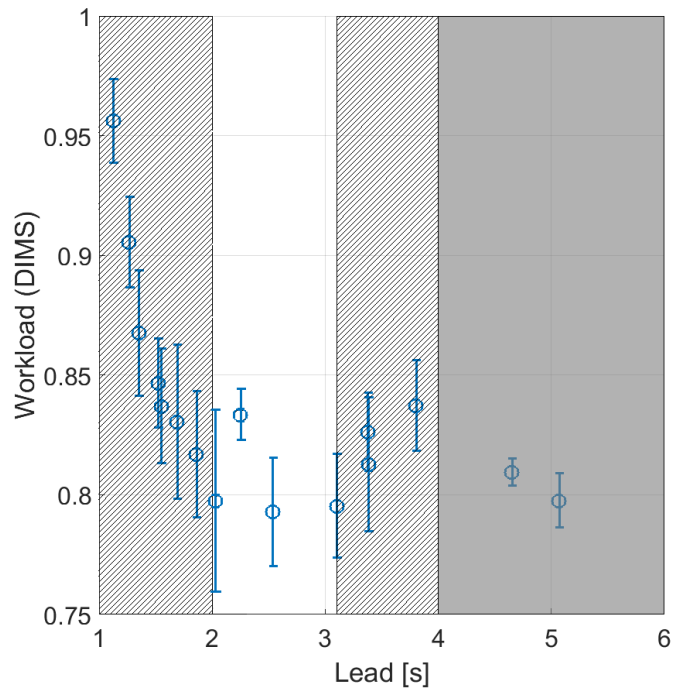
(a)
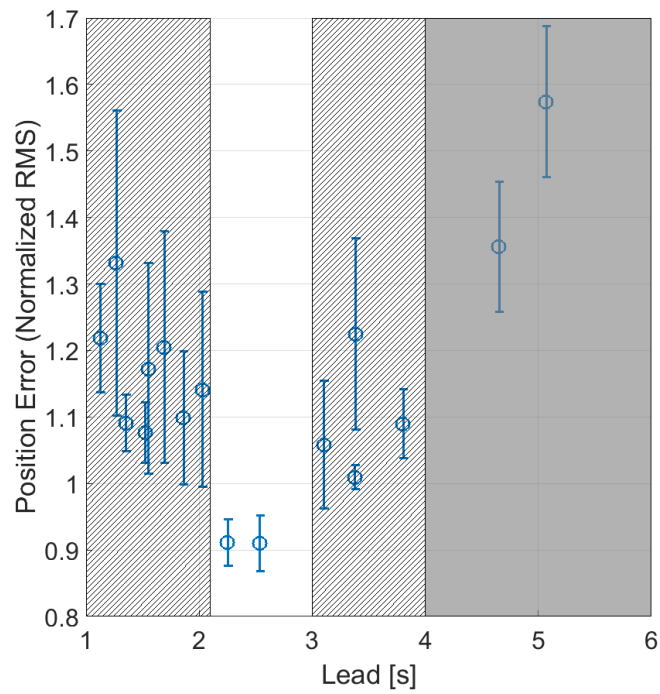
(b)

Figure 16: Performance (position error) and workload (DIMS) vs *Lead*. White region indicates favourable response. Light grey hatching indicates marginal/poor response. Dark grey shading indicates anomalous region of low control workload but high position error.

corrected, that small deviation would translate to a large helicopter acceleration (and thus a larger position excursion).

The control activity, or DIMS, followed similar trends as position error, adhering to the underlying assumption that control activity should increase in response to worsening performance. Interestingly, control workload is greater with insensitive cueing than with sensitive cueing. This may be an issue of control strategy: recognizing that the cue was too volatile to properly track at small K_a values, the participant allows larger cue excursions prior to applying corrective action in order to avoid "chasing" the cue. Thus, a with highly sensitive acceleration cues (low K_a) the participant applies less-frequent, pulsing inputs, resulting in lower control activity. This strategy is studied and modelled by Bachelder et. al [72], in which it was demonstrated that pulsing control was the preferred method when controlling higher order vehicle dynamics (e.g. controlling the acceleration cue) in a continuous tracking task. Conversely, due to the insensitivity of the cue at large K_a values, large-amplitude inputs would be required to regulate the acceleration cue.

4.1.2 Velocity Cue Scaling

The effects of veloctiy cue scaling as found in Figure 15b) produce conflicting performance and control activity trends in that they are mutually inverted—this is counter to the assumption described above which states that control activity should increase with increasing position error. In considering these trends, be aware that analyzing the velocity cue trends in isolation must be done judiciously while recognizing that the participant would not necessarily control the helicopter using the velocity cue directly, but that it represents a source of intermediate information. Namely, it indicates how quickly the helicopter is deviating from its hover position, but it is not the primary source of information regarding when the helicopter *begins* deviating, nor by *how much* it is currently offset from the target location. The author therefore posits that the velocity cue behaviours may be artifacts produced as a result of participants adopting a control strategy not requiring full use of the velocity vector (e.g. "put the ball in the box" strategy from Section 3.10). If this is the case, the DIMS metric may be capturing an effect not related to the velocity scaling, and should therefore be ignored. Alternatively, consider that in a multi-axis task the velocity cue is equally responsible for indicating the *direction* of travel (track angle) as it is the rate of travel. When collapsed to a single-axis task, the information represented by the velocity cue

loses an amount of saliency and the cue may therefore have been internally ignored. Finally, it is possible that the range of velocity cue scaling tested was not adequate to capture the values which would promote low position error and low control activity. Further investigation must be conducted to test these hypotheses.

4.1.3   Position Cue Scaling

The position cue scaling K_x as seen in Figure 15c) yields a decreasing trends for both position error and workload, though as was the case with the acceleration cue scaling the error bars mask any distinct minima. Within the tested range, it can be stated that the minimum position error and workload lie between $K_x = 125$ and $200 \frac{ft}{screen}$. The $K_x = 200 \frac{ft}{screen}$ is taken as a suggested value, however the change from $K_x = 175$ to $200 \frac{ft}{screen}$ is arguably a discountable amount considering the error.

A sharp increase in position error is observed when the cue becomes more sensitive at small K_x. This occurs for a few reasons: first, similar control logic is applied to the position cue as the acceleration cue in that the participant must regulate its position in the hover phase. A more sensitive cue means more rapid cue motion, and is therefore more difficult to keep stationary. Second, recall from Section 3.3.2 that the position cue scaling changes not only the position cue's behaviour, but also the size of the cue displayed on the screen. At small K_x, the total distance represented from the top to the bottom of the display is reduced, and the position cue is therefore drawn larger on the display (as though the display is "zoomed in"). Regulating the position of a larger symbol is more challenging because the nominal symbol center is not accurately discernible. As a means of example, consider the two cases in Figure 17: the degree of accuracy with which the symbol is regulated falls off as the participant necessarily delineates the symbol center as a *region* within the larger position cue. Third, the larger position error for sensitive cues may also be a result of distance misinterpretation: in Figure 17, both position cues denote an offset of 50 feet, but are located at different places on the display due to their respective scaling levels. At first glance, the participant recognizes that the cue in Figure 17a) is further away from the center of the screen, but does not recognize that it tracks across the screen twice as fast as the smaller cue in Figure 17b). This could lead to a more aggressive control strategy, and thus larger position error (i.e. more aggressive input to bring the seemingly-father cue to the origin, resulting in substantial overshoot).

As the position cue sensitivity is varied, the changes in performance are reflected
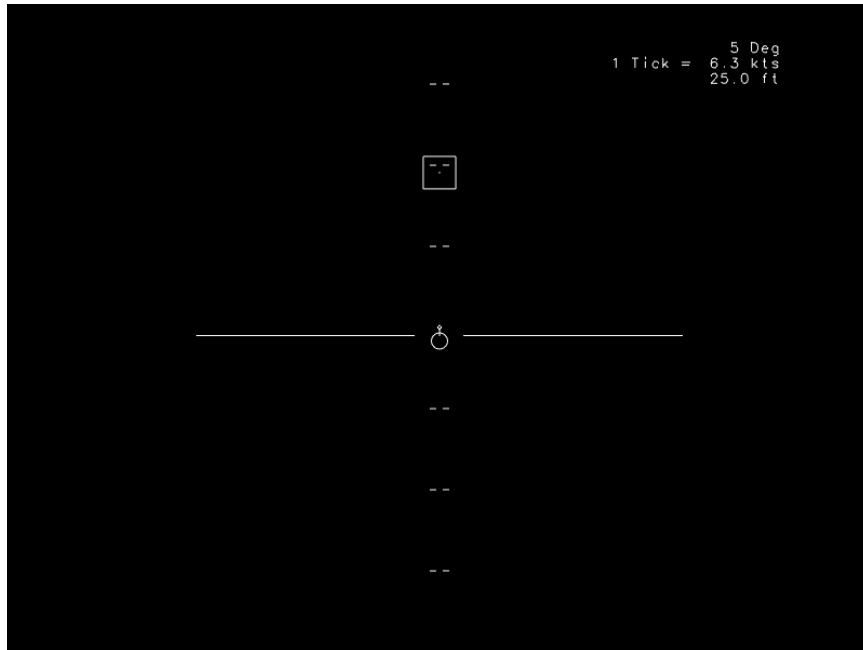
(a)
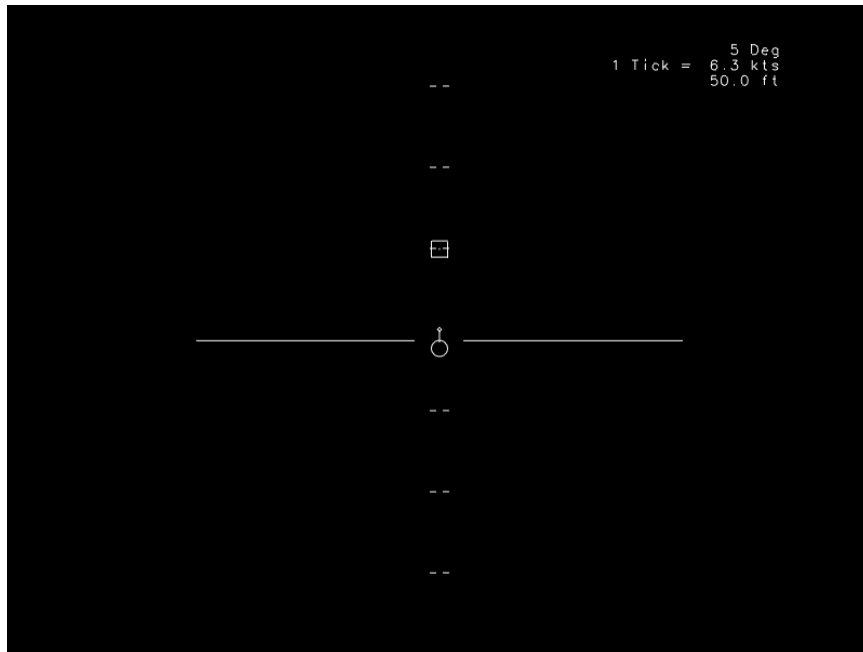
(b)

Figure 17: Changes in position cue size according to position cue scaling. a) $K_x = 100 \frac{ft}{screen}$, b) $K_x = 200 \frac{ft}{screen}$.

in participant control efforts: as position error increases, workload increases, with the opposite also being true. This once more confirms the underlying assumption of control activity increasing in response to worsening performance. As a means of explanation, it can be surmised that highly sensitive position cues elicit high levels of control activity because the participant's task is fundamentally to regulate the vehicle's position. In other words, since a position cue excursion will prompt participant response, *sensitive* position cues will result in higher frequency control activity because they visually deviate from the nominal hover position more so than insensitive cues.

4.1.4 Lead

As stated previously, *Lead* represents the amount of time it takes for the tip of the velocity vector to catch up to the position of the acceleration cue. An alternate way of describing *Lead* is the amount of time it takes for the symbology to indicate that constant velocity has been achieved (recall that the acceleration cue is referenced to the tip of the velocity cue, and when their positions coincide there is no acceleration). *Lead* is therefore a visual representation of the inertial effects of the helicopter, and an appropriate value is accordingly a function of the underlying helicopter dynamics.

Figure 16a) presents an area of high control workload when less than roughly 2 seconds of *Lead* is afforded, with a minimum likely occurring between 2 and 3.25 seconds. This behaviour is largely reflected in Figure 16b): small *Lead* values (less than 2 seconds) result in noticeable position error increases, and a *Lead* value in the range of 2.5 seconds yields a distinctly minimum position error. The poor performance and high control activity at small *Lead* values can be explained as a human-user limitation, since they can only respond to events in a finite amount of time (this was introduced in Section 1.4.4). At higher values of *Lead* (4 seconds and upward), the performance and control workload trends diverge noticeably. Task abandonment is a probable cause, which would explain the very poor performance yet minimal control efforts at correction. This cause is revisited in later sections.

Aside from offering an additional means of assessing the symbology, *Lead* enables system designers to compute appropriate values for either K_a or K_v given only one of the two. In the case of the present work, the suggested *Lead* value is 2.5 seconds—combining it with the suggested K_a from Figure 15a) would therefore yield a K_v value despite the K_v trends not exhibiting any recognizable minima.

4.1.5 Two-Way Interactions

To say an interaction between two variables is present is to imply that the effect of one independent variable (e.g. K_a) on the dependent variable (position error or DIMS) depends on the level of the other independent variable (e.g. K_x). That is, does the level of one independent variable influence how *changes in another independent variable* affect the response. As an illustration of two variables with no interaction effects whatsoever, consider Figure 18: the lines are entirely parallel, indicating that the effect of variable 1 on the response in no way depends on the level of variable 2. An example of the extreme opposite is presented in Figure 19, where the level of variable 2 greatly influence how the responds to variable 1. More moderate levels of interaction are not always evident, and one must therefore defer to the p-value to determine if interactions of statistical significance are present (refer to Table 11). Surprisingly, no two-way interactions of statistical significance were observed between any of the main variable effects for either position error or DIMS. This is apparent through the two-way interaction Figures, found in Appendix A. Such indifference towards the *combinations* of cue scaling may be a result of the single-axis task and equivalently reduced symbology set, though further investigations must be conducted to conclusively determine if this is the case.
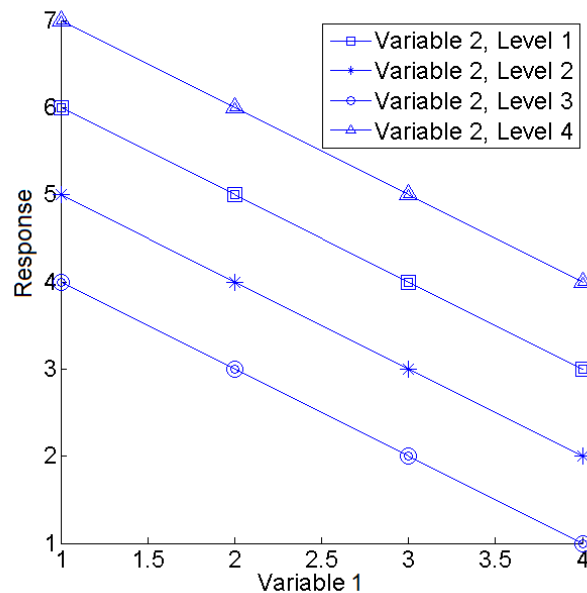
Figure 18: Illustration of lack of 2-way interaction
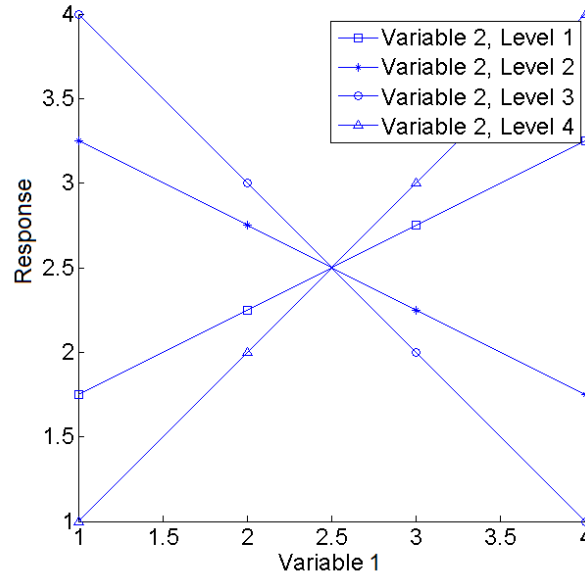
Figure 19: Illustration of significant 2-way interaction

4.1.6 Summary

The suggested scaling levels according to position error and control activity are listed in Table 10, and are selected for having promoted a combination of low position error and low control activity. Be aware that these values are preliminary in that subjective workload ratings (Bedford) have not yet been considered; further analysis is forthcoming in Section 4.2. The suggested K_v value is obtained as the product of *Lead* and K_a value since no minima are present in the K_v plot of Figure 15.

A large p-value ($p \geq 0.05$) means that the null hypothesis cannot be rejected because the data is either extremely scattered (i.e. random) or does not display enough variation in response to indicate a definite effect (i.e. flat line). A small p-value ($p < 0.05$) indicates the opposite. The ANOVA-generated p-values are listed in Table 11, and show that all main-variable effects are statistically significant for the position error. However, only K_x, K_a, and *Lead* comfortably produce statistically significant main-variable effects for DIMS—with a p-value of 0.05 for K_v, significance is rejected. This supports the notion presented in Section 4.1.2 that the K_v-DIMS trend may be capturing an outside effect and should therefore be discarded. Two-way p-values are all equal to or larger than 0.05, indicating no interactions of statistical significance.

Table 10: Suggested scaling levels per performance and control workload

Acceleration Cue Scaling K_a	15 $[\frac{\frac{ft}{s^2}}{screen}]$
Velocity Cue Scaling K_v	22 $[\frac{kts}{screen}]$ **
Position Cue Scaling K_x	200 $[\frac{ft}{screen}]$
Lead	2-2.5 $[sec]$

** Obtained by multiplying *Lead* and K_a and converting to appropriate units

Table 11: ANOVA p-values for performance and control workload results

Main or Interaction Effect	Performance (Normalized RMS Position Error) p-value	Workload (DIMS) p-value
K_a $[\frac{\frac{ft}{s^2}}{screen}]$	0.03	<0.01
K_v $[\frac{kts}{screen}]$	0.01	0.05
K_x $[\frac{ft}{screen}]$	<0.01	<0.01
Lead $[s]$	0.02	<0.01
K_a-K_v	0.21	0.28
K_a-K_x	0.36	0.89
K_v-K_x	0.33	0.80

4.2 Subjective Workload Ratings

The DIMS metric is an incomplete measure of participant workload because it does not consider the participant's cognitive (perceived) workload. The participant's perceived workload is therefore recorded according to the Bedford rating system (refer to Section 3.11.5) to complement the DIMS ratings. With the Bedford metric, it will be possible to determine whether elevated DIMS values are due to deliberate participant strategies (e.g. high-activity control strategy, where DIMS would be high but Bedford not necessarily so) or due to difficulties with the task (where one would expect high DIMS and Bedford ratings). The Bedford workload ratings undergo a

non-parameterized analysis equivalent to the factorial ANOVA, called Align-Rank-Tranform (ART) [71]—refer again to Section 3.11.5 for the procedure description. As with the DIMS ratings, the non-parameterized Bedford ratings are a relative measure, and their values should be used only to compare the perceived effort between scaling levels. Further, since the ratings are *subjective*, the numerical values to which the non-parameterized Bedford results are assigned do not truly reflect a quantitative scale. For example, one cannot infer from the results that doubling the rating implies double the perceived effort. The subjective ratings can only be used to describe workload in a binary sense (i.e. greater or lesser). This is reflected in Figure 20 through 23 where the markers are connected through arrows to ease visual interpretation, but are not connected in the sense of an algebraic trend. The y-axis limits are kept consistent from Figure 20 to Figure 22, which enables the reader to compare the degree of subjective workload variation across main variables (these limits are more restricted than those in Figure 23 so that the error bars can be seen). Statistical significance of the Bedford ratings is determined through p-values found in Table 13; though these are generated through ART, they are analogous to ANOVA-generated p-values. Adjustments to the scaling levels from Table 10 as a result of subjective workload considerations are listed in Table 12 in Section 4.2.6.

4.2.1 Acceleration Cue Scaling

Qualitatively, the Bedford ratings illustrated in Figure 20 reflect the performance (position error) and control workload (DIMS) trends found in Figure 15a): within the data set generated, there is a distinct minimum at $K_a = 15 \ \frac{ft}{s^2}$, with a steep increase in subjective workload at either extreme. Such strong conformity confirms that the suggested value of $K_a = 15 \ \frac{\frac{ft}{s^2}}{screen}$ will enable good performance while minimizing both participant control activity and, most importantly, the mental exertion of the participant. It can therefore be stated that the suggested K_a value is not a misrepresentation born of control strategy (consider, for example, a strategy in which the acceleration cue position was precisely regulated, but doing so required intense mental concentration on the part of the participant). The consistency observed between the performance, DIMS, and Bedford results reinforces the existence of a predictable quantitative relationship between cue scaling and pilot response.
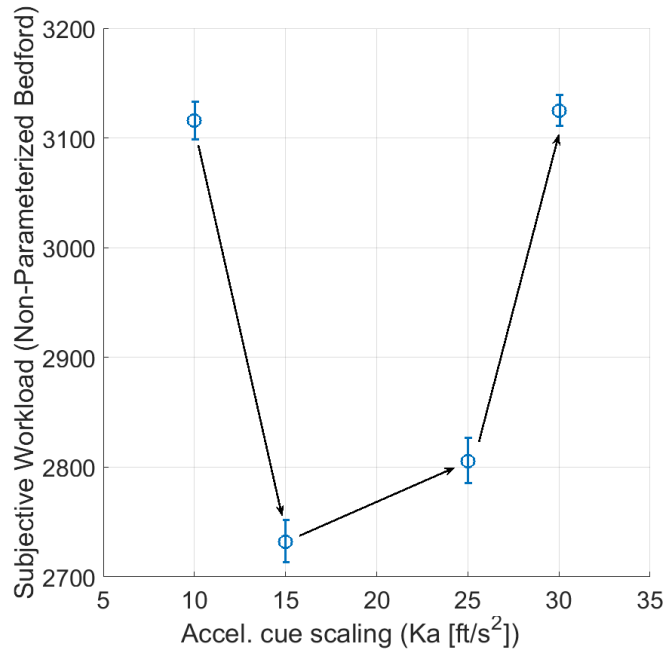
Figure 20: Subjective workload (non-parameterized Bedford ratings) as a function of acceleration cue scaling

4.2.2 Velocity Cue Scaling

The p-values in Table 11 indicate that the control workload ratings (DIMS) do not produce statistically significant results ($p \geq 0.05$) when varied against K_v. In this case, it is because too little variation is observed between levels of K_v to establish a trend, and the null hypothese therefore cannot be rejected. This is shown graphically in Figure 21, where participants are largely indifferent to the velocity cue scaling. In Section 4.1.2 it is noted that the K_v-DIMS results are anomalous, and it is posited that the trend is capturing effects not related to the velocity scaling. This notion is supported through the Bedford analysis since large changes in control activity are unlikely if the participant were not exerting more effort. The large change in control activity responses found in Figure 15b) is therefore likely an artifact.

4.2.3 Position Cue Scaling

As per Figure 22, the non-parameterized Bedford ratings are low at intermediate position cue scaling levels and increase abruptly at the extreme levels. The trend
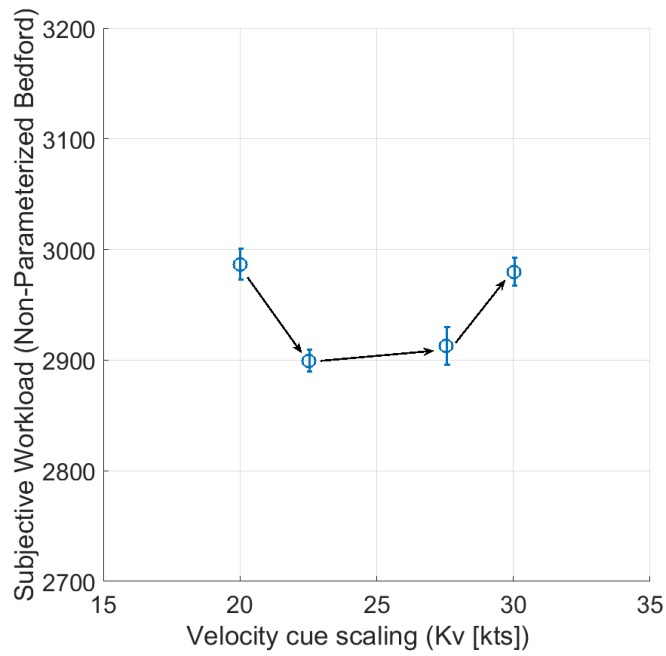
Figure 21: Subjective workload (non-parameterized Bedford ratings) as a function of velocity cue scaling
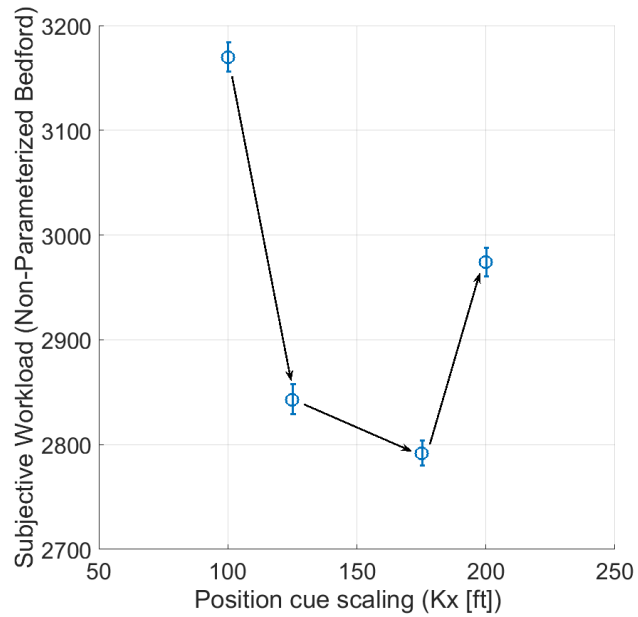
Figure 22: Subjective workload (non-parameterized Bedford ratings) as a function of position cue scaling

exhibited in the lower end of the K_x spectrum (corresponding to $K_x = 100, 125,$ and $175 \frac{ft}{screen}$) largely reflects that of the control workload (DIMS) plot in Figure 15c). Namely, an increase in workload is observed at lower levels of K_x. A significant increase is seen in the Bedford ratings at large levels of K_v, a trend which is not seen on the DIMS plot in Figure 15c) (though due to the error tolerance on the DIMS plot this conclusion cannot be taken as an absolute, since the increase in DIMS at large K_x may in fact be more pronounced than the means would suggest). According to the Bedford trend, a K_x value of $175 \frac{ft}{screen}$ should be selected since a well-defined minimum perceived effort is produced at that scaling level. As mentioned earlier, the effect of position cue scaling on position error and DIMS is arguably discountable between $K_x = 175$ and $200 \frac{ft}{screen}$ due to the large error (refer to Figure 15c)). Thus, modifying the suggested K_x value to $175 \frac{ft}{screen}$ to support the Bedford conclusions is equally agreeable with the conclusions of Section 4.1.3.

4.2.4 Lead

Three items of note are present in the *Lead* plot of Figure 23. First, the Bedford ratings increase sharply below 1.5 seconds. This supports the behaviours seen in Figures 15a) and b), and again reflects the finite response time of human-users. Second, the ratings trend towards a minimum somewhere between 1.75 and 3 seconds of *Lead* (though the large errors make a more precise conclusion difficult). Nonetheless, the perceived workload reached a minimum in the same region of *Lead* as control workload (DIMS) in Figure 16. The agreement between the trends reinforces the assumption that *Lead* is a critical element in participant control capabilities, and is thereby a strong indicator of symbology suitability. The third item of note is the upswing in Bedford ratings at large *Lead* values, a trend which is seen in position error (Figure 16b)) but not DIMS (Figure 16a)). These large *Lead* values correspond to the quotients of large K_v values and small K_a values, i.e. insensitive velocity cue and sensitive acceleration cue. Under this configuration, the issue likely becomes one of incompatibility between helicopter dynamics and display lead. A low-gain helicopter (i.e. one in which control inputs produce small or sluggish respones) should be flown using low-gain primary symbology cues (acceleration cue, in this case) so that the physical response of the helicopter is accurately depicted on the display. Recalling that the primary symbol in this rate-controlled system is the acceleration cue, it appears that a large delay between acceleration and velocity cue motion negatively

impacts the perceived workload. The helicopter model implemented in the experiment is that of the UH-1H, a single-engine military helicopter of medium weight (and therefore higher-gain dynamics), so a delay in the visually-depicted acceleration-velocity coupling could promote poor pilot responses.

When considering the performance and DIMS as a function of *Lead* in Section 4.1.4, it was suggested that behaviours at large *Lead* values could be a result of task abandonment—and indeed, the high Bedford ratings seem to suggest such an occurrence. At high *Lead* values the participants perceive the task as extremely demanding, score poorly in terms of performance, and yet engaged in little control activity, the combination of which suggests that the scaling levels resulted in an uncontrollable system. This hypothesis is explored in later Sections.
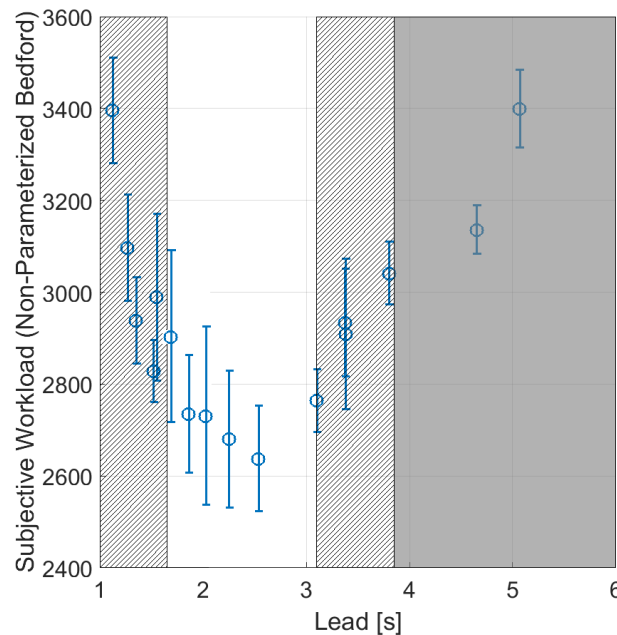
Figure 23: Subjective workload (non-parameterized Bedford ratings) as a function of *Lead*

4.2.5   Two-Way Interactions

Unlike the DIMS and performance metrics, Bedford ratings demonstrated statistically significant two-way interactions. As a refresher, a statistically significant two-way interaction means that the manner in which one independent variable affects the dependent variable *relies* on the level of a second independent variable. For example,
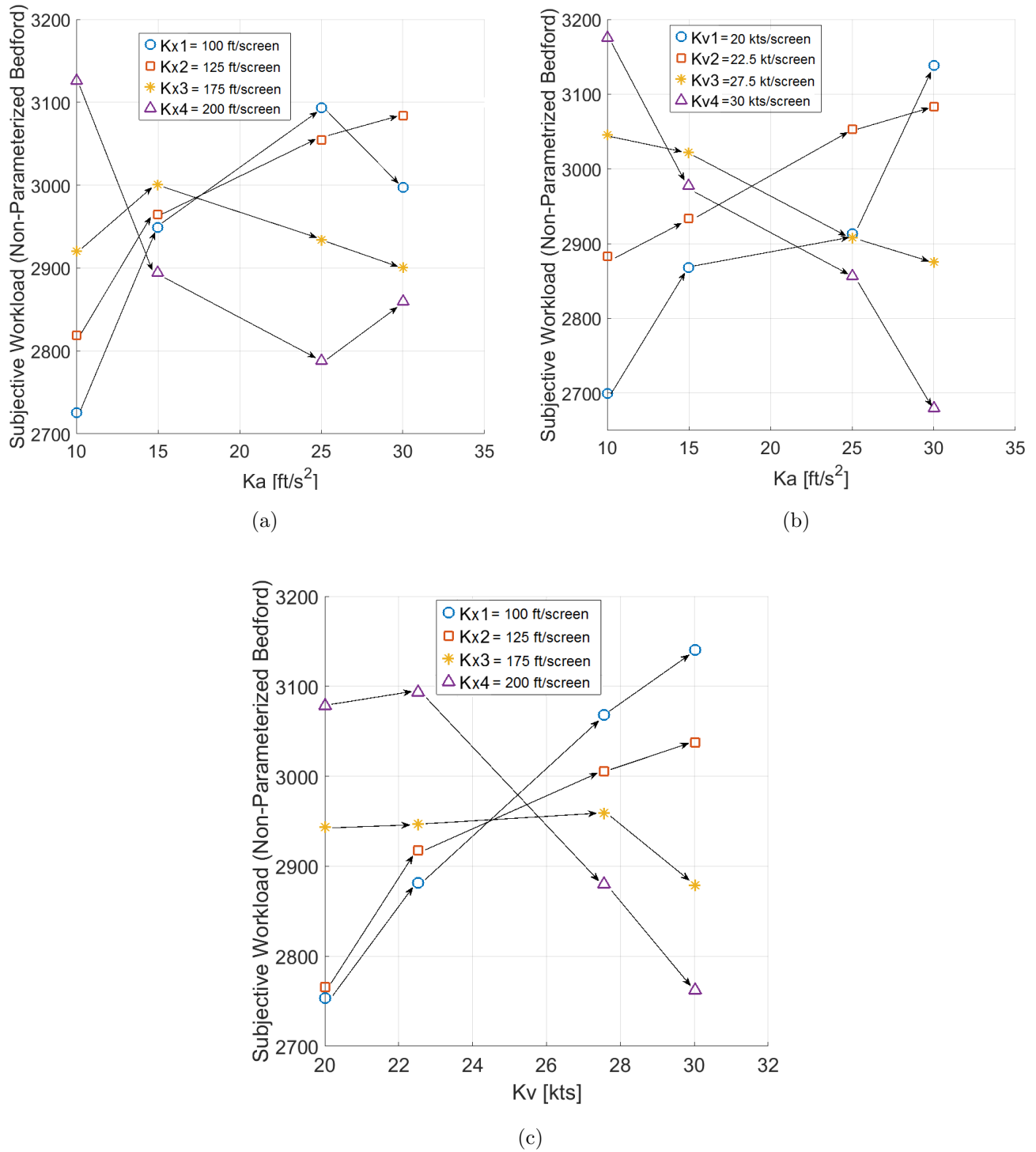
Figure 24: Two-way interaction effects on non-parameterized Bedford workload ratings. a) Acceleration-Position scaling combinations, b) Acceleration-Velocity scaling combiantions, c) Velocity-Position scaling combinations.

note how in Figure 24c) the level of K_x distinctly influences how changes in K_v affect the response: with a low K_x, low K_v produces low Bedford, and high K_v produces high Bedford; with a high K_x, the K_v-Bedford trend is reversed. That combinations of cue scaling affecting the perceived effort of the participants, but not their control activity or performance, is difficult to rationalize, but may suggest the interaction of cue sizing as a dominant factor (as opposed to cue behavioural interactions, i.e. *Lead*). For example, recall that the size of the position cue changes with the cue's scaling. At $K_a = 10 \ \frac{\frac{ft}{s^2}}{screen}$ and $K_x = 200 \ \frac{ft}{screen}$, the acceleration cue and the position cue overlap, making it difficult to distinguish individual symbol motion (see Figure 25). This theory in part explains the trends, where in Figure 24a) one of the largest subjective workload rating is in fact observed at $K_x = 200 \ \frac{ft}{screen}$ and $K_a = 10 \ \frac{\frac{ft}{s^2}}{screen}$.

Figure 25: Visual overlap between acceleration cue and position cue

While other two-way behaviours are not so easily explained, the Bedford ratings still provides insight which would have been overlooked had the analysis been restricted to position error and DIMS. Furthermore, the 2-way Bedford interactions are sufficient to draw the following rules from Figure 24a) through c), which can be used to check the consistency of the suggested scaling levels. Recalling that "sensitive" refers to low scaling level and "insensitive" to high scaling levels:

1. Sensitive acceleration cues pair best with sensitive position cues (producing low Bedford ratings as per Figure 24a))

2. Insensitive acceleration cues pair best with insensitive position cues (producing low Bedford ratings as per Figure 24a))

3. Sensitive acceleration cues pair best with sensitive velocity cues (producing low Bedford ratings as per Figure 24b))

4. Insensitive acceleration cues par best with insensitive velocity cues (producing low Bedford ratings as per Figure 24b))

5. Sensitive velocity cues pair best with sensitive position cues (producing low Bedford ratings as per Figure 24c))

6. Insensitive velocity cues pair best with insensitive position cues (producing low Bedford ratings as per Figure 24c))

The suggested velocity scaling and acceleration scaling levels (Table 12) are at the lower end of their tested values and are therefore consistent with the above guidelines. Interestingly, the K_x value of 175 $\frac{ft}{screen}$, having been selected instead of 200 $\frac{ft}{screen}$ after considering the Bedford trends (refer to Section 4.2.3), does not adhere to the proposed guidelines. According to Figure 24a) and c), a K_v of 22 $\frac{kts}{screen}$ and a K_a of 15 $\frac{\frac{ft}{s^2}}{screen}$ pair best with a K_x of 100 $\frac{ft}{screen}$ and 200 $\frac{ft}{screen}$, respectively. A few things must be recalled: first, the trends associated with the velocity cue (Figures 15b) are suspect given the large p-values and overall anomalous behaviours, and the suggestion to ignore these trends was in fact support by the K_v-Bedford results (Figure 21). Futhermore, any of the above guidelines associated with the velocity scaling must be applied while recognizing that the suggested K_v value was obtained through manipulation of the *Lead* and K_a, not as a direct result of the K_v behaviours. Second, the error bars on the position error and DIMS graphs (Figure 15c) are both very large at the upper limits of K_x, so a value of $K_x = 200$ $\frac{ft}{screen}$ conceivably produces the same effects as one of $K_x = 175$ $\frac{ft}{screen}$. With these points in mind, the fact that the suggested K_x in Table 12 does not conform with item 5 in the above table can be discounted. Furthermore, the Bedford ratings in Figure 22 strongly suggest a K_x value of 175 $\frac{ft}{screen}$, so this value will be retained.

4.2.6 Summary

The suggested scaling levels, having considered the Bedford ratings in addition to the performance and control workload, are found in Table 12. Changes made relative to the preliminary scaling levels in Table 10 are noted. As these levels are the product of all performance, control workload, and perceived workload analyses, they are the final recommendations. The ART-generated p-values are listed in Table 13.

Table 12: Suggested scaling levels per performance & control and Bedford workloads

Acceleration Cue Scaling K_a	15 $\left[\frac{\frac{ft}{s^2}}{screen}\right]$
Velocity Cue Scaling K_v	22 $\left[\frac{kts}{screen}\right]$ **
Position Cue Scaling K_x	175 $\left[\frac{ft}{screen}\right]$ ***
Lead	2-2.5 $[sec]$

** Obtained by multiplying *Lead* and K_a and converting to appropriate units
*** Modified from 200 $\frac{ft}{screen}$ from Table 10

Table 13: ART p-values for non-parameterized Bedford workload results

Main or Interaction Effect	Non-Parameterized Bedford p-value
K_a $\left[\frac{\frac{ft}{s^2}}{screen}\right]$	<0.01
K_v $\left[\frac{kts}{screen}\right]$	0.386
K_x $\left[\frac{ft}{screen}\right]$	<0.01
Lead $[s]$	<0.01
K_a-K_v	<0.01
K_a-K_x	<0.01
K_v-K_x	<0.01

4.3 Pilot Aggression

Participant control strategy greatly affects performance and control activity, but is not properly captured by either measure. This is particularly the case for the DIMS metric where high degrees of control activity may result from a preferred control technique and not truly reflect elevated levels of workload. In the following sections, scaling levels which promote aggressive versus cautious behaviour are established through the time-to-approach (TTA) the target position and through maximum attitude excursions.

4.3.1 Time-to-Approach

At the start of each trial, the participant is located 50 feet rearward of the target location; as per Section 3.1 it is their task to translate the helicopter to the target position (phase 1) and subsequently maintain a hover for 20 seconds (phase 2). The time elapsed during phase 1 is a strong indicator of the participant's aggression, where a lower TTA means a more aggressive strategy. This relationship may be used to confirm the performance and control workload results presented thus far. In assessing the time-to-approach, note that the y-limits in Figure 26 through 29 are kept constant to enable at-a-glance comparison. ANOVA-generated p-values are presented in Table 14. where once again p-values equal to or greater than 0.05 indicate no effects of statistical significance. Two-way interactions are not considered.

Table 14: ANOVA p-values for time-to-approach results

Main Effect	Time-to-Approach
$K_a \left[\frac{\frac{ft}{s^2}}{screen} \right]$	<0.01
$K_v \left[\frac{kts}{screen} \right]$	0.9
$K_x \left[\frac{ft}{screen} \right]$	<0.01
$Lead \ [s]$	0.24

Figure 26 shows TTA decreasing with increasing K_a levels, indicating that low-sensitivity acceleration cues promote more aggressive control strategies. Such behaviour agrees with the performance trends found in Figure 15a), where more aggressive strategies are more likely to precipitate position overshoot, and in turn poorer performance and higher control workload. The greater perceived exertion at large K_a levels in Figure 20 do not contradict the assertion of intentional aggression—in fact, approaching a task in an aggressive manner would necessarily leave the participants with less spare mental capacity.

As seen in Figure 27, and as is supported by the large p-value in Table 14, the TTA is virtually unaffected by variations in K_v. This behaviour yet again reinforces the decision to exclude direct consideration of K_v insofar as control activity and Bedford trends. However, variations in position cue scaling have a large effect on aggression, as found in Figure 28. In this case, a decrease in K_x (resulting in a larger, quicker-moving position cue) yields a lower TTA, thus indicating more aggressive control strategies. These findings agree with the performance and DIMS trends found in Figure 15c) in that the aggressive strategy at low K_x results in overshooting the position cue, and thus performance and control activity are impacted. Bedford workload ratings in Figure 22 likewise support the notion that the overall degradation in participant response at low K_x levels was in fact an attempt at engaging the task in a more aggressive manner (perhaps inappropriately so).

The TTA dispays extreme levels of scatter when plotted against *Lead* in Figure 29—this is reflected through the p-value found in Table 14. Therefore, the hypothesis of task abandonment at large *Lead* values cannot be definitively confirmed through this avenue.

Note that despite these findings indicating that participants may have *selected* control strategies which reduced performance and increased workload, the conclusions drawn insofar as appropriate scaling levels still remain. A symbology configuration which elicits poor pilot response, regardless of it being the result of deliberate action, is still deficient. The TTA analysis therefore reinforces the scaling level selections in Table 12 as one should prefer scaling levels which promote safe, if protracted, strategies.
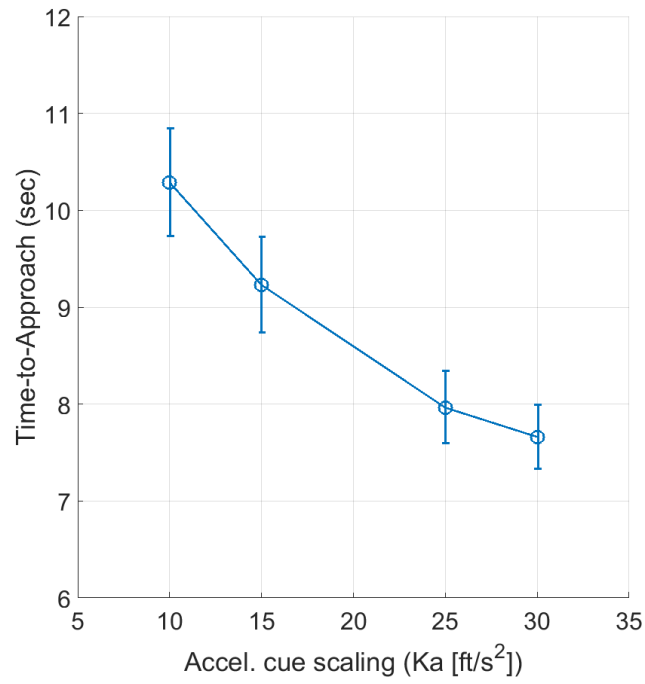
Figure 26: Time-to-approach as a function of acceleration cue scaling
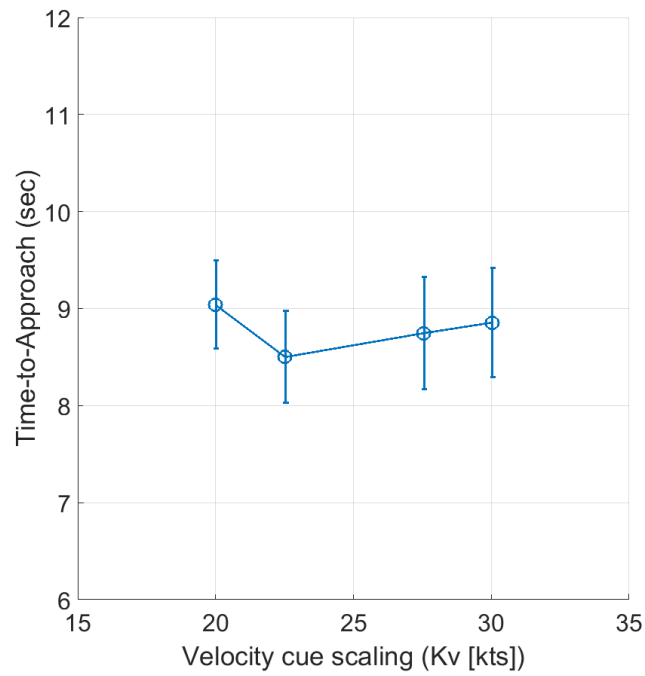
Figure 27: Time-to-approach as a function of velocity cue scaling
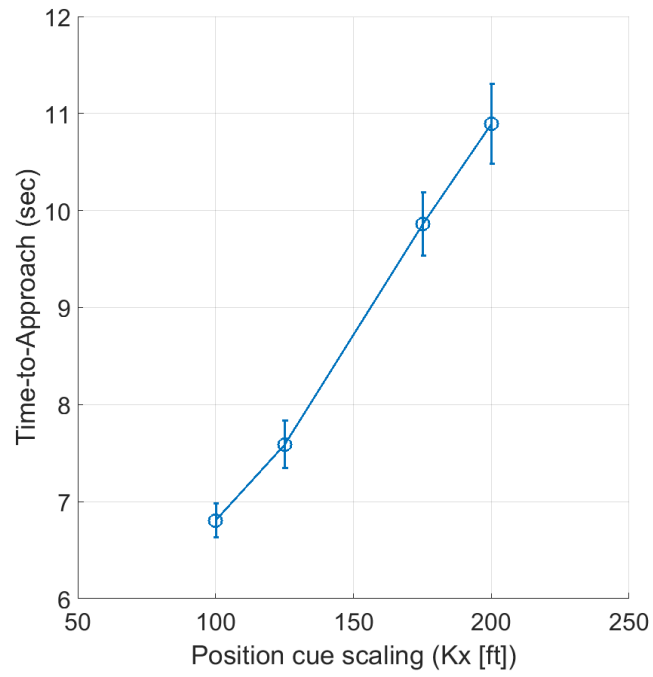
Figure 28: Time-to-approach as a function of position cue scaling
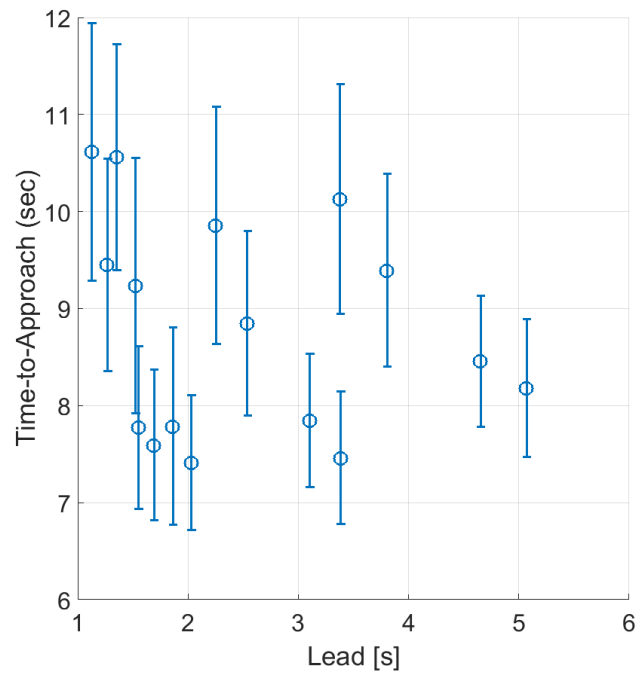
Figure 29: Time-to-approach as a function of *Lead*

4.3.2 Maximum Attitude Excursions

Both measures of control aggression, maximum attitude excursion and TTA, are products of the same action (i.e. larger control input during phase 1), and thus one would not expect the trends to suggest different conclusions. For the case of K_x, K_v, and K_a, that is indeed the case. However, as suggested by comparing Figures 29 and 30, one difference between the two measures of control aggression is that the attitude excursions are affected by the *Lead* time, whereas TTA is not. At first glance, this new behaviour demonstrates that *Lead* values less than 2 seconds greatly increase the likelihood that the participant adopts an aggressive strategy. Due to limitations on human-user response time, however, the large excursions may simply be a result of participant inability to properly control the helicopter at small *Lead* values. The gross degree of scatter in the sub-2 second data, as well as the "step" in maximum attitudes observed at 2 seconds rather than a gradual trend, likewise suggest an abrupt *loss* of control rather than a concerted change in control technique. The *Lead*-pitch relation is likely complex because there are two degrees of separation between the measures (Pitch→Acceleration →*Lead*), and would require dedicated experiments to fully understand why and how it affects attitude excursions in such a manner.

(a)   (b)
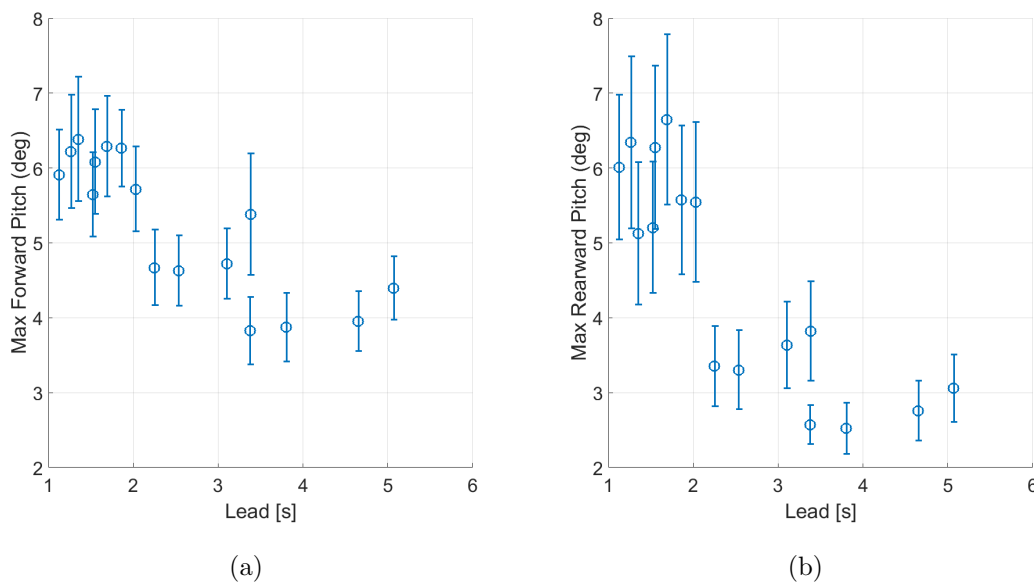
Figure 30: Maximum attitude excursions as a function of *Lead*. a) Forward pitch, b) Rearward pitch.

Chapter 5

Conclusions and Recommendations

Through this investigation, it has been proven that there exists a predictable relationship between non-conformal symbology display scaling and pilot response. By considering the position error RMS and pilot control activity (DIMS), levels of display scaling are identified which promote good performance and low workload simultaneously. These trends are supported by the Bedford workload ratings, which capture the perceived (subjective) pilot effort during the experiment according to spare cognitive ability. Through these metrics, reliable suggestions are made insofar as the position cue scaling K_x, acceleration cue scaling K_a, and *Lead*; however, the effect of velocity cue scaling K_v is anomalous in that the position error RMS and DIMS trends are mutually inverted. This indicates that factors not considered in the experiment influenced the use of the velocity vector, or that it was ignored altogether. For example, the pilots may have discounted the velocity vector due to lack of saliency since track angle is not required a single-axis task. This notion was supported by the K_v-Bedford trend, which points to participant indifference when it come to levels of K_v. An appropriate K_v value is instead obtained indirectly by manipulating *Lead* and K_a. For the implemented helicopter model, the suggested display scaling levels are:

$$K_x = 175 \ \frac{ft}{screen}$$

$$K_a = 15 \ \frac{\frac{ft}{s^2}}{screen}$$

$$Lead = 2\text{-}2.5 \ s$$

$$K_v \approx 22 \ \frac{kts}{screen}$$

By implementing these values, system designers are now afforded a quantitative and defendable basis for their tuning suggestions, and are able to conduct their tuning

through simulator trials. Furthermore, the suggested scaling will in theory provide an appropriate range for helicopters of similar make to the UH-1H (i.e. mid-weight utility helicopters) in low-speed manoeuvres.

The time-to-approach the hover phase (TTA) is considered as a means of assessing pilot control aggression. When plotted against TTA, the K_a and K_x trends support the scaling level suggestions obtained through the performance, DIMS, and Bedford analyses. The K_v-TTA trend displays nothing of statistical significance, supporting the idea of participant indifference towards the K_v level. *Lead* likewise produces no discernible effect on the TTA. However, the TTA is verified by the maximum attitude excursion: since both measures of control aggression depend on the same action (i.e. larger control inputs during the approach phase), the trends should be very similar. This is the case for all but the *Lead*, where a disjointed step increase in maximum pitch is seen at *Lead* <2 seconds, rather than a gradual increase. The *Lead*-pitch relation in complex, but may indicate *loss* of control, which would be consistent with human-user responsiveness limitations.

In expanding the research to capture a more representative set of effects, the following advancements are suggested:

- Extend the range of K_x to larger values to capture a proper minimum for one or both of the performance and DIMS metrics (if one exists)

- Refine the range of *Lead* values tested to better capture the transition from near-optimal to loss-of-control

- Expand the helicopter model to a multi-axis system

  $\implies$ in doing so, design a K_v-specific set of tasks to test for velocity vector saliency when direction of travel is required

- Reproduce experiment for a different helicopter model (of similar dynamcis to the UH-1H) to validate results

Bibliography

[1] "Beating brownout." http://www.aviationtoday.com/av/military/Beating-Brownout67142.html. Accessed Feb 1, 2017.

[2] S. Jennings, P. Holst, G. Craig, *et al.*, "Rotary wing brown-out symbology: The dvest test," in *SPIE Conference on Head- and Helmet-Mounted Displays; and Display Technologies and Applications for Defense, Security and Avionics*, 2012.

[3] M. Couch and J. Lindell, "Study on rotorcraft safety and survivability," in *Proc. of the American Helicopter Society 66th Annual Forum*, 2010.

[4] "Synthetic vision for helicopters by cobham avionics." www.sea-specialmissions.com/brochures/EFISHelicopter.pdf. Accessed Feb 1, 2017.

[5] D. Wickens and T. Prevett, "Exploring the dimensions of egocentricity in aircraft navigation displays," *Journal of Experimental Psychology*, vol. 1, pp. 110–135, 1995.

[6] M. McGreevy and S. Ellis, "The effect of perspective geometry on judged direction in spatial information instruments," *Human Factors*, vol. 28, pp. 439–56, 1986.

[7] R. McCann and D. Foyle, "Scene-linked symbology to improve situational awareness," in *Proc. in AGARD Conference No. 555, Aerospace Medical Panel Conference on Situational Awareness*, 1995.

[8] R. Becklen and D. Cervone, "Selective looking and the noticing of unexpected events," *Memory and Cognition*, vol. 11, pp. 601–608, 1983.

[9] R. Emerson and C. Wickens, "Superimposition, symbology, visual attention, and the head-up display," *Human Factors*, vol. 39, pp. 581–601, 1997.

[10] L. Hennessey, "The effects of a pathway-in-the-sky display on performance of a two axis tracking task by instrument rated pilots," Master's thesis, Embry-Riddle Aeonautical University, 1995.

[11] C. Knox and J. Leavitt, *Description of path-in-the-sky contact analog piloting display.* Washington, DC: NASA TM 74057, 1977.

[12] S. Roscoe, L. Colr, and R. Jensen, "Flight display dynamics revisited," *Human Factors*, vol. 23, pp. 341–53, 1981.

[13] Neiswander, "Improving rotorcraft deceleration guidance for brownout landing," Master's thesis, University of Iowa, 2010.

[14] D. Wickens and J. Long, "Object versus space based models of visual attention: Implications for the design of displays," *Journal of Experimental Psychology*, vol. 1, pp. 179–93, 1995.

[15] V. Merrick, G. Farris, and A. Vanags, *A head up display for application to V/STOL aircraft approach and landing.* Ames Research Center: NASA TM 102216, 1990.

[16] Z. Szoboszlay, T. Turpin, and R. McKinley, "Symbology for brown-out landings: The first simulation for the 3d-lz program," in *Proc. in the 65th Annual American Helicopter Society Forum*, 2009.

[17] D. Wickens, C. Liang, T. Prevett, *et al.*, "Egocentric and exocentric displays for terminal navigation areas," in *Proc. in the 38th Annual Meeting of the Human Factors and Ergonomics Society Annual Meeting*, pp. 16–20, 1994.

[18] Z. Szoboszlay, W. Albery, T. Turpin, and G. Neiswander, "Brown-out symbology simulation (boss) on the nasa ames vertical motion simulation," in *Proc. in the 64th Annual American Helicopter Society Forum*, 2008.

[19] U. S. Army, *Operator's Manual for Helicopter, Attack, AH-64A Apache.* Washington DC: TM 1-1520-238-10, 1994.

[20] I. Haskell and D. Wickens, "Two- and three-dimensional displays for aviation: A theoretical and empricial comparison," *International Journal of Aviation Psychology*, vol. 3, pp. 87–109, 1993.

[21] R. Newman and K. Greeley, *Helmet-Mounted Display Design Guide*. Ames Research Center, Moffett Field, CA: Defense Technical Information Center TR-97-11, 1997.

[22] P. Ververs and C. Wickens, "The effect of clutter and lowlighting symbology on pilot performance with head-up displays," in *Proc. in the Human Factors and Ergonomics Society 40th Annual Meeting*, pp. 62–66, 1996.

[23] "Fa90x operational evaluation board report." www.tc.gc.ca/eng/civilaviation/standards/commerce-3780.htm. Accessed July 5, 2017.

[24] H. Dudfield, T. Hardiman, and S. Selcon, *Human factors issues in the design of helment-mounted displays*. Man Machine Integration Department, Defence Research Agenecy, UK, 1995.

[25] R. Farrell and J. Booth, *Design Handbook for Imagery Interpretation*. Boeing Aerospace Company, Seattle, Washington, 1984.

[26] J. Randle, S. Roscoe, and J. Petitt, *Effects of magnification and accommodation of aimpoint estimation in simulated landings with real and virtual image display*. NASA Technical Report 1635, 1980.

[27] I. Larish and C. Wickens, *Divided attention with superimposed and separated imagery: implications for head-up displays*. University of Illinois, Aviation Research Center: TR 91-4/NASA HUD 91-1, 1991.

[28] R. Newman, *Head-Up Displays: Designing the Way Ahead*. Aldershot, England: Avebury, 1995.

[29] A. Alexander, E. Stelzer, S. Kim, *et al.*, *Bottom-up and top-down contributors to pilots perceptions of display clutter in advanced flight deck technologies*. Proc. in the Human Factors and Ergonomics Society 52nd Annual Meeting, 2008.

[30] A. Alexander, C. Wickens, and T. Hardy, "Synthetic vision systems: the effects of guidance symbology, display size, and field of view," *Human Factors*, vol. 47, pp. 693–707, 2005.

[31] P. Ververs and C. Wickens, "Head-up displays: effect of clutter, display intensity, and display location on pilot performance," *The International Journal of Aviation Psychology*, vol. 4, pp. 377–403, 1998.

[32] A. Doyle, *An improved attitude display for high elevation angle tasks.* DRA Technical Report DRA/AS/MMI/TR/94034, 1994.

[33] R. Hosman and H. Stassen, "Pilot's perception in the control of aircraft motions," *Control Engineering Practice*, vol. 7, pp. 1421–1428, 1999.

[34] S. Fadden and D. Wickens, *Maximizing traffic awareness with a head-up flightpath highway display.* Aviation Research Laboratory, Savoy, IL: University of Illinois Institute of Aviation, TR ARL-97-1/FAA-97-1, 1997.

[35] M. Yeh, D. Wickens, and F. Seagull, "Target cuing in visual search: the effects of conformality and display location on the allocation of visual attention," *Human Factors*, vol. 41, pp. 524–42, 1999.

[36] M. Velger, *Helmet-Mounted Displays and Sights.* Boston, MA: Artech House, 1998.

[37] R. Patterson, M. Winterbottom, and B. Pierce, "Perceptual issues in the use of head-mounted visual displays," *Human Factors*, vol. 48, pp. 555–573, 2006.

[38] R. Kruk and D. Runnings, "Low level flight performance and air combat manoeuvering performance in a simulator with a fibre optic helmet mounted display system," in *In Proc. of the American Institute of Aeronautics and Astronautics Conference*, pp. 1989–1992, 1989.

[39] J. Richman, J. Stanfield, and B. Dyre, "Small fields of view interfere with perception of heading during active contol but not passive viewing," in *Proc. in the Human Factors and Ergonomics Society 42nd Annual Meeting*, 1998.

[40] Z. Szoboszlay, L. Haworth, and T. Reynolds, "Field-of-view study for rotorcraft visionics," in *Proc. in Helmet- and Head-Mounted Displays and Symbology Design Requirements*, 1995.

[41] M. Konicke, "747-400 flight displays development," in *Aircraft Design, Systems and Operations*, 1988. DOI: 10.2514/6.1988-4439.

[42] U. Military, *Human Factors Engineering Design Criteria for Helicopter Cockpit Electro-Optical Display Symbology, MIL-STD-1295A*. Washington, DC: U.S. Department of Defense, 1984.

[43] M. Bernsten, M. Mulder, and M. vanPassen, "Modelling human visual perception and control of the direction of self-motion," in *Proc. in the AIAA Modeling and Simulation Technologies Conference and Exhibit*, vol. AIAA-2005-5893, 2005.

[44] B. Kantowitz, *Human Information Processing: Tutorials in Performance and Cognition*. John Wiley and Sons Inc, Jan 1975.

[45] A. Morris and P. Hamilton, *Visual Acuity and Reaction Time in Navy Fighter Pilots*. Naval Air Station, Pensacola, FL: United States Department of Defense, NAMRL-1324, 1986.

[46] J. Pollard, *All digital simulation for manned flight in turbulence*. Wright-Patterson AFB, Ohio: Air Force Institute of Technology AFFDL-TR-75-82, 1975.

[47] W. Barkhuizen, J. Schepers, and J. Coetzee, "Rate of information processing and reaction time of aircraft pilots and non-pilots," *Journal of Industrial Psychology*, vol. 2, pp. 67–76, 2002.

[48] R. Cummings, "The analysis of driving skills," *Journal of the Australian Road Research Board*, pp. 4–14, 1964.

[49] K. Schweizer, "Complexity of information processing and the speed-ability relationship," *Journal of General Psychology*, vol. 1, pp. 89–102, 1998.

[50] R. Hosman and M. Mulder, "Perception of flight information from efis displays," *Control Engineering Practice*, vol. 5, pp. 383–90, 1997.

[51] B. Korn, S. Schmerwitz, B. Lorenz, *et al.*, "Combining enhanced and synthetic vision for autonomous all-weather approach and landing," *The International Journal of Aviation Psychology*, vol. 19, pp. 49–72, 2009.

[52] C. Rash, B. Mozo, W. McLean, *et al.*, *Assessment Methodology for Integrated Helmet and Display Systems in Rotary-Wing Aircraft*. USAARL Report 96-1, 1996.

[53] D. Hans-Ulrich, "Improving visual-conformal displays for helicopter guidance," in *Proc. SPIE 5162, p.1-3. doi: 10.1117/12.01310.*

[54] J. Schroeder and M. Eshow, "Improvements in hover display dynamics for a combat helicopter," in *Proc. in Piloting Vertical Aircraft: A Conference on Flying Qualities and Human Factors*, (San Francisco, California), 1993.

[55] R. Hess and P. Gorder, "Design and evaluation of a cockpit display for hovering flight," in *Proc. in AIAA/AHS/ASEE Aircraft Design, Systems and Operations Meeting*, (Atlanta, GA), 1988.

[56] W. Aiken, *A mathematical representation of an advanced helicopter for piloted simulator investigations of control system and display variations.* Ames Research Center, Moffett Field, CA: U.S. Army Research and Technology Laboratories (AVRADCOM), TM 80-A-2, 1980.

[57] W. Aiken and K. Merrill, *Results of a Simulator Investigation of Control System and Display Variations for an Attack Helicopter mission.* Ames Research Center, Moffett Field, CA: U.S. Army Research and Technology Laboratories (AVRADCOM), TM 80-A-28, 1980.

[58] T. Muensterer, "Method for presenting the drift values of an aircraft," Feb. 4 2014. US Patent 8,645,008.

[59] L. Stiles and M. MacIsaac, "Integrated hover display with radar altitude predictor for indicating height above ground," Oct. 26 2006. US Patent App. 11/471,087.

[60] U. Military, *Aeronautical Design Standard, Performance Specification, Handling Qualities Requirements for Military Rotorcraft, ADS-33E-PRF.* Redstone Arsenal, AL: US Army Aviation and Missile Command, 2000.

[61] D. Caughey, "Introduction to aircraft stability and control." Cornell University Lecture Notes, Sibley School of Mechanical and Aerospace Engineering, 2011.

[62] H. O'Neill, "Calculation of the longitudinal stability derivatives and modes of motion for helicopter aircraft," Master's thesis, Naval Postgraduate School, Nibtereym California, 1982.

[63] G. Padfield, *Helicopter flight dynamics: the theory and application of flying qualities and simulation modelling, 2nd Ed.* American Institute of Aeronautics and Astronautics, 1996.

[64] R. Heffley, W. Jewell, J. Lehman, *et al.*, *A Compilation and Analysis of Helicopter Handling Qualities Data: Volume One.* Ames Research Center: NASA Contractor Report 3144, 1971.

[65] J. Bittner, "The use of texture in improving simulation of low-level flight," Master's thesis, University of Toronto, 1997.

[66] G. Mather and R. Sharman, "Decision-level adaptation in motion perception," in *Royal Society Open Science*, 2015. http://dx.doi.org/10.1098/rsos.150418.

[67] A. Roscoe and G. Ellis, *A Subjective Rating Scale for Assessing Pilot Workload in Flight: A Decade of Practical Use.* Royal Aerospace Establishment Technical Report 90019, 1990.

[68] J. Cohen, *Statistical Power Analysis for the Behavioral Sciences, 2nd ed.* New York, NY: Psychology Press, 2009.

[69] R. Bray, *Vertical Motion Requirements for Landing Simulation.* Ames Research Center, Moffat Field, CA: NASA Technical Memorandum TM X-62,236, 1973.

[70] S. Jennings *et al.*, "Evaluating control activity as a measure of workload in flight test," in *Proc. of the Human Factors and Ergonomics Society, 49th Annual Meeting*, pp. 64–67, 2005.

[71] J. Wobbrock, L. Findlater, D. Gergle, *et al.*, "The aligned rank transform for nonparametric factorial analysis using only anova procedures," in *Proc. in the ACM Conference on Human Factors in Computing*, pp. 143–146, 2011.

[72] E. Bachelder, B. Aponso, and M. Godfroy, "Characterization of pilot technique," in *Proc. in the AHS International 73rd Annual Forum and Technology Display*, 2017.

Appendix A
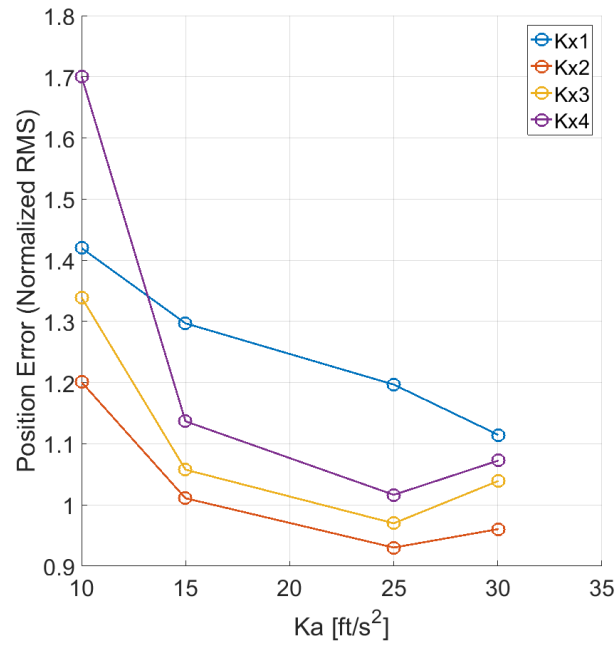
Figure 31: Performance (position error) as a function of combinations of acceleration cue scaling and position cue scaling. $\mathrm{K}_{x_1} = 100\ \frac{ft}{screen}$, $\mathrm{K}_{x_2} = 125\ \frac{ft}{screen}$, $\mathrm{K}_{x_3} = 175\ \frac{ft}{screen}$, and $\mathrm{K}_{x_4} = 200\ \frac{ft}{screen}$.
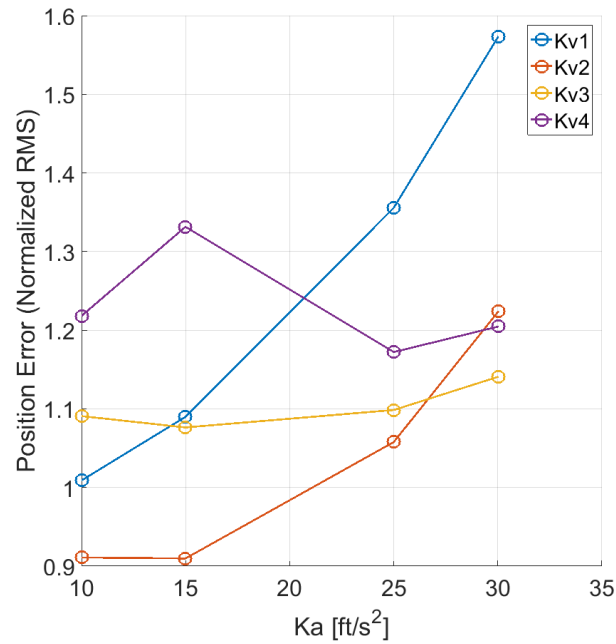
Figure 32: Performance (position error) as a function of combinations of acceleration cue scaling and velocity cue scaling
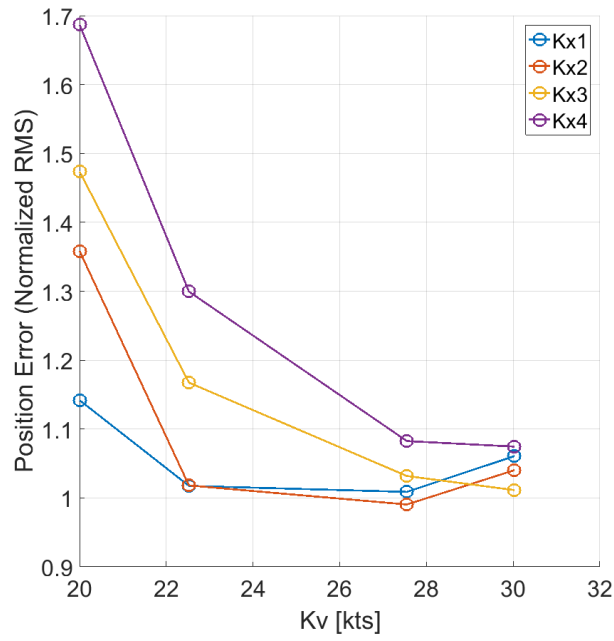
Figure 33: Performance (position error) as a function of combinations of velocity cue scaling and position cue scaling
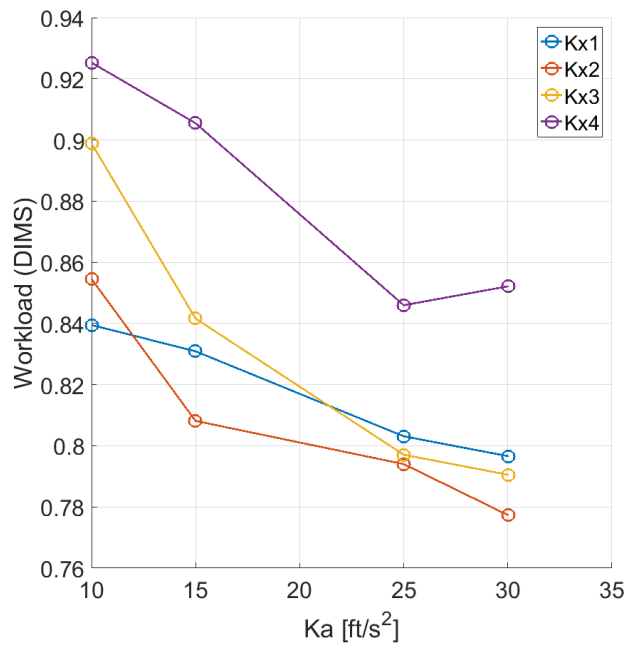
Figure 34: Workload (DIMS) as a function of combinations of acceleration cue scaling and position cue scaling
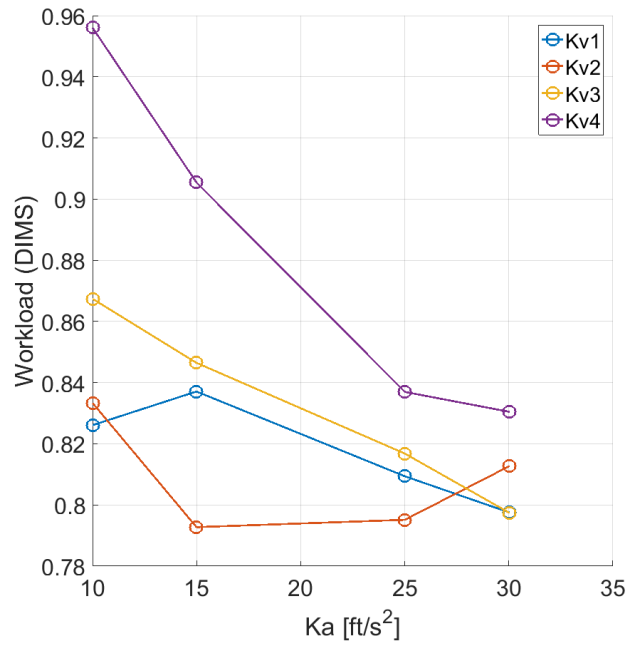
Figure 35: Workload (DIMS) as a function of combinations of acceleration cue scaling and velocity cue scaling
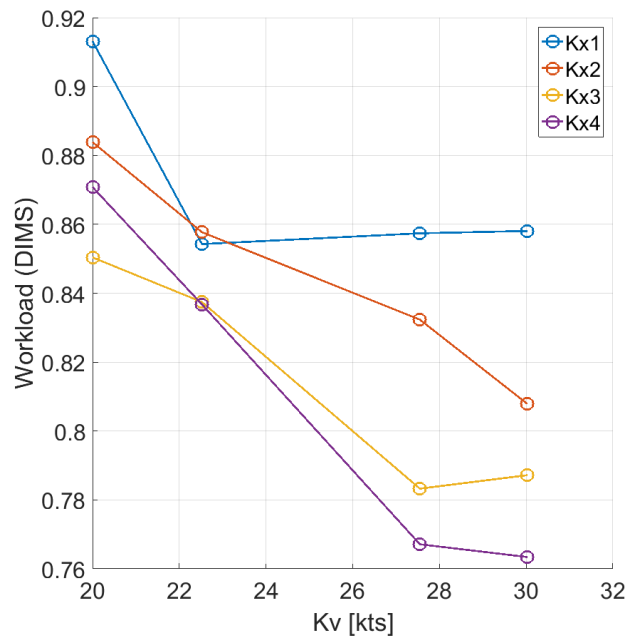
Figure 36: Workload (DIMS) as a function of combinations of velocity cue scaling and position cue scaling

Appendix B
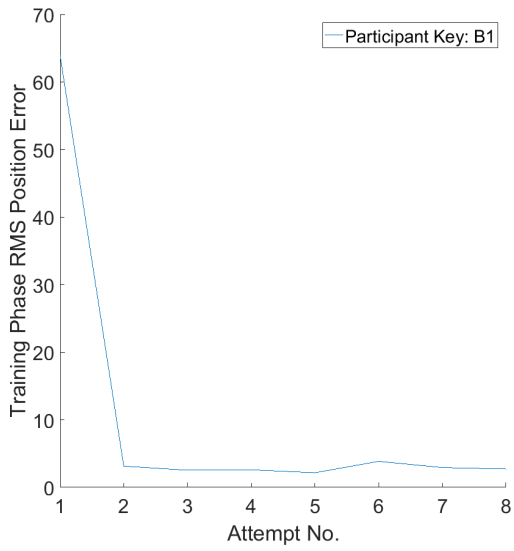
Figure 37: Participant B1 training
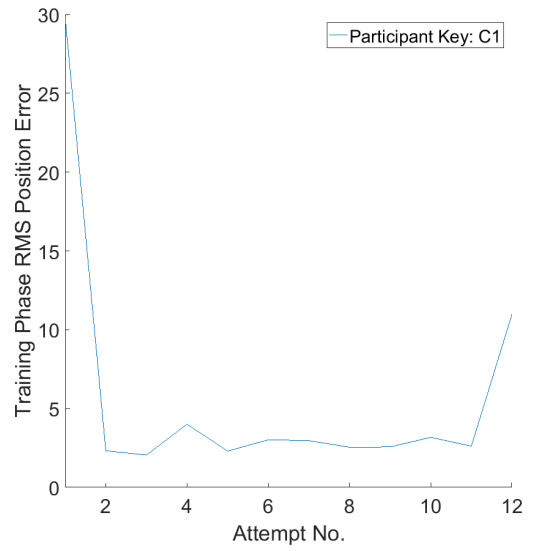
Figure 38: Participant C1 training
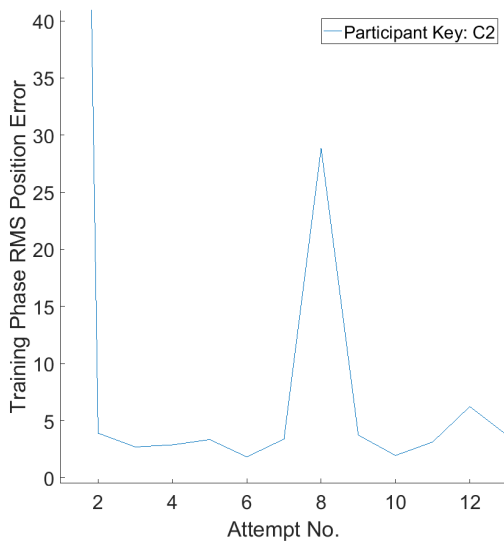
Figure 39: Participant C2 training
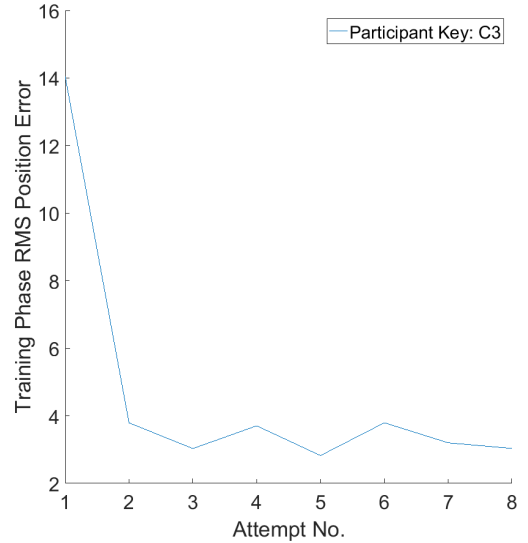
Figure 40: Participant C3 training
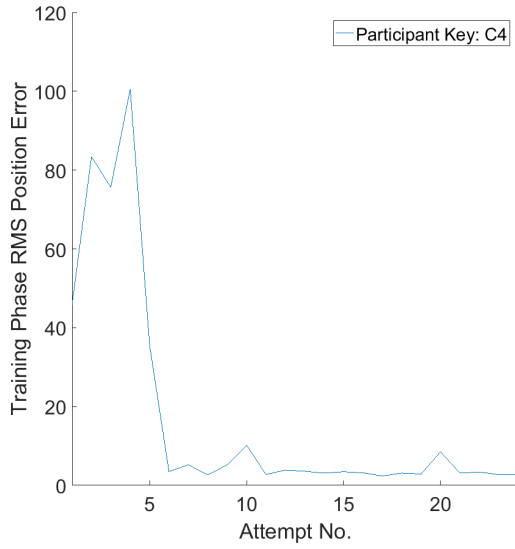
Figure 41: Participant C4 training
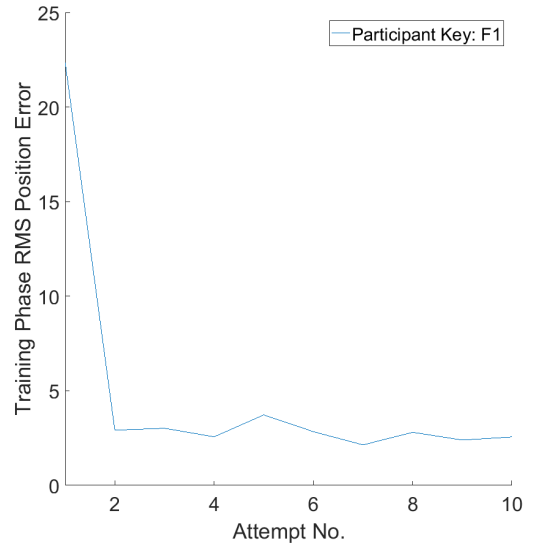
Figure 42: Participant F1 training
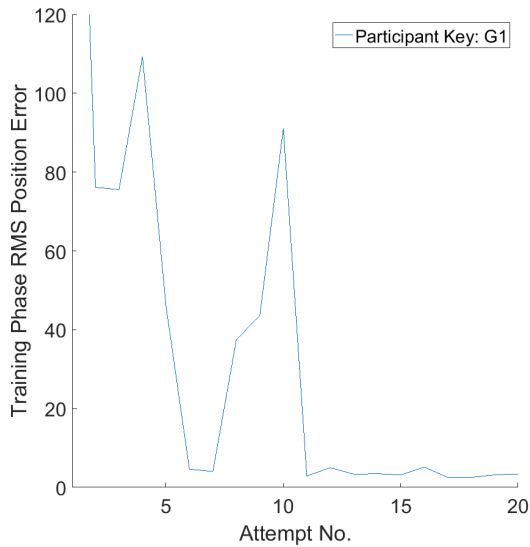
Figure 43: Participant G1 training
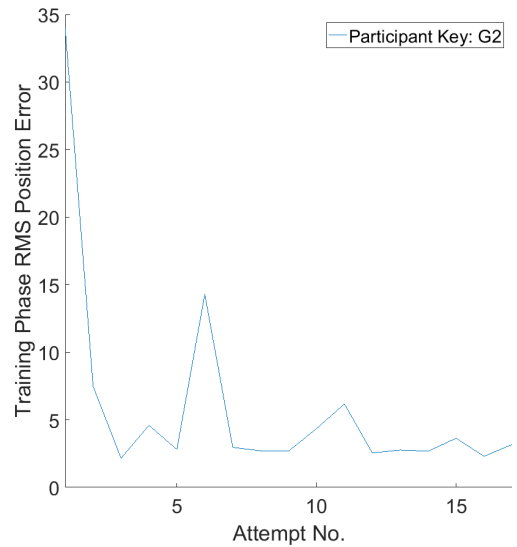
Figure 44: Participant G2 training
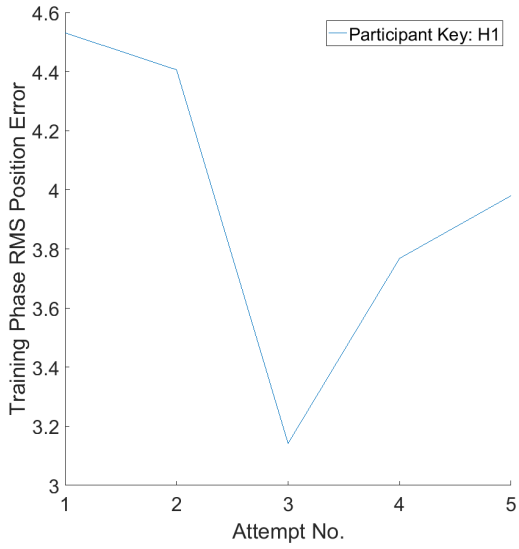
Figure 45: Participant H1 training
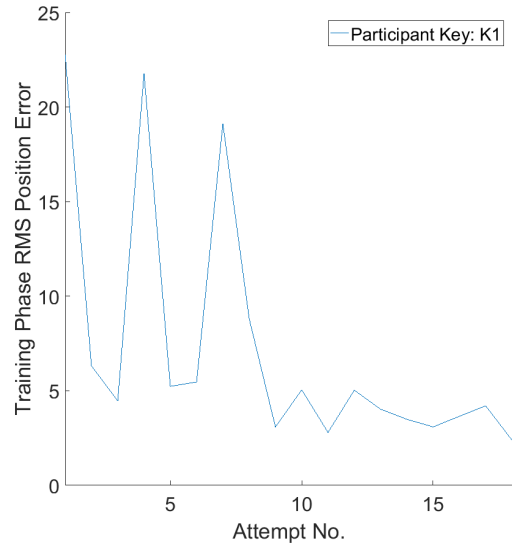
Figure 46: Participant K1 training
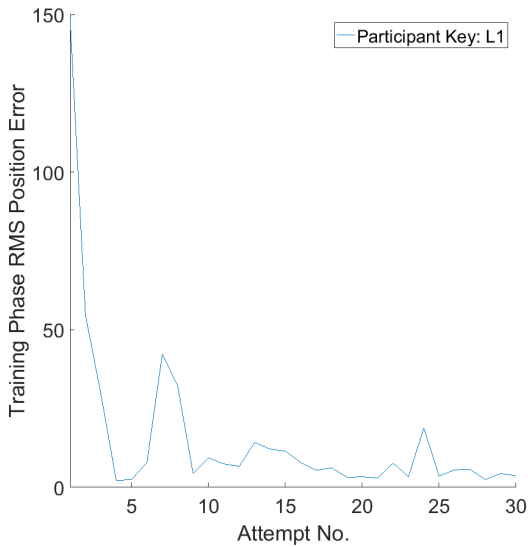
Figure 47: Participant L1 training
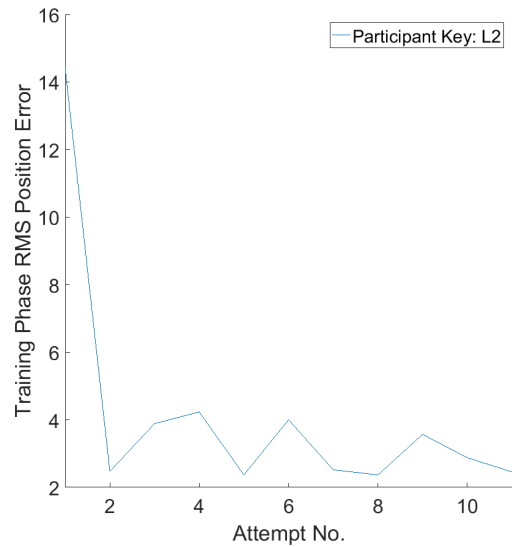
Figure 48: Participant L2 training
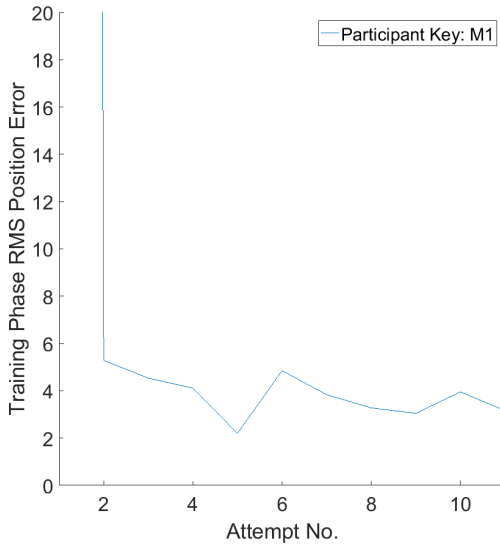
Figure 49: Participant M1 training
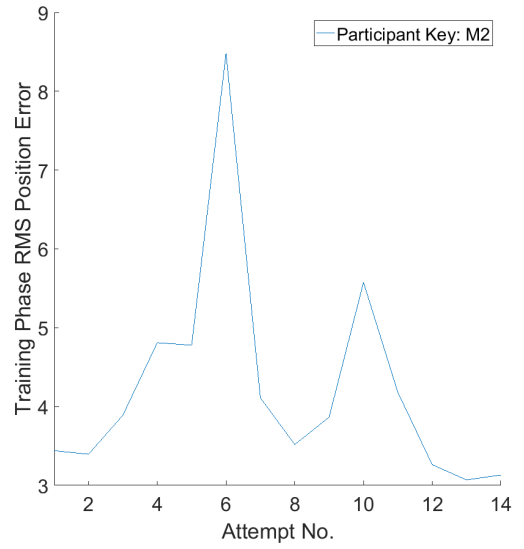
Figure 50: Participant M2 training
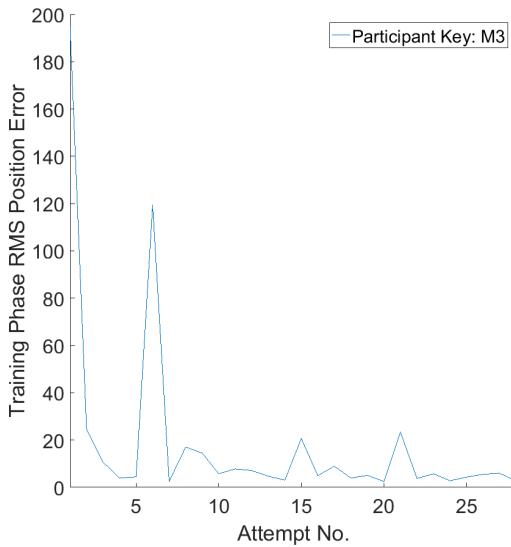
Figure 51: Participant M3 training
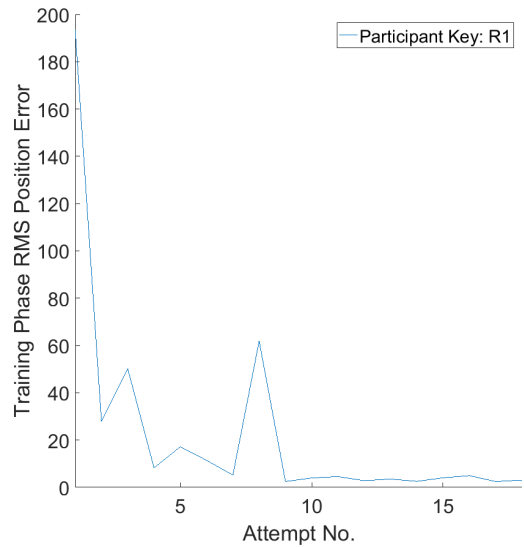
Figure 52: Participant R1 training
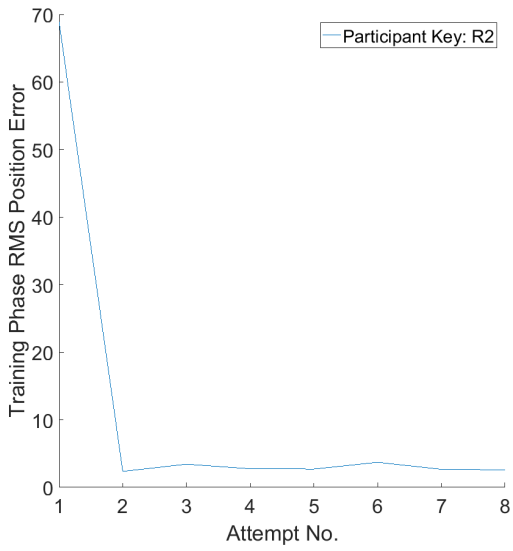
Figure 53: Participant R2 training
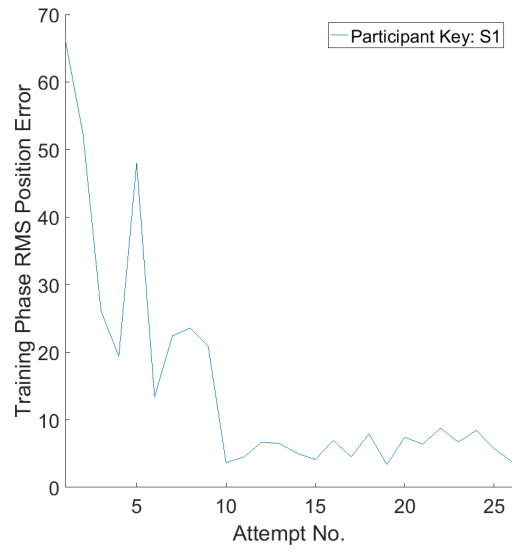
Figure 54: Participant S1 training
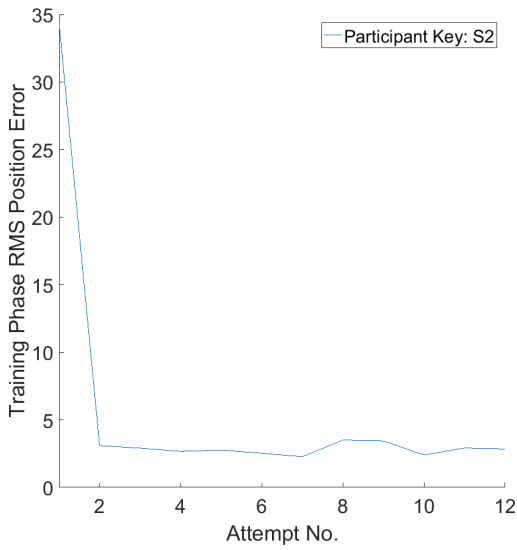
Figure 55: Participant S2 training
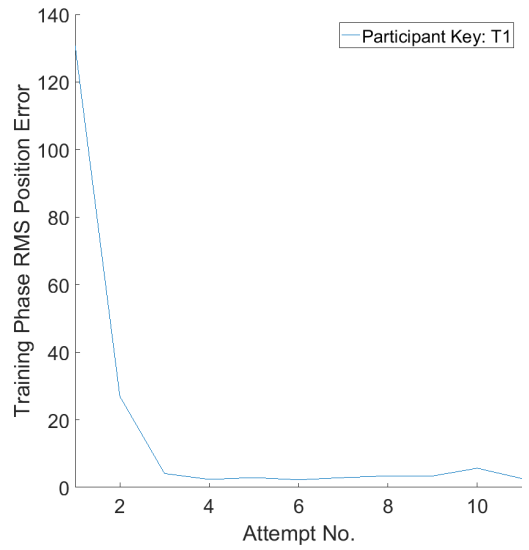
Figure 56: Participant T1 training
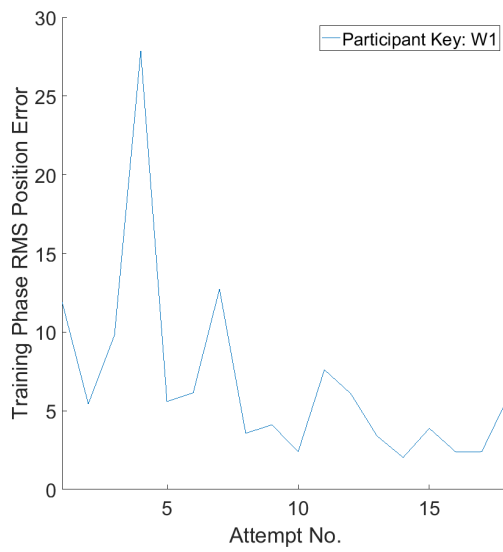
Figure 57: Participant W1 training
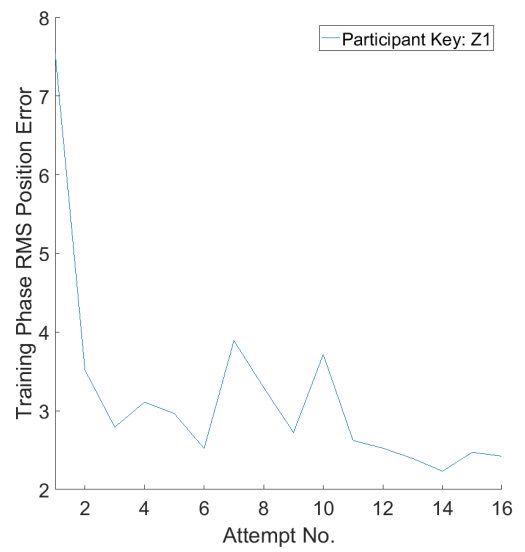
Figure 58: Participant Z1 training

Appendix C

Table 15: Complete experiment matrix

Trial No.	$K_x \left[\frac{ft}{screen}\right]$	$K_v \left[\frac{kt}{screen}\right]$	$K_a \left[\frac{\frac{ft}{s^2}}{screen}\right]$
1	100	30	10
2	100	30	15
3	100	30	25
4	100	30	30
5	100	27.5	10
6	100	27.5	15
7	100	27.5	25
8	100	27.5	30
9	100	22.5	10
10	100	22.5	15
11	100	22.5	25
12	100	22.5	30
13	100	20	10
14	100	20	15
15	100	20	25
16	100	20	30
17	125	30	10
18	125	30	15
19	125	30	25
20	125	30	30
21	125	27.5	10
22	125	27.5	15

23	125	27.5	25
24	125	27.5	30
25	125	22.5	10
26	125	22.5	15
27	125	22.5	24
28	125	22.5	30
29	125	20	10
30	125	20	15
31	125	20	25
32	125	20	30
33	175	30	10
34	175	30	15
35	175	30	25
36	175	30	30
37	175	27.5	10
38	175	27.5	15
39	175	27.5	25
40	175	27.5	30
41	175	22.5	10
42	175	22.5	15
43	175	22.5	25
44	175	22.5	30
45	175	20	10
46	175	20	15

47	175	20	25
48	175	20	30
49	200	30	10
50	200	30	15
51	200	30	25
52	200	30	30
53	200	27.5	10
54	200	27.5	15
55	200	27.5	25
56	200	27.5	30
57	200	22.5	10
58	200	22.5	15
59	200	22.5	25
60	200	22.5	30
61	200	20	10
62	200	20	15
63	200	20	25
64	200	20	30

Appendix D

Table 16: Experiment schedule

Session	Minutes Allotted
Forms	5
Briefing	10
Training	30
Experiment Proper	190
Debriefing	5
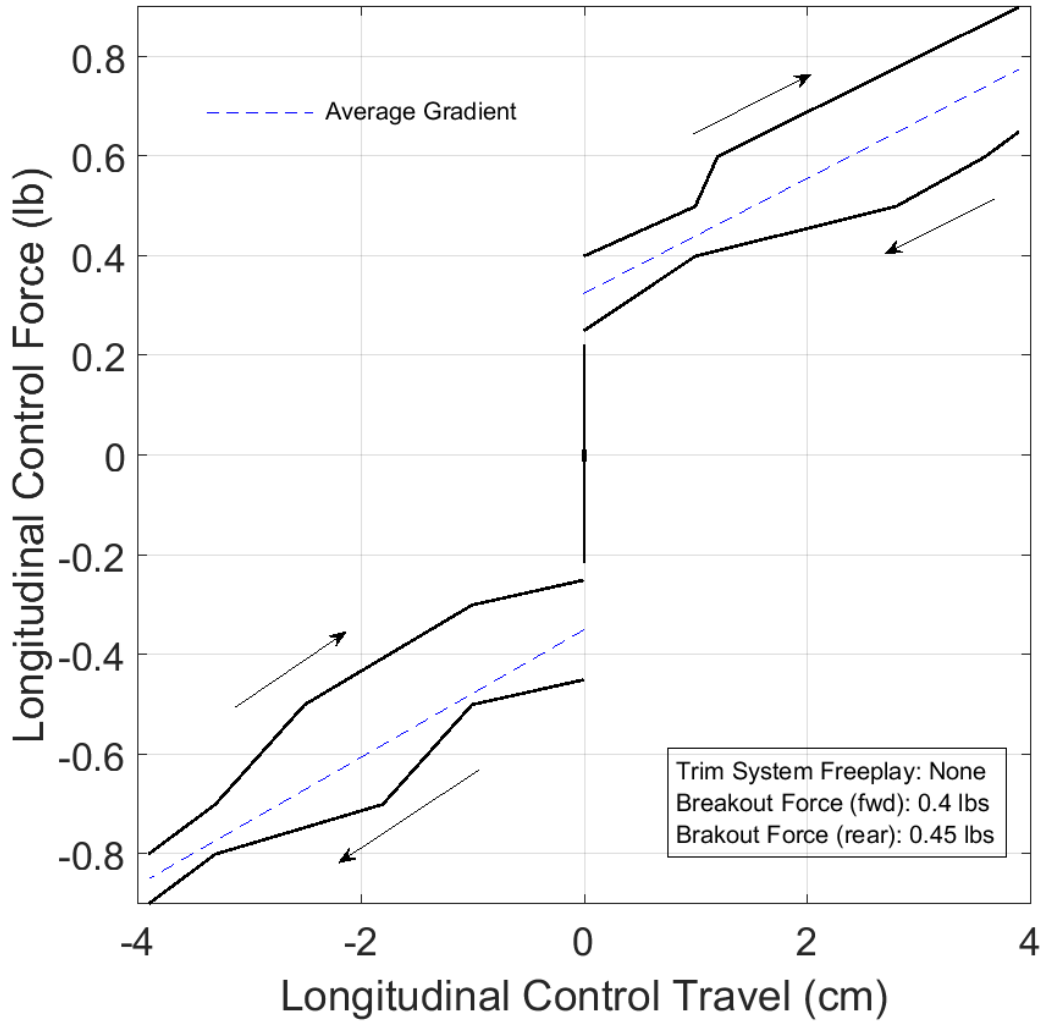
Figure 59: Joystick characterization
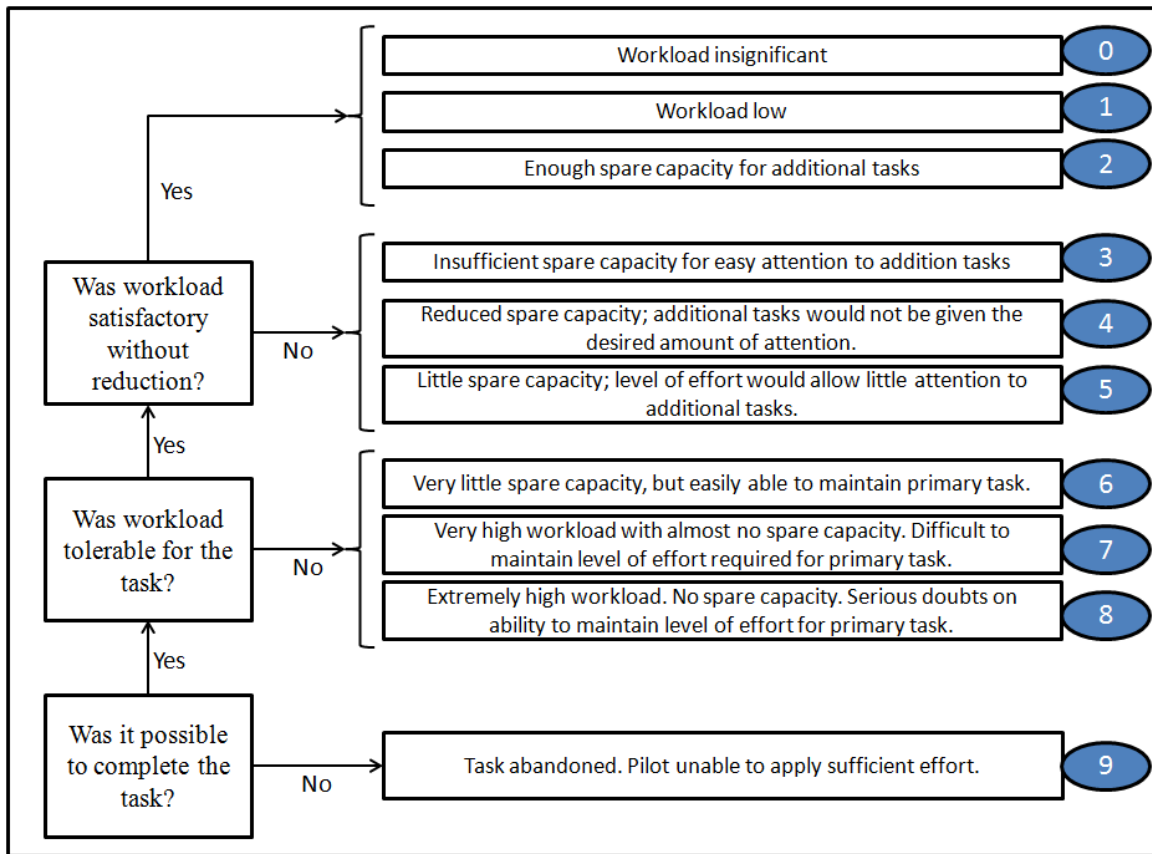
Figure 60: Bedford workload rating scale. Modified to lie in 0-9 range (from commonly adopted 1-10 range) to ease selection using a numpad.

National Research Council
Canada

Conseil national de recherches
Canada

NRC·CNRC

7 November 2016   SENT BY E-MAIL ONLY

Dr. Sion Jennings
NRC - Aerospace
Sion.jennings@nrc-cnrc.gc.ca

Dear Dr. Jennings:

Re: Ethics approval for Project 2016-79
       Helicopter Symbology Assessment Metric

I reviewed the application for ethics approval of the above-titled project submitted to the NRC
Research Ethics Board. I am pleased to inform you that this protocol is eligible for Chair review,
and the request you submitted has received ethics approval as of 7 November 2016.

The ethics approval lasts one year and expires on 6 November 2017.
In accordance with national norms in research ethics, please note that this ethics approval
comes with the understanding that you will submit to the NRC-REB the following:

*   any proposed changes to the project or informed consent;
*   any adverse events or unexpected outcomes
*   a request for ethics renewal on an annual basis; and
*   a final report at the conclusion of the trial.

I wish you continued success in your research endeavours.

Sincerely,

Gordon DuVal, SJD
Chair, NRC-REB

E-copies only to: Jerzy Komorowski, GM, NRC Aerospace
                        Stephen Parkinson, Director, NRC Aerospace
                        Louise de Ruiter, NRC-REB

Canada

Figure 61: National Research Council Ethics Board project approval

National Research Council Conseil national de recherches
Canada Canada

NRC·CNRC

31 January 2017 SENT BY E-MAIL ONLY

Dr. Sion Jennings
NRC - Aerospace
Sion.jennings@nrc-cnrc.gc.ca

Dear Dr. Jennings:

**Re: Ethics approval of Amendment #1 for Project 2016-79
Helicopter Symbology Assessment Metric**

I reviewed the application for an amendment to the above-titled project submitted to the NRC Research Ethics Board. I am pleased to inform you that your request has been approved as of 31 January 2017.

The expiry date remains the same (6 November 2017). If this project and its human research elements are to endure beyond the expiration date, please contact the NRC Research Ethics Board Secretariat to renew or confirm ethics approval at least 30 days in advance.

In accordance with national norms in research ethics, please note that this ethics approval comes with the understanding that you will submit to the NRC-REB the following:

- any proposed changes to the project or informed consent;
- any adverse events or unexpected outcomes
- a request for ethics renewal on an annual basis; and
- a final report at the conclusion of the trial.

I wish you continued success in your research endeavours.

Sincerely,

Gordon DuVal, SJD
Chair, NRC-REB

Copies: Jerzy Komorowski, GM, NRC Aerospace
Stephen Parkinson, Director, NRC Aerospace
Louise de Ruiter, NRC-REB

Canada

Figure 62: National Research Council Ethics Board approval of project amendments

CERTIFICATION OF INSTITUTIONAL ETHICS CLEARANCE

The Carleton University Research Ethics Board-B (CUREB-B) has granted ethics clearance for the research project described below and research may now proceed.

CUREB-B is constituted and operates in compliance with the *Tri-Council Policy Statement: Ethical Conduct for Research Involving Humans (TCPS2)*.

Ethics Protocol Clearance ID: Project # 106515

Faculty Supervisor: Jason Etele

Research Team: Jason Etele (Primary Investigator)
Fabian Erazo (Student Research: Master's Student)

Project Title: Helicopter Symbology Assessment Metric

Funding Source (If applicable):

Effective: **March 03, 2017**   Expires: **March 31, 2018**.

Restrictions:

This certification is subject to the following conditions:

1. Clearance is granted only for the research and purposes described in the application.
2. Any modification to the approved research must be submitted to CUREB-B via a Change to Protocol Form. All changes must be cleared prior to the continuance of the research.
3. An Annual Status Report for the renewal of ethics clearance must be submitted and cleared by the renewal date listed above. Failure to submit the Annual Status Report will result in the closure of the file. If funding is associated, funds will be frozen.
4. A closure request must be sent to CUREB-B when the research is complete or terminated.
5. Should any participant suffer adversely from their participation in the project you are required to report the matter to CUREB-B.

Failure to conduct the research in accordance with the principles of the *Tri-Council Policy Statement: Ethical Conduct for Research Involving Humans 2ndedition* and the *Carleton University Policies and Procedures for the Ethical Conduct of Research* may result in the suspension or termination of the research project.

Please contact the Research Compliance Coordinators, at ethics@carleton.ca if you have any questions or require a clearance certificate with a signature.

CLEARED BY: **Date: March 03, 2017**

Andy Adler, PhD, Chair, CUREB-B
Shelley Brown, PhD, Vice-Chair, CUREB-B

Figure 63: Carleton University Ethics Board project approval

DEMOGRAPHIC QUESTIONS

Project identification
Project title: **HELICOPTER SYMBOLOGY ASSESSMENT METRIC**
Project identification number: assigned by NRC REB Secretariat: 2016-79

Online questionnaire:

1.   DEMOGRAPHIC INFORMATION

1. What is your age?_____ (Years)
2. You identify your gender as
    ○ Woman   ○ Man   ○ _____ (fill in the blank)
3. Are you a pilot? If so, how many years of flight experience do you have?
    ○ Yes ○ No _____ (Years of experience)
4. Do you have any previous experience flying or testing helicopter symbology?
    ○ Yes ○ No

2.   VISION

1. Are you currently wearing eyeglasses or corrective contacts? ○ Yes ○ No
    a.   If you selected "Yes", is your vision considered normal when wearing your glasses or contact lenses?
       ○ Yes ○ No
       i.   If you selected "No", please elaborate? _____

3.   HANDEDNESS

1. Which hand do you prefer to use when you write?
    ○ Left ○ Right ○ No preference

National Research   Conseil national
Council Canada   de recherches Canada

Canada

Data captured directly from the device used by the participant:
(We will automatically record the following information from your trials)

1. Simulated helicopter position as indicated by the "Landing zone" symbol
2. Simulated helicopter velocity as indicated by the "Velocity vector" symbol
3. Simulated helicopter acceleration as indicated by the "Acceleration cue" symbol
4. Joystick position

Screening:
Participants shall be selected from the National Research Council's Flight Research Laboratory's staff members. The participants must be 1) 18 years of age or older, 2) must complete the entire experiment for their data set to be included in the results, 3) have normal or corrected-to-normal vision, 4) be comfortable performing the experiment in a semi-private room, separated by curtains, and 5) be comfortable performing the experiment while wearing a standard-issue helicopter helmet.

Questions during debriefing phase:

1. Are there any factors that might have influenced your performance?
2. Other comments/feedback?

Figure 64: Demographic questionnaire

Helicopter Symbology Assessment Metric Project

Why are you being asked to read this information?
You are being asked to participate in a study meant to improve the quality of helicopter symbology systems for use in low-visibility operations. The information on this page is intended to help you understand your tasks in this experiment so that you can decide whether or not you wish to proceed. Please read this consent form carefully before making your decision. Take all the time that is necessary. Your participation is entirely voluntary.

Why is the study being undertaken?
The purpose of this study is to better understand the manner in which scaling the symbol dynamics of 2D (non-conformal) helicopter symbology affects pilot performance. In particular, the tasks are tailored towards station-keeping performance, and are restricted to single-axis movement.

What will you be asked to do?
Should you consent to participate in the experiment, we will be asking you to attempt to keep a square symbol, indicative of the simulated helicopter's position, centered on the symbology display. Responses will be made using a 568 Combatstick USB joystick. There will be 216 trials broken into 4 blocks of 64, with each trial taking roughly 30 seconds. Prior to each trial, some aspect of the symbology scaling will be altered – you will **not** be informed as to how the scaling was altered.s

Privacy and confidentiality
All data collected during the experiment will be stored on secure servers accessible only to the research team. All information gathered from you will be confidential and all data used in the analyses will be anonymized so that no link can be made between data and participant. If you choose to withdraw from the research and stop using the system, only the information you shared before withdrawal will remain in the system for research purposes.

Confidentiality will be respected, and unless required by law, no information that might directly or indirectly reveal your identity will be released or published without your specific consent to the disclosure.

NRC's Research Ethics Board will have access to the data, for monitoring purposes.

Potential harms / inconveniences / benefits
There are no known harms associated with your participation in this research other than that possibility of mild temporary eyestrain. You will not benefit directly from your participation in this study.

National Research Council Canada   Conseil national de recherches Canada

Canada

Compensation for injury, legal rights
By consenting to participate in the research you are not waiving your legal rights.

You have the right to change your mind
Your participation is entirely voluntary, and you may exit the experiment at any time during the study.

Who to contact if you have any further concerns or questions?
If you have any questions or comments about this experiment, please contact Sion Jennings at
Sion.Jennings@nrc-cnrc.gc.ca ; 613-990-3607.

Ethics review
This study has been reviewed by the NRC Research Ethics Board (REB). REB review seeks to ensure that research projects involving humans as participants meet Canadian standards of ethics. Any questions or concerns about the ethics of this study may be directed to the NRC-REB Secretariat, NRC-REB@nrc-cnrc.gc.ca, (613) 949-8681.

Statement of consent – please check the appropriate box
- ☐ I have read and understand the information given in this informed consent and all my questions have been answered to my satisfaction. I have had sufficient time to consider whether to participate in this study. I understand that my participation in this study is entirely voluntary and that I may withdraw from the study at any time without penalty. I voluntarily consent to participate in this study.
- ☐ I do not consent to participate in this study

Participant Name (Print): _____

Participant Signature: _____

Date: _____

Location (City): _____

Witness Name (Print): _____

Witness Signature: _____

Date: _____

Location (City): _____

Figure 65: Consent form

Appendix E

Table of critical values for the F distribution (for use with ANOVA):

How to use this table:
There are two tables here. The first one gives critical values of F at the p = 0.05 level of significance.
The second table gives critical values of F at the p = 0.01 level of significance.
1. Obtain your F-ratio. This has (x,y) degrees of freedom associated with it.
2. Go along x columns, and down y rows. The point of intersection is your critical F-ratio.
3. If your obtained value of F is equal to or larger than this critical F-value, then your result is
significant at that level of probability.
An example: I obtain an F ratio of 3.96 with (2, 24) degrees of freedom.
I go along 2 columns and down 24 rows. The critical value of F is 3.40. My obtained F-ratio
is larger than this, and so I conclude that my obtained F-ratio is likely to occur by chance with a p<.05.

Critical values of F for the 0.05 significance level:

	1	2	3	4	5	6	7	8	9	10
1	161.45	199.50	215.71	224.58	230.16	233.99	236.77	238.88	240.54	241.88
2	18.51	19.00	19.16	19.25	19.30	19.33	19.35	19.37	19.39	19.40
3	10.13	9.55	9.28	9.12	9.01	8.94	8.89	8.85	8.81	8.79
4	7.71	6.94	6.59	6.39	6.26	6.16	6.09	6.04	6.00	5.96
5	6.61	5.79	5.41	5.19	5.05	4.95	4.88	4.82	4.77	4.74
6	5.99	5.14	4.76	4.53	4.39	4.28	4.21	4.15	4.10	4.06
7	5.59	4.74	4.35	4.12	3.97	3.87	3.79	3.73	3.68	3.64
8	5.32	4.46	4.07	3.84	3.69	3.58	3.50	3.44	3.39	3.35
9	5.12	4.26	3.86	3.63	3.48	3.37	3.29	3.23	3.18	3.14
10	4.97	4.10	3.71	3.48	3.33	3.22	3.14	3.07	3.02	2.98
11	4.84	3.98	3.59	3.36	3.20	3.10	3.01	2.95	2.90	2.85
12	4.75	3.89	3.49	3.26	3.11	3.00	2.91	2.85	2.80	2.75
13	4.67	3.81	3.41	3.18	3.03	2.92	2.83	2.77	2.71	2.67
14	4.60	3.74	3.34	3.11	2.96	2.85	2.76	2.70	2.65	2.60
15	4.54	3.68	3.29	3.06	2.90	2.79	2.71	2.64	2.59	2.54
16	4.49	3.63	3.24	3.01	2.85	2.74	2.66	2.59	2.54	2.49
17	4.45	3.59	3.20	2.97	2.81	2.70	2.61	2.55	2.49	2.45
18	4.41	3.56	3.16	2.93	2.77	2.66	2.58	2.51	2.46	2.41
19	4.38	3.52	3.13	2.90	2.74	2.63	2.54	2.48	2.42	2.38
20	4.35	3.49	3.10	2.87	2.71	2.60	2.51	2.45	2.39	2.35
21	4.33	3.47	3.07	2.84	2.69	2.57	2.49	2.42	2.37	2.32
22	4.30	3.44	3.05	2.82	2.66	2.55	2.46	2.40	2.34	2.30
23	4.28	3.42	3.03	2.80	2.64	2.53	2.44	2.38	2.32	2.28
24	4.26	3.40	3.01	2.78	2.62	2.51	2.42	2.36	2.30	2.26
25	4.24	3.39	2.99	2.76	2.60	2.49	2.41	2.34	2.28	2.24
26	4.23	3.37	2.98	2.74	2.59	2.47	2.39	2.32	2.27	2.22
27	4.21	3.35	2.96	2.73	2.57	2.46	2.37	2.31	2.25	2.20
28	4.20	3.34	2.95	2.71	2.56	2.45	2.36	2.29	2.24	2.19
29	4.18	3.33	2.93	2.70	2.55	2.43	2.35	2.28	2.22	2.18
30	4.17	3.32	2.92	2.69	2.53	2.42	2.33	2.27	2.21	2.17
31	4.16	3.31	2.91	2.68	2.52	2.41	2.32	2.26	2.20	2.15
32	4.15	3.30	2.90	2.67	2.51	2.40	2.31	2.24	2.19	2.14
33	4.14	3.29	2.89	2.66	2.50	2.39	2.30	2.24	2.18	2.13
34	4.13	3.28	2.88	2.65	2.49	2.38	2.29	2.23	2.17	2.12
35	4.12	3.27	2.87	2.64	2.49	2.37	2.29	2.22	2.16	2.11

36	4.11	3.26	2.87	2.63	2.48	2.36	2.28	2.21	2.15	2.11
37	4.11	3.25	2.86	2.63	2.47	2.36	2.27	2.20	2.15	2.10
38	4.10	3.25	2.85	2.62	2.46	2.35	2.26	2.19	2.14	2.09
39	4.09	3.24	2.85	2.61	2.46	2.34	2.26	2.19	2.13	2.08
40	4.09	3.23	2.84	2.61	2.45	2.34	2.25	2.18	2.12	2.08
41	4.08	3.23	2.83	2.60	2.44	2.33	2.24	2.17	2.12	2.07
42	4.07	3.22	2.83	2.59	2.44	2.32	2.24	2.17	2.11	2.07
43	4.07	3.21	2.82	2.59	2.43	2.32	2.23	2.16	2.11	2.06
44	4.06	3.21	2.82	2.58	2.43	2.31	2.23	2.16	2.10	2.05
45	4.06	3.20	2.81	2.58	2.42	2.31	2.22	2.15	2.10	2.05
46	4.05	3.20	2.81	2.57	2.42	2.30	2.22	2.15	2.09	2.04
47	4.05	3.20	2.80	2.57	2.41	2.30	2.21	2.14	2.09	2.04
48	4.04	3.19	2.80	2.57	2.41	2.30	2.21	2.14	2.08	2.04
49	4.04	3.19	2.79	2.56	2.40	2.29	2.20	2.13	2.08	2.03
50	4.03	3.18	2.79	2.56	2.40	2.29	2.20	2.13	2.07	2.03
51	4.03	3.18	2.79	2.55	2.40	2.28	2.20	2.13	2.07	2.02
52	4.03	3.18	2.78	2.55	2.39	2.28	2.19	2.12	2.07	2.02
53	4.02	3.17	2.78	2.55	2.39	2.28	2.19	2.12	2.06	2.02
54	4.02	3.17	2.78	2.54	2.39	2.27	2.19	2.12	2.06	2.01
55	4.02	3.17	2.77	2.54	2.38	2.27	2.18	2.11	2.06	2.01
56	4.01	3.16	2.77	2.54	2.38	2.27	2.18	2.11	2.05	2.01
57	4.01	3.16	2.77	2.53	2.38	2.26	2.18	2.11	2.05	2.00
58	4.01	3.16	2.76	2.53	2.37	2.26	2.17	2.10	2.05	2.00
59	4.00	3.15	2.76	2.53	2.37	2.26	2.17	2.10	2.04	2.00
60	4.00	3.15	2.76	2.53	2.37	2.25	2.17	2.10	2.04	1.99
61	4.00	3.15	2.76	2.52	2.37	2.25	2.16	2.09	2.04	1.99
62	4.00	3.15	2.75	2.52	2.36	2.25	2.16	2.09	2.04	1.99
63	3.99	3.14	2.75	2.52	2.36	2.25	2.16	2.09	2.03	1.99
64	3.99	3.14	2.75	2.52	2.36	2.24	2.16	2.09	2.03	1.98
65	3.99	3.14	2.75	2.51	2.36	2.24	2.15	2.08	2.03	1.98
66	3.99	3.14	2.74	2.51	2.35	2.24	2.15	2.08	2.03	1.98
67	3.98	3.13	2.74	2.51	2.35	2.24	2.15	2.08	2.02	1.98
68	3.98	3.13	2.74	2.51	2.35	2.24	2.15	2.08	2.02	1.97
69	3.98	3.13	2.74	2.51	2.35	2.23	2.15	2.08	2.02	1.97
70	3.98	3.13	2.74	2.50	2.35	2.23	2.14	2.07	2.02	1.97
71	3.98	3.13	2.73	2.50	2.34	2.23	2.14	2.07	2.02	1.97
72	3.97	3.12	2.73	2.50	2.34	2.23	2.14	2.07	2.01	1.97
73	3.97	3.12	2.73	2.50	2.34	2.23	2.14	2.07	2.01	1.96
74	3.97	3.12	2.73	2.50	2.34	2.22	2.14	2.07	2.01	1.96
75	3.97	3.12	2.73	2.49	2.34	2.22	2.13	2.06	2.01	1.96
76	3.97	3.12	2.73	2.49	2.34	2.22	2.13	2.06	2.01	1.96
77	3.97	3.12	2.72	2.49	2.33	2.22	2.13	2.06	2.00	1.96
78	3.96	3.11	2.72	2.49	2.33	2.22	2.13	2.06	2.00	1.95
79	3.96	3.11	2.72	2.49	2.33	2.22	2.13	2.06	2.00	1.95
80	3.96	3.11	2.72	2.49	2.33	2.21	2.13	2.06	2.00	1.95
81	3.96	3.11	2.72	2.48	2.33	2.21	2.13	2.06	2.00	1.95
82	3.96	3.11	2.72	2.48	2.33	2.21	2.12	2.05	2.00	1.95
83	3.96	3.11	2.72	2.48	2.32	2.21	2.12	2.05	2.00	1.95
84	3.96	3.11	2.71	2.48	2.32	2.21	2.12	2.05	1.99	1.95
85	3.95	3.10	2.71	2.48	2.32	2.21	2.12	2.05	1.99	1.94

Figure 66: F-distribution table

8.4 SAMPLE SIZE TABLES 381

Table 8.4.1

n to detect f by F test at a = .01
for u = 1, 2, 3, 4

$$\frac{u = 1}{f}$$

Power	.05	.10	.15	.20	.25	.30	.35	.40	.50	.60	.70	.80
.10	336	85	39	22	15	11	9	7	5	4	4	3
.50	1329	333	149	85	55	39	29	22	15	11	9	7
.70	1924	482	215	122	79	55	41	32	21	15	12	9
.80	2338	586	259	148	95	67	49	38	25	18	14	11
.90	2978	746	332	188	120	84	62	48	31	22	17	13
.95	3564	892	398	224	144	101	74	57	37	26	20	16
.99	4808	1203	536	302	194	136	100	77	50	35	26	21

$$\frac{u = 2}{f}$$

Power	.05	.10	.15	.20	.25	.30	.35	.40	.50	.60	.70	.80
.10	307	79	36	21	14	10	8	6	5	4	3	3
.50	1093	275	123	70	45	32	24	19	13	9	7	6
.70	1543	387	173	98	63	44	33	26	17	12	10	8
.80	1851	464	207	117	76	53	39	30	20	14	11	9
.90	2325	582	260	147	95	66	49	38	25	18	14	11
.95	2756	690	308	174	112	78	58	45	29	21	16	12
.99	3658	916	408	230	148	103	76	59	38	27	20	16

$$\frac{u = 3}{f}$$

Power	.05	.10	.15	.20	.25	.30	.35	.40	.50	.60	.70	.80
.10	278	71	32	19	13	9	7	6	4	3	3	2
.50	933	234	105	59	38	27	20	16	11	8	6	5
.70	1299	326	146	83	53	37	28	22	14	10	8	7
.80	1548	388	175	98	63	44	33	25	17	12	9	8
.90	1927	483	215	122	78	55	41	31	21	15	11	9
.95	2270	568	253	143	92	64	48	37	24	17	13	10
.99	2986	747	333	188	121	84	62	48	31	22	17	13

$$\frac{u = 4}{f}$$

Power	.05	.10	.15	.20	.25	.30	.35	.40	.50	.60	.70	.80
.10	253	64	29	17	12	8	7	5	4	3	3	2
.50	820	206	92	52	34	24	18	14	10	7	6	5
.70	1128	283	127	72	46	33	24	19	13	9	7	6
.80	1341	336	150	85	55	38	29	22	15	11	8	7
.90	1661	416	186	105	68	47	35	27	18	13	10	8
.95	1948	488	218	123	79	55	41	32	21	15	11	9
.99	2544	640	286	160	103	76	53	41	27	19	14	11

388   8   **F** TESTS ON MEANS IN THE ANALYSIS OF VARIANCE AND COVARIANCE

Table 8.4.8

n to detect f by F test at a = .10
for u = 5, 6, 8, 10

u = 5

f

Power	.05	.10	.15	.20	.25	.30	.35	.40	.50	.60	.70	.80
.50	343	86	39	22	14	10	8	6	4	3	3	2
.70	551	139	61	35	23	16	12	9	6	5	4	3
.80	693	174	77	44	28	20	15	12	8	6	4	4
.90	922	231	103	58	37	26	20	15	10	7	6	4
.95	1128	283	126	71	46	32	24	18	12	9	7	5
.99	1564	392	175	98	63	44	33	25	16	12	9	7

u = 6

f

Power	.05	.10	.15	.20	.25	.30	.35	.40	.50	.60	.70	.80
.50	317	80	36	20	13	9	7	6	4	3	3	2
.70	506	127	57	32	21	15	11	9	6	4	3	3
.80	635	159	71	40	26	18	14	11	7	5	4	3
.90	838	210	94	53	34	24	18	14	9	7	5	4
.95	1022	256	114	65	42	29	22	17	11	8	6	5
.99	1408	353	157	89	57	40	30	23	15	11	8	6

u = 8

f

Power	.05	.10	.15	.20	.25	.30	.35	.40	.50	.60	.70	.80
.50	278	70	32	18	12	9	6	5	4	3	2	2
.70	436	110	49	28	18	13	10	8	5	4	3	3
.80	545	137	61	35	23	16	12	9	6	5	4	3
.90	717	180	80	46	29	21	15	12	8	6	4	4
.95	870	218	97	55	36	25	19	14	9	7	5	4
.99	1190	298	133	75	49	34	25	19	13	9	7	5

u = 10

f

Power	.05	.10	.15	.20	.25	.30	.35	.40	.50	.60	.70	.80
.50	250	63	28	16	11	8	6	5	3	3	2	2
.70	390	98	44	25	16	11	9	7	5	4	3	3
.80	482	121	54	31	20	14	11	8	6	4	3	3
.90	633	159	71	40	26	18	14	11	7	5	4	3
.95	765	192	86	49	31	22	16	13	8	6	5	4
.99	1040	261	116	66	42	30	22	17	11	8	6	5

8.4   SAMPLE SIZE TABLES   389

Table 8.4.9

n to detect f by F test at a = .10
for u = 12, 15, 24

u = 12

f

Power	.05	.10	.15	.20	.25	.30	.35	.40	.50	.60	.70	.80
.50	229	58	26	15	10	7	5	4	3	2	2	2
.70	355	89	40	23	15	11	8	6	4	3	3	2
.80	437	110	49	28	18	13	10	8	5	4	3	3
.90	571	143	64	36	24	17	12	10	6	5	4	3
.95	688	173	77	44	28	20	15	11	8	5	4	4
.99	931	233	104	59	38	27	20	15	10	7	5	4

u = 15

f

Power	.05	.10	.15	.20	.25	.30	.35	.40	.50	.60	.70	.80
.50	205	52	23	13	9	6	5	4	3	2	2	2
.70	315	79	35	20	13	9	7	6	4	3	2	2
.80	386	97	43	25	16	12	9	7	5	4	3	2
.90	502	126	56	32	21	15	11	9	6	4	3	3
.95	603	151	68	38	25	17	13	10	7	5	4	3
.99	812	203	91	51	33	23	17	13	9	6	5	4

u = 24

f

Power	.05	.10	.15	.20	.25	.30	.35	.40	.50	.60	.70	.80
.50	161	41	18	11	7	5	4	3	2	2	--	--
.70	246	62	27	16	10	7	6	5	3	2	2	2
.80	298	75	34	19	12	9	7	5	4	3	2	2
.90	382	96	43	25	16	11	8	7	5	3	3	2
.95	456	114	52	30	19	13	10	8	5	4	3	3
.99	607	152	68	39	25	17	13	10	7	5	4	3

Table 8.4.2

n to detect f by F test at a = .01
for u = 5, 6, 8, 10

u = 5

Power	.05	.10	.15	.20	.25	.30	.35	.40	.50	.60	.70	.80
.10	233	59	27	16	11	8	6	5	4	3	2	2
.50	737	185	82	47	30	22	16	13	9	6	5	4
.70	1009	253	113	64	41	29	22	17	11	8	6	5
.80	1193	299	134	76	49	34	26	20	13	10	7	6
.90	1469	368	164	93	60	42	31	24	16	12	9	7
.95	1719	431	192	109	70	49	36	28	18	13	10	8
.99	2235	560	249	141	91	63	47	36	24	17	13	10

u = 6

Power	.05	.10	.15	.20	.25	.30	.35	.40	.50	.60	.70	.80
.10	218	55	25	15	10	7	6	5	3	3	2	--
.50	673	169	76	43	28	20	15	12	8	6	5	4
.70	917	230	103	58	38	27	20	15	10	8	6	5
.80	1080	271	121	68	44	31	23	18	12	9	7	6
.90	1326	332	148	84	54	38	28	22	14	10	8	6
.95	1547	388	173	98	63	44	33	25	17	12	9	7
.99	2003	502	224	126	81	57	42	33	21	15	11	9

u = 8

Power	.05	.10	.15	.20	.25	.30	.35	.40	.50	.60	.70	.80
.10	194	49	23	13	9	6	5	4	3	3	2	2
.50	580	146	65	37	24	17	13	10	7	5	4	3
.70	785	197	88	50	32	23	17	13	9	7	5	4
.80	918	230	103	58	38	27	20	15	10	8	6	5
.90	1122	281	126	71	46	32	24	19	12	9	7	6
.95	1303	327	146	83	53	37	28	22	14	10	8	6
.99	1676	420	187	106	68	48	36	27	18	13	10	8

u = 10

Power	.05	.10	.15	.20	.25	.30	.35	.40	.50	.60	.70	.80
.10	176	45	21	12	8	6	5	4	3	2	2	2
.50	515	129	58	33	21	15	12	9	6	5	4	3
.70	691	173	78	44	29	20	15	12	8	6	5	4
.80	810	203	91	51	33	23	18	14	9	7	5	4
.90	982	246	110	62	40	28	21	16	11	8	6	5
.95	1138	285	127	72	47	33	24	19	12	9	7	6
.99	1456	365	163	92	60	42	31	24	16	11	9	7

Table 8.4.3

n to detect f by F test at a = .01
for u = 12, 15, 24

u = 12

Power	.05	.10	.15	.20	.25	.30	.35	.40	.50	.60	.70	.80
.10	162	41	19	11	8	5	4	4	3	2	2	2
.50	467	117	53	30	20	14	10	8	6	4	3	3
.70	623	157	70	40	26	18	14	11	7	5	4	3
.80	726	182	82	46	30	21	16	12	8	6	5	4
.90	881	221	99	56	36	25	19	15	10	7	6	5
.95	1017	255	114	65	42	29	22	17	11	8	6	5
.99	1297	325	145	83	53	37	28	21	14	10	8	6

u = 15

Power	.05	.10	.15	.20	.25	.30	.35	.40	.50	.60	.70	.80
.10	147	37	17	10	7	5	4	3	2	2	2	--
.50	413	104	47	27	17	12	9	7	5	4	3	3
.70	548	138	62	35	23	16	12	10	6	5	4	3
.80	632	159	71	41	26	19	14	11	7	5	4	4
.90	769	193	86	49	32	22	17	13	9	6	5	4
.95	885	222	99	56	36	26	19	15	10	7	6	4
.99	1125	282	126	72	46	32	24	19	12	9	7	5

u = 24

Power	.05	.10	.15	.20	.25	.30	.35	.40	.50	.60	.70	.80
.10	118	30	14	8	6	4	3	3	2	2	--	--
.50	318	80	36	21	14	10	7	6	4	3	3	2
.70	417	105	47	27	17	12	9	7	5	4	3	2
.80	485	121	55	31	20	15	11	8	6	4	3	3
.90	578	145	65	37	24	17	13	10	7	5	4	3
.95	662	166	74	42	27	19	14	11	8	6	4	4
.99	831	209	92	53	34	24	18	14	9	7	5	4

Table 8.4.4

n to detect f by F test at a = .05
for u = 1, 2, 3, 4

u = 1
f

Power	.05	.10	.15	.20	.25	.30	.35	.40	.50	.60	.70	.80
.10	84	22	10	6	5	4	3	3	2	--	--	--
.50	769	193	86	49	32	22	17	13	9	7	5	4
.70	1235	310	138	78	50	35	26	20	13	10	7	6
.80	1571	393	175	99	64	45	33	26	17	12	9	7
.90	2102	526	234	132	85	59	44	34	22	16	12	9
.95	2600	651	290	163	105	73	54	42	27	19	14	11
.99	3675	920	409	231	148	103	76	58	38	27	20	15

u = 2
f

Power	.05	.10	.15	.20	.25	.30	.35	.40	.50	.60	.70	.80
.10	84	22	10	6	5	4	3	3	2	--	--	--
.50	662	166	74	42	27	19	15	11	8	6	5	4
.70	1028	258	115	65	42	29	22	17	11	8	6	5
.80	1286	322	144	81	52	36	27	21	14	10	8	6
.90	1682	421	188	106	68	48	35	27	18	13	10	8
.95	2060	515	230	130	83	58	43	33	22	15	12	9
.99	2855	714	318	179	115	80	59	46	29	21	16	12

u = 3
f

Power	.05	.10	.15	.20	.25	.30	.35	.40	.50	.60	.70	.80
.10	79	21	10	6	4	3	3	2	2	--	--	--
.50	577	145	65	37	24	16	13	10	7	5	4	3
.70	881	221	99	56	36	25	19	15	10	7	6	5
.80	1096	274	123	69	45	31	23	18	12	9	7	5
.90	1415	354	158	89	58	40	30	23	15	11	8	7
.95	1718	430	192	108	70	49	36	28	18	13	10	8
.99	2353	589	262	148	95	66	49	38	24	17	13	10

u = 4
f

Power	.05	.10	.15	.20	.25	.30	.35	.40	.50	.60	.70	.80
.10	74	19	9	6	4	3	2	2	--	--	--	--
.50	514	129	58	33	21	15	11	9	6	5	4	3
.70	776	195	87	49	32	22	17	13	9	6	5	4
.80	956	240	107	61	39	27	20	16	10	8	6	5
.90	1231	309	138	78	50	35	26	20	13	10	7	6
.95	1486	372	166	94	60	42	31	24	16	11	9	7
.99	2021	506	225	127	82	57	42	33	21	15	11	9

Table 8.4.5

n to detect f by F test at a = .05
for u = 5, 6, 8, 10

u = 5
f

Power	.05	.10	.15	.20	.25	.30	.35	.40	.50	.60	.70	.80
.10	69	18	9	5	4	3	2	2	--	--	--	--
.50	467	117	53	30	19	14	10	8	6	4	3	--
.70	698	175	78	44	29	20	15	12	8	6	5	3
.80	856	215	96	54	35	25	18	14	9	7	5	4
.90	1098	275	123	69	45	31	23	18	12	9	7	5
.95	1320	331	148	83	54	38	28	22	14	10	8	6
.99	1783	447	199	112	72	50	37	29	19	13	10	8

u = 6
f

Power	.05	.10	.15	.20	.25	.30	.35	.40	.50	.60	.70	.80
.10	66	17	8	5	4	3	2	2	--	--	--	--
.50	429	108	49	28	18	13	10	8	5	4	3	--
.70	638	160	72	41	26	18	14	11	7	5	4	3
.80	780	195	87	50	32	22	17	13	9	6	5	4
.90	995	250	112	63	41	29	21	16	11	8	6	5
.95	1192	299	133	75	49	34	25	20	13	9	7	6
.99	1604	402	179	101	65	46	34	26	17	12	9	7

u = 8
f

Power	.05	.10	.15	.20	.25	.30	.35	.40	.50	.60	.70	.80
.10	60	16	7	5	3	2	2	--	--	--	--	--
.50	374	94	42	24	16	11	8	7	5	4	3	2
.70	548	138	61	35	23	16	12	9	6	5	4	3
.80	669	168	75	42	27	19	14	11	8	6	4	4
.90	848	213	95	54	35	24	18	14	9	7	5	4
.95	1012	254	113	64	41	29	22	17	11	8	6	5
.99	1351	338	151	86	55	39	29	22	14	10	8	6

u = 10
f

Power	.05	.10	.15	.20	.25	.30	.35	.40	.50	.60	.70	.80
.10	55	14	7	4	3	2	2	--	--	--	--	--
.50	335	84	38	21	14	10	8	6	4	3	3	2
.70	488	123	55	31	20	14	11	8	6	4	3	3
.80	591	148	66	38	24	17	13	10	7	5	4	3
.90	747	187	84	48	31	22	16	13	8	6	5	4
.95	888	223	99	56	36	26	19	15	10	7	5	4
.99	1177	295	132	75	48	34	25	19	13	9	7	6

Table 8.4.6

n to detect f by F test at a = .05
for u = 12, 15, 24

u = 12
f

Power	.05	.10	.15	.20	.25	.30	.35	.40	.50	.60	.70	.80
.10	51	13	7	4	3	2	2	--	--	--	--	--
.50	306	77	35	20	13	9	7	6	4	3	3	2
.70	443	111	50	28	18	13	10	8	5	4	3	3
.80	534	134	60	34	22	16	12	9	6	5	4	3
.90	673	169	75	43	28	20	15	11	8	6	4	4
.95	796	200	89	51	33	23	17	13	9	6	5	4
.99	1052	264	118	67	43	30	22	17	11	8	6	5

u = 15
f

Power	.05	.10	.15	.20	.25	.30	.35	.40	.50	.60	.70	.80
.10	47	12	6	4	3	2	---	--	--	--	--	--
.50	272	69	31	18	12	8	6	5	4	3	2	2
.70	391	98	44	25	16	12	9	7	5	4	3	2
.80	471	118	53	30	20	14	10	8	6	4	3	3
.90	588	148	66	38	24	17	13	10	7	5	4	3
.95	697	175	78	44	29	20	15	12	8	6	4	4
.99	915	229	102	58	38	26	20	15	10	7	6	4

u = 24
f

Power	.05	.10	.15	.20	.25	.30	.35	.40	.50	.60	.70	.80
.10	38	10	5	3	2	---	---	--	--	--	--	--
.50	213	54	24	14	9	7	5	4	3	2	2	--
.70	303	76	34	20	13	9	7	5	4	3	2	2
.80	363	91	41	23	15	11	8	6	4	3	3	2
.90	457	115	51	29	19	13	10	8	5	4	3	3
.95	525	132	59	34	22	15	11	9	6	4	4	3
.99	680	171	76	44	28	20	15	11	8	6	4	4

Table 8.4.7

n to detect f by F test at a = .10
for u = 1, 2, 3, 4

u = 1
f

Power	.05	.10	.15	.20	.25	.30	.35	.40	.50	.60	.70	.80
.50	542	136	61	35	22	16	12	9	6	5	4	3
.70	942	236	105	60	38	27	20	15	10	7	6	5
.80	1237	310	138	78	50	35	26	20	13	9	7	6
.90	1713	429	191	108	69	48	36	27	18	13	10	8
.95	2165	542	241	136	87	61	45	35	22	16	12	9
.99	3155	789	351	198	127	88	65	50	32	23	17	13

u = 2
f

Power	.05	.10	.15	.20	.25	.30	.35	.40	.50	.60	.70	.80
.50	475	119	53	30	20	14	11	8	6	4	3	3
.70	797	200	89	50	32	23	17	13	9	6	5	4
.80	1029	258	115	65	41	29	22	17	11	8	6	5
.90	1395	349	156	88	57	40	29	23	15	11	8	6
.95	1738	435	194	109	70	49	36	28	18	13	10	8
.99	2475	619	276	155	100	70	51	33	21	15	11	9

u = 3
f

Power	.05	.10	.15	.20	.25	.30	.35	.40	.50	.60	.70	.80
.50	419	105	47	27	18	12	9	7	5	4	3	3
.70	690	173	77	43	28	20	15	11	8	6	4	4
.80	883	221	99	56	36	25	19	15	10	7	5	4
.90	1180	296	132	74	48	34	25	19	13	9	7	5
.95	1458	365	163	92	59	41	30	24	15	11	8	7
.99	2051	513	229	129	83	58	43	33	21	15	11	9

u = 4
f

Power	.05	.10	.15	.20	.25	.30	.35	.40	.50	.60	.70	.80
.50	376	95	43	24	16	11	9	7	5	4	3	3
.70	612	154	68	38	25	18	13	10	7	5	4	3
.80	773	193	87	49	32	22	17	13	9	6	5	4
.90	1031	258	115	65	42	29	22	17	11	8	6	5
.95	1267	317	141	80	51	36	27	21	13	10	7	6
.99	1768	443	197	111	71	50	37	28	19	13	10	8

Figure 67: Cohen n'-tables. Source: [68].